Insights into the formation of oncogenic chromosome rearrangements

Dissertation

Zur Erlangung des Grades

Doktor der Naturwissenschaften

Am Fachbereich Biologie

Der Johannes Gutenberg-Universität Mainz

Vera Minneker

geb. am 25.06.1989 in Lengerich (Westf.)

Mainz, 2022

Table of Contents

1 Zusammenfassung

Chromosomenabberationen wie Translokationen können direkt krebsauslösend zu sein. Sie treten sehr selten auf, können Zellen aber einen Wachstumsvorteil verschaffen, was die Untersuchung der für ihre Entstehung erforderlichen Schritte erschwert. Paradoxerweise ist die zelluläre Maschinerie zur Reparatur von Doppelstrangbrüchen (DSB), auch dafür verantwortlich, gebrochene Chromosomenenden auf unzulässige Weise zu Translokationen zu verbinden. Es wird davon ausgegangen, dass einfache Chromosomenfusionen auf einem der End Joining (EJ) Prozesse beruhen: classical non-homologous EJ (cNHEJ) oder alternativem EJ (aEJ).

Mehrere Studien, in denen verschiedene Versuchsanordnungen zur Auslösung von Translokationen und zur Bestimmung ihrer Häufigkeit verwendet wurden, kamen zu dem Schluss, dass Translokationen durch aEJ verursacht werden und, dass cNHEJ die Zellen vor ihrer Bildung schützt. Zuletzt haben Studien, bei denen TALENs und CRISPR zur Auslösung von Translokationen und PCR-basierte Methoden zur Quantifizierung verwendet wurden, jedoch ergeben, dass weniger und nicht mehr Translokationen in Abwesenheit von cNHEJ gebildet werden. Zur Klärung dieser Kontroverse, verfolgten wir einen systematischen Ansatz unter Verwendung isogener menschlicher Zelllinien, mit Deletionen verschiedener EJ-Faktoren und unter Verwendung verschiedener Arten der DSB-Induktion. Um die Bildung von Translokationen zu quantifizieren, haben wir eine Kombination aus Fluoreszenz *in situ* Hybridisierung, Hochdurchsatz-Bildgebung und automatisierter Bildanalyse verwendet, die wir im Laufe dieser Studie so verbessert haben, dass sie eine höhere Spezifität und Sensitivität erreicht, die nun eine Quantifizierung ähnlicher Translokationsraten wie PCR-basierte Ansätze ermöglicht. Wir konnten zeigen, dass unabhängig von der DSB-induzierenden Methode in Abwesenheit von cNHEJ mehr Translokationen gebildet werden und fanden Beweise dafür, dass der Nachweis von weniger Translokationen nach CRISPR in cNHEJ-defizienten Zellen unter Verwendung von PCR Methoden auf höhere Resektionsraten zurückzuführen sein könnte, die eine Primerbindung verhindern.

Topoisomerase 2 (Top2)-Gifte werden häufig als Chemotherapeutika eingesetzt, können aber durch spezifische Translokationen sekundäre Krebserkrankungen hervorrufen. In einem weiteren Teil dieser Studie untersuchten wir die Beteiligung verschiedener zellulärer Prozesse an der Translokationsbildung nach Verabreichung verschiedener Top2-Gifte und untersuchten Faktoren, die an der Umwandlung von „vergiftetem" Top2 in offene DSBs beteiligt sind. Dabei stellten wir fest, dass die ATPase VCP eine wichtige Rolle spielen könnte und, dass die durch verschiedene Top2-Gifte induzierte DSBs auf unterschiedlichen zellulären Prozessen beruhen.

2 Summary

Chromosomal rearrangements like translocations can directly induce cancerogenesis. They occur very rarely but can give a growth advantage, which makes the steps required for their formation difficult to study. Paradoxically, double strand break repair (DSB) machinery, which protects from effects of these detrimental lesions, is also responsible for fusing broken chromosome ends in an illegitimate manner to form rearrangements.

It is believed that simple chromosome fusions rely one of the end joining (EJ) pathways: the classical non-homologous EJ (cNHEJ) or the alternative EJ pathway. Several studies using different setups to induce translocations and to read out their frequencies concluded that translocation frequency increases in the absence of cNHEJ and that its presence protects cells from their formation. More recently, studies using TALENs and CRISPR to induce translocations and PCR-based approaches to quantify their frequencies have found, that in the absence of cNHEJ, less translocations are formed. In order to shed light on this controversy, we followed a systematic approach using isogenic human cell lines null for different EJ factors and different ways of DSB induction. In order to quantify translocation formation, we made use of a combination of fluorescence *in situ* hybridisation, high-throughput imaging and automated image analysis in interphase cells. During the course of this study, we improved this method further to yield higher specificity and sensitivity, which now allows quantification of similar rates of translocations as PCR-based approaches. We could show that independently of the DSB inducing method, more rearrangements are formed in the absence of cNHEJ and found proof that the detection of less translocations after CRISPR in cNHEJ deficient cells could be due to higher rates of resection, which prevent primer binding.

So-called Topoisomerase 2 (Top2) poisons are widely used chemotherapeutics and are known to induce secondary cancers due to the induction of poison specific translocations. In another part of this study using the before described method, we investigated the involvement of different cellular processes on translocation formation after administration of different Top2 poisons and studied factors involved in the conversion of trapped Top2 to open DSBs. We found that VCP may be an important contributor and that DSBs induced by the Top2 poisons etoposide and mitoxantrone rely on different cellular pathways.

3 Introduction

3.1 DNA double strand break repair pathways

Our genomes are constantly target of endogenous (e. g. replication or oxidative stress) and exogenous (e. g. chemical exposure or X-ray/UV irradiation) sources of genotoxic stress [1]. Fortunately, mechanisms that deal with the resulting DNA lesions have been established in the form of the DNA damage response (DDR). The DDR first detects the damage, signals the damage and then finally repairs the damage. While the DDR is active, many cellular processes are on hold until the damage is repaired or, if that is not possible, to allow a fast switch towards an (un-)programmed cell death, depending on the severity and kind of DNA damage. Furthermore, the DDR allows cells to maintain their genome stability in a precisely coordinated network of different repair pathways, again depending on the type of DNA lesion. In case of a defective DDR, genomic instability can confer a selective advantage to the damaged cell. Consistently, genetic instability is a hallmark of cancer cells and syndromes that result from a defect in DDR are associated with genomic instability often leading to a higher cancer predisposition and premature aging.

Among all types of DNA lesions (Figure 1), the DNA double-strand break (DSB) is considered the most detrimental. A persistent DSB during mitosis can lead to under-replication during S-phase, the loss of genomic information in the daughter cells, or the formation of genomic rearrangements. However, DSBs are also needed for genetic diversity in cellular processes like meiosis, V(D)J recombination and class switch recombination to allow a versatile immune response [2].
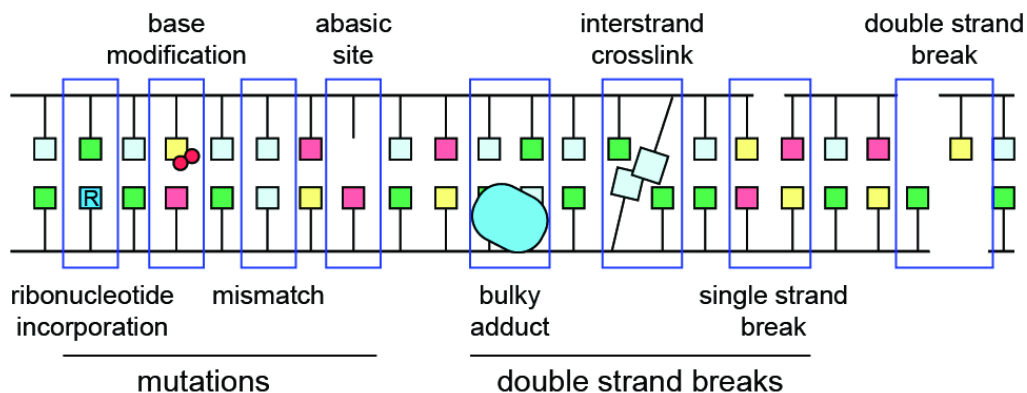
Figure 1: Different types of DNA lesions and their potential outcome. Lesions that interfere with perfect base pairing such as the incorporation of ribonucleotides, base modifications, mismatches or abasic sites, often trigger the development of mutations. Other lesions that interfere with the structure of the DNA helix, like DNA-bound proteins, inter-strand crosslinks perturb processes like replication or transcription and often lead to the formation of DSBs.

Two main pathways mediate the repair of DSBs, homologous recombination (HR) and non-homologous end-joining (NHEJ). While both pathways require end processing by nucleases, utilization of DNA polymerases and a final ligation step to finalise DNA repair, they both exhibit remarkable differences. HR on one hand uses the sister chromatid or the homolog as a template to repair DSBs and is therefore only active during S- and G2- phase of the cell cycle whereas NHEJ on the other hand is active throughout the cell cycle [3] and can in principle directly ligate broken DNA ends together. However, NHEJ may involve losing a few nucleotides at the repair junctions [2].

While some consider NHEJ to be some sort a bouquet of instruments [4], the majority of studies think of it as a compilation of different but competing pathways, which can potentially make us of the same factors. One of these NHEJ pathways is the canonical NHEJ pathway, cNHEJ, which depends on the binding of the Ku heterodimer (Ku70/80) to broken chromosome ends and the recruitment of the catalytically active subunit of DNA-PK (DNA-PKcs) to form the DNA-PK holoenzyme [5]. Direct ligation of broken DNA ends is often not possible due to end incompatibility caused by mismatching overhangs or chemical modifications at the DNA ends.

Nucleases process these mismatched or modified ends to prepare them for ligation, which often involves removing short passages of the 5' or 3' overhangs by exo- or endonucleolytic processing that can result in short regions of microhomology (≤4 nt) between the strands and can facilitate end joining [2]. Extensive end resection of more than 20 nt occurs during the initiation of homologous recombination (HR) or single-strand annealing (SSA) pathways. The presence of Ku is the main determinant to distinguish the end processing of NHEJ from other DSB repair pathways [4], but when DNA resection is required for NHEJ, DNA-PKcs is recruited in complex with the nuclease Artemis to Ku-bound DNA ends. DNA-PKcs interacts with the flexible C terminus of Ku80, undergoes autophosphorylation and activates Artemis, which then gains the ability to cut DNA ends at boundaries between single-strand and double-strand DNA (ss-dsDNA boundaries), e. g. at overhangs [6]. Artemis is a member of the metallo-β-lactamase family of nucleases and has the ability to hydrolyze DNA or RNA in various configurations [7]. In addition to 5' exonuclease activity on ssDNA, Artemis possesses a DNA-PKcs-dependent endonuclease activity on both 5' and 3' DNA overhangs at ss-dsDNA boundaries.

If the addition of additional nucleotides is required, members of the Pol X family of polymerases participate in DSB repair by NHEJ. In human cells, DNA Pol λ and Pol μ are the two members involved in NHEJ [8,9] and both have an N-terminal BRCT domain that allows them to interact with Ku [10] and can incorporate nucleotides in a template-dependent or template-independent

manner [11]. In the final step of cNHEJ, the cNHEJ ligase complex consisting of DNA ligase 4 (Lig4), Xrcc4 and XLF, ligates the ends [12,13]. The high abundance of Ku70/80 and its high affinity to DSB ends makes cNHEJ the predominantly used pathway for DSB repair [2,14].

Importantly, residual EJ activity is observed in the absence of cNHEJ factors, suggesting that there is at least one alternative way to join broken DNA ends (that is not HR) [15]. This pathway is referred to as alternative EJ (aEJ) or microhomology-mediated end joining (MMEJ) - the term MMEJ can however be confusing as cNHEJ is associated with the occurrence of microhomologies to a certain extent as well (see above).

The decision which pathway is to be used for DSB repair may likely happen in two steps [16–18]: First, a decision between cNHEJ and more extensive resection has to be made. If a DSB is not repaired fast enough by cNHEJ, the endonuclease CtIP or the MRN (Mre11/Rad50/Nbs1) complex initiate DSB end resection and homology search can begin. This in turn demands a choice between HR and aEJ. The MRN complex is important for the resection step of the HR and SSA pathways to generate extensive 3' overhangs. The intrinsic 3'$\rightarrow$5' exonuclease activity of Mre11 cannot generate 3' overhangs by acting directly on DNA ends. MRN relies on the C-terminal-binding protein interacting protein (CtIP) to stimulate MRN endonuclease activity, which allows the incision of regions further apart from the break site [4] and the 3'$\rightarrow$5' exonuclease activity can thereafter degrade DNA from the incision site towards the DSB. This process leaves behind 3' ssDNA overhangs that can further undergo long-range resection (e.g. by nucleases such as Exo1 in yeast or DNA2-BLM in human cells) and potentially has implications on the binding of Ku as Mre11 endonuclease activity occurs upstream of the Ku-bound DNA end [19,20].

Resection outcome and cell cycle phase probably play important roles in the decision between HR and aEJ when cNHEJ is not suitable for repair, as HR is restricted to S and G2 phase while aEJ can be used throughout the entire cell cycle [21]. aEJ sometimes describes all EJ activity that is present in the absence of cNHEJ factors [22].

DNA Polymerase θ (Pol θ) has been one of the factors implicated in aEJ [23] and it has been shown that a Pol θ-associated helicase function can reveal microhomologies at DNA ends by displacing RPA from ssDNA, while its polymerase function can stabilize joint ends [24]. Additional DNA polymerases eventually may thereafter be required for fill-in synthesis. In general, data suggests that Pol θ evolved to be able to repair associated DNA lesions that are not efficiently repaired via cNHEJ, e.g. certain replication-associated lesions [25–27]. The repair of DSBs by aEJ is, as for cNHEJ, completed by a DNA ligase once ligatable DNA are present. Since DNA ligase 4 (Lig4) only functions in cNHEJ, the DNA ligases encoded by the LIG1 and LIG3 genes

served as the candidate enzymes for aEJ in many studies, which these indicate that Lig3 is the major DNA ligase in the aEJ pathway [28,29]. Further proposed factors of the aEJ pathway include the end processing enzymes Mre11 and CtIP and the poly(ADP-ribose)polymerase1 (Parp1). In the nucleus, Lig3 forms a stable complex with XRCC1, a scaffold protein that interacts with several DNA repair proteins [30]. Both Lig3 and XRCC1 preferentially interact with poly(ADP-ribosylated) Parp1 and the Lig3/XRCC1 furthermore complex interacts with the MRN complex to digest and join DNA duplexes with DNA ends that were not directly ligatable by uncovering and utilizing stretches of microhomologies [31,32].

Other studies have impicated MMEJ in the formation of chromosomal translocations due to the presence of aberrant class switch recombination in cNHEJ deficient mice [33] and in some studies translocation formation was not dependent on XRCC1 [34]. Although there may be sufficient residual nuclear Lig3 activity for translocation formation in the absence of XRCC1 [35], it is also possible that in the absence of nuclear Lig3, translocation formation occurs by a Lig1-dependent pathway [36] although it remains unclear how Lig1 is recruited to the repair site.

3.2 Chromosomal rearrangements in cancer

Cancer is very frequently associated with genomic instability and in fact, genomic instability is a hallmark of human cancers and leads to genomic changes scaling from individual nucleotides variations to the gain or loss of entire chromosomes. While Theodor Boveri already postulated the causality of chromosome aberrations for cancer development in 1914 [37], the famous Philadelphia chromosome was the first genetic abnormality that could be linked to a specific cancer as early as 1960 [38,39].

Chromosomal rearrangements like deletions, insertions, inversions and translocations often play key roles in the initial steps of tumorigenesis and frequently cause haematological cancers and solid tumours [3,40]. Translocations can lead to the formation and expression of oncogenic fusion genes (e.g. *BCR-ABL*), the deregulated expression of a tumour-suppressor or oncogene (e.g. *IGH-MYC*) or to a loss-of-function mutation in a tumour-suppressor [3]. This in turn can lead to genomic instability, deregulated proliferation, or resistance to cell death, which are all further known hallmarks of cancer [40]. Both, the expression of a fusion gene, as well as the deregulated expression of an oncogene can directly initiate cancer development [41,42].

Inter-chromosomal   Intra-chromosomal
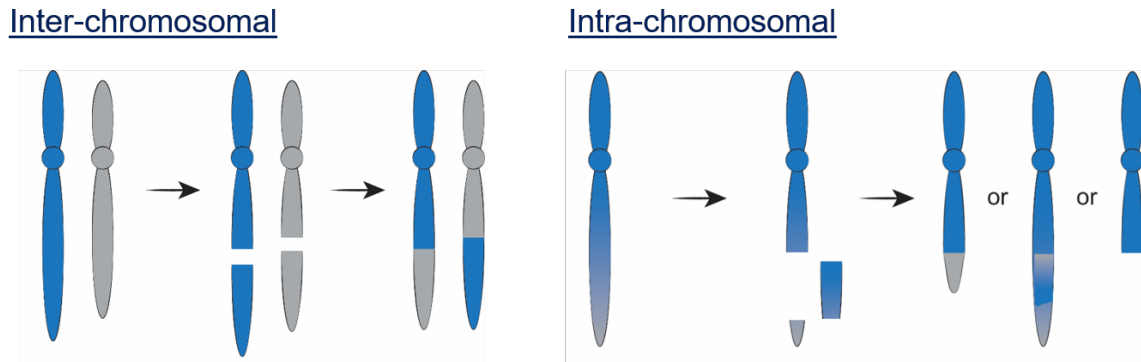
Figure 2: Different kinds of chromosomal rearrangements. Inter-chromosomal rearrangements occur as chromosome translocations. Intra-chromosomal translocations can present as deletions, inversions, insertions (not depicted) or even the partial loss of a chromosome arm.

The world's largest resource on genome alternations in human cancer, the COSMIC database (Catalogue Of Somatic Mutations In Cancer), holds information about more than 10,000 gene fusions and more than 60,000 other genome rearrangements found in human tumours [43]. *BCR-ABL* and *IGH-MYC* translocations are often found in haematological cancers whereas in thyroid cancers, inversions and translocations, such as *RET/PTC*, are frequently observed [44].

The first deletion event found to cause oncogenesis was the deletion of the *RB* locus, which causes the development of retinoblastoma [45,46] and in the 1960s, Nowell and Hungerford characterized for the first times the famous Philadelphia chromosome, a reciprocal translocation between chromosomes 9 and 21, in patients with chronic myeloid leukaemia [39]. Nevertheless, the arguments for a primary role of chromosome abnormalities in the direct causation of human tumours remained unconvincing until finally in the mid-1960s, Levan and van Steenis gave further indications that certain chromosome types tend to be more and others less frequent in human tumours [47,48]. The "non-randomness" of these changes in chromosome numbers and structure was then also demonstrated in specific types of human solid tumours and leukaemia. The invention of chromosome banding techniques in the 1970s made the studies on cancer cytogenetics more precise and stringent [49,50] and led to the development of an increasing number of various fluorescence in situ hybridization (FISH) technologies. These FISH techniques even allow the analyses of gene specific breakpoints and the investigation of their role in structural chromosome rearrangements [51,52].
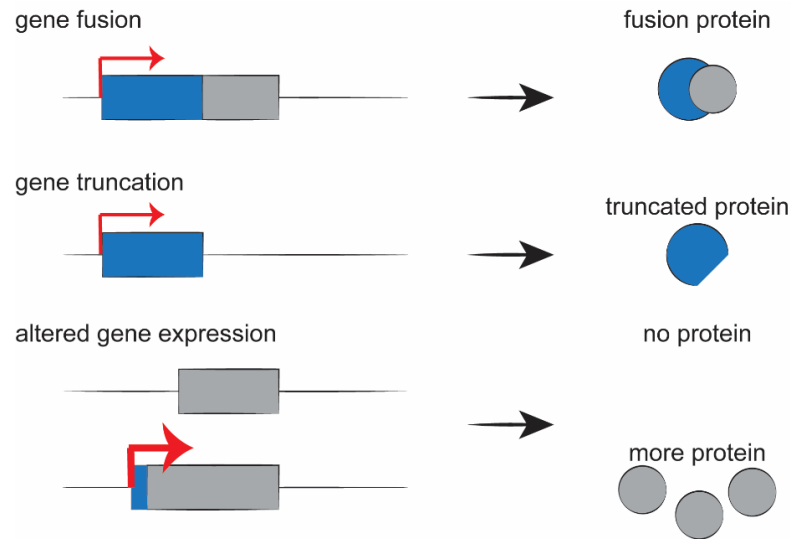
Figure 3: Chromosome rearrangements can have different outcomes and can potentially trigger cancer. If two genes are fused, this leads to the expression of a fusion protein with potentially changed regulatory behavior or response. The same is true for the expression of a truncated protein after gene truncation. In case of altered gene expression, e.g. in case of promotor swap, this can lead to altered protein expression levels.

Until the early 2000s, more than 600 recurrent cancer-associated chromosome aberrations have been identified. Interestingly, solid tumours account for less than one-third of this number. Probably because there is less information available on the cytogenetics of solid tumours as their chromosome preparation is more challenging. Additionally, in contrast to haematological tumours, solid tumours often acquired a multitude of aberrations at the time of diagnosis [53], which makes their cytogenetic characterization difficult. However, some tumour types have been studied to a depth that allows conclusions on specificity or even uniqueness of a distinct chromosomal rearrangement to a certain malignancy. This includes haematological cancers, lymphomas and mesenchymal, germ cell and epithelial tumours [53].

Interestingly, simple and disease-specific chromosome fusions dominate in leukaemia, but make up less than 1% of the studied epithelial tumours (see Figure 4 adapted from [53]). The underlying reasons for this discrepancy remain highly discussed in the field of cancer research. In acute myeloid leukaemia (AML), probably the best studied neoplastic disease, but also other leukaemia types, chromosomal rearrangements are found to be remarkably specific [42,54] and associated with distinct clinical features and gene expression profiles [55,56]. This kind of information has gained increasing importance in the development of treatment strategies for cancer patients and in the prediction of the outcome of a chosen anti-cancer therapy.

simple & disease-specific	multiple & non-specific

chronic myeloid leukaemia

acute leukaemias

malignant lymphomas

mesenchymal tumours

epithelial tumours
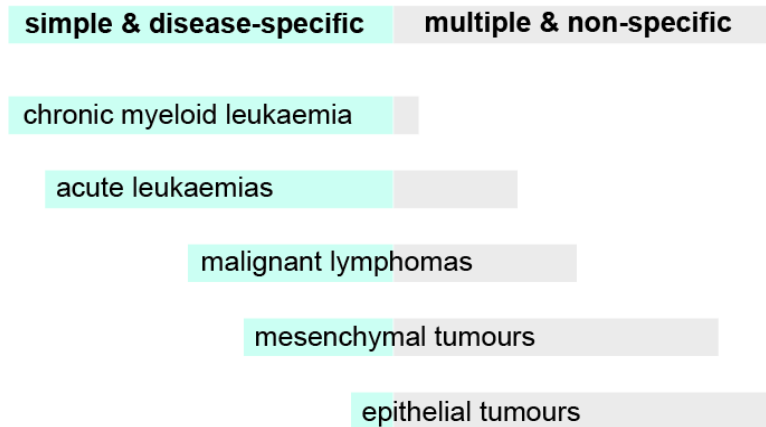
Figure 4: Distribution of different chromosome rearrangements within different malignancies (modified from [53]).

Some genes involved in fusions are found to recombine with many different partner genes; a well-known example that will appear at different points throughout this thesis, is the mixed lineage leukaemia gene (*KMT2A*, coding for the MLL1 protein) with around 50 characterized fusion partners whose fusions all trigger the development of AML [57]. Nevertheless, the prevalence of a specific gene fusion remains low, and only few of them have been found in larger groups of patients. Also, malignancies characterized by specific gene fusions represent a minority of haematological disorders [42]. Examples to be mentioned here are *BCR–ABL1* in CML, *IGH–CCND1* in mantle cell lymphoma, MYC deregulation in Burkitts lymphoma and *PML–RARA* in acute promyeloid leukaemia. In these special cases, nearly all malignancies present the same chromosomal aberration pattern.

3.3 Factors influencing the formation of chromosome rearrangements

When we think about the steps, which have to happen in order for a chromosomal rearrangement to occur, this naturally summarizes the areas, where different factors can influence their frequency.

First, a chromosome break has to occur. There are known and most likely further unknown factors, which influence a genomic region and make it more or less susceptible to breakage (see 3.3.1)

Figure 5: steps in the formation of a chromosome translocation. First, chromosomes have to break, and then the DSEs of the two chromosomes have to encounter each other in the nuclear space in order to be finally fused by DSE ligation.

Second, in order for DNA double strand ends (DSEs) to be fused in an illegitimate way, two ends have to meet in the nuclear space. Here, differ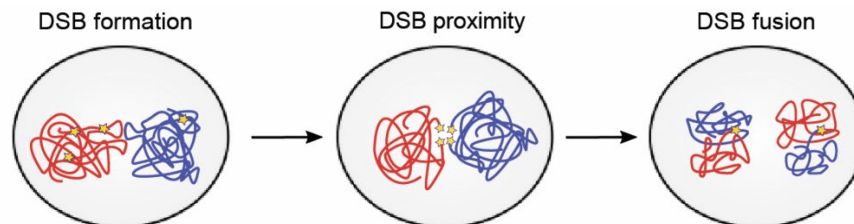ent processes are influencing the probability of this to happen. DSE mobility for example, but also the complexity of the DSE and thereby the time that it remains unrepaired. If two loci are in close proximity in the nuclear space from the start on, they will be more likely to be fused in an incorrect way (see 3.3.2).

Third, these DSEs not only have to meet, but they also have to be fused by the DSB repair machinery. Here, probably blunt ends will be fused more easily as they do not require DSE processing. Therefore, the nature and structure of DSEs most likely also plays a major role in this process (see 3.3.3).

3.3.1 Genome Fragility and DSB formation

Endogenous sources of DSBs include errors in DNA metabolism (e. g. replication across single-strand nicks and replication fork collapse), endogenous nucleases, programmed genome rearrangements (e. g. during antibody maturation, class switch recombination), physical forces, reactive oxygen species and fragile sites.

So-called fragile sites are regions in the genome that are prone to instability and breakage under different circumstances. More than 120 fragile sites have been characterized in the human genome, which are also often found rearranged in cancer [58]. Early replicating fragile sites (ERFS) are enriched in highly transcribed clusters of genes and harbour higher levels of repetitive elements and CpG dinucleotide sites, which lead to an interference between transcription and replication, in turn resulting in recurrent replication stress [1]. Common fragile sites (CFS) have also been described as replication stress-related sites of fragility and breakage and are characterized by faulty condensin loading [58,59]. Other than CFS, ERFSs are replicated early and therefore have a high probability of triggering collisions between replication and transcription intermediates [60]. Although several mechanisms seem to account for the appearance of CFS, they share some common features: CFS are enriched in stretches of AT repeats which allow for high DNA helix flexibility and the ability to form stable non-B DNA secondary structures, which may in turn inhibit or slow DNA replication [61], furthermore they are mainly found in long genes [62]. Since replication origins (ORIs) are not equally distributed along the genome, some regions that are poor in ORIs are unable to compensate for slow replication progression in case of replicative problems. This can result in cells entering mitosis with under-replicated regions. Because the replication program is cell-type specific, the position and occurrence of CFS is, other than in the case of ERFSs, cell-type specific [63]. Following S-phase, CFS may contain intertwined

sister chromatids or unresolved DNA repair intermediates which can be cleaved by nucleases, such as Mus81 and Gen1, or unwound by BLM. CFS are sequestered and shielded in 53BP1/γH2AX bodies, decorated by RPA and transmitted to the resulting daughter cells to be processed when an appropriate repair process (other than HR) is available [60,64–67]. Under normal circumstances, CFS are relatively stable, in cancer cells however, breaks and genomic rearrangements accumulate at these sites. This may be due to the accelerated rate of replication in some cancer cells [68]. More recently, it has also been discovered, that CFS are often marked by faulty condensin loading and compaction and that they coincide with mitotic DNA synthesis (MIDAS) [59]. Suggesting that, under replication stress, aberrant condensin loading leads to CFS expression, which allows for MIDAS to occur, which in turn, can result in genome fragility [59].

A study from our lab [69] showed in 2019 that DSBs occurring due to incomplete topoisomerase 2 (Top2) activity are enriched in highly transcribed genes, which are located proximal to chromatin loop anchors. Transcriptional activity as well as loop anchor proximity have been shown to influence the frequencies of Top2 mediated chromosome breaks independently [69]. Other studies have shown a similar transcription-coupled chromosome fragility and some furthermore show the dependency on chromosome architecture [70–72].

Besides transcriptional activity, also certain chromatin marks have been associated with chromosome fragility independent of transcriptional activity at the fragile loci. An enrichment of methylated H3K4 in genomic areas prone to translocate was shown in a computational analysis of chromatin features at recurrent breakpoints comparing freely accessible ChIP-seq data by comparing sets of control genes with translocating genes [73]. These areas enriched for H3K4 methylation further showed increased abundance of H3K27ac and increased DNase I hypersensitivity as a mark of open chromatin. As these chromatin marks are furthermore associated with active transcription, control genes were chosen to have the same transcriptional output. Interestingly, the increased fragility still depended on the H3 modifications. This study furthermore showed that cells overexpressing H3K4 methyl-transferases showed higher frequencies of chromosome breaks in known translocating genes after irradiation, suggesting that methylation of H3K4 predisposes genomic loci even more to chromosome breakage [73].

Intriguingly, certain DNA structures and sequence specificities can prime genomic regions to DNA lesions. For example, G-quadruplexes (G4), which consist of a stretch of guanines in a stacked structure, presumably act as roadblocks for molecular mechanisms sliding along the DNA strands such as replication and transcription [74,75]. The annealing of inverted or palindromic sequences can create cruciform structures that, when accidentally processed by resolvases like Mus81 and Slx1-Slx4, are converted to DSBs as they resemble Holliday junctions [76]. Furthermore, regions

prone to Z-DNA formation, which can form in GC-rich regions during transcription, have been identified next to breakpoint junctions and seem to play a role in DNA fragility [77,78].

3.3.2   DSB proximity

It only seems logic, that loci, which are more mobile or in closer proximity to each other, show an increased probability of forming a chromosome rearrangement. The proof for this has however been difficult. The recent rapid developments in NGS techniques have allowed exploring this hypothesis further in the last couple of years and it has been shown using an NGS-based translocation capture technique (HTGTS: high-throughput genome-wide translocation sequencing [62]) that intra- and inter-chromosomal rearrangements correlate with Hi-C contact probability [79]. Before these recent advances, most studies relied on live cell imaging to study spatial movement and clustering of DSBs [80].

Previously, there were indications in yeast that loci proximity does not pre-dispose DSBs to translocate. Here, it has been shown that there is no correlation between pre-damage contact frequency of DSB loci as predicted by chromatin crosslinking and translocation frequency mediated specifically by NHEJ [81]. These results were distinct from earlier studies in yeast where proximity always showed a strong influence on HR mediated gene conversion [82,83]. Other studies suggest that DSBs follow a Brownian motion model during homology search [84] but interestingly, DSBs have been observed to cluster over time in yeast and also in mammals [67,85]. This has however mainly been shown for DSBs that rely on repair via HR and not NHEJ. Importantly, DNA damage increases the chromosome mobility of both damaged and undamaged loci overall [86] and in yeast damaged chromatin explores nuclear space more efficiently than undamaged chromatin [87]. However, the question remains how DSBs move throughout the nucleus.
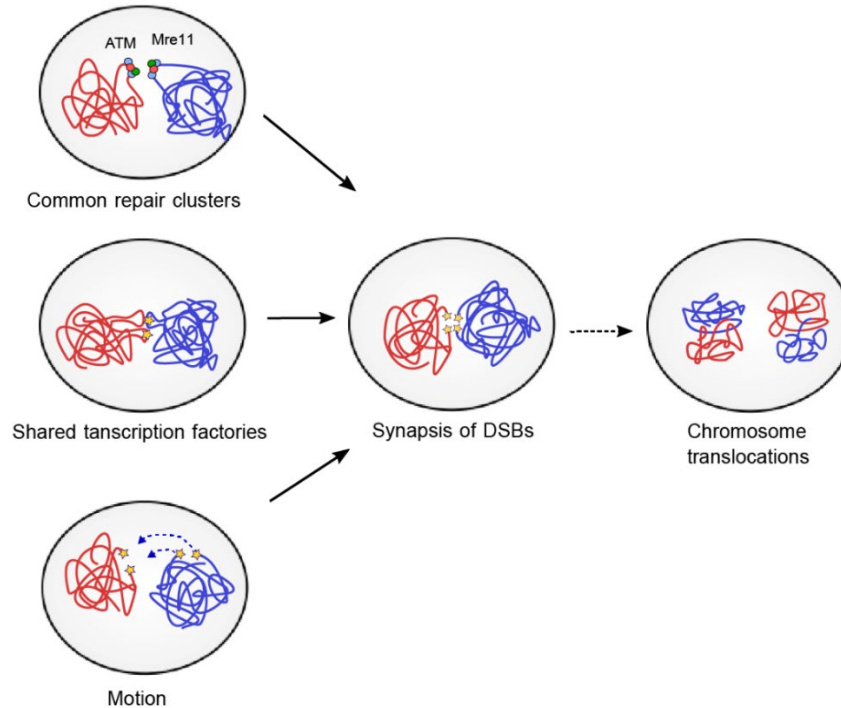
Figure 6: Factors influencing proximity of DSBs. DSBs that need to be repaired by HR are often found to cluster during G1-phase of the cell cycle until cells enter S-phase and the sister-chromatid is available as repair template. loci that share transcription factories are also clustering together and more mobile loci/DSBs also increase the probability for two DSBs to be proximal in the nuclear space. All these factors increase the probability for DSBs to meet in the nuclear space and to synapse. It does not necessarily mean that the DSB repair machinery fuses them (from [88]).

To find out more about the nature of DSB motion and movement, many hypotheses have been tested. The simplest one would be that they move randomly following Brownian motion. This would however mean that they are repaired equally as frequent with the proper DSE in *cis* as they are fused to an improper DSE in *trans* and this is not what has been observed in experiments [81,89] where DSBs are by far more frequently repaired in a *cis* way. Here, the possibility remains that DSBs are rapidly repaired in *cis* and only if they remain unrepaired, they can undergo random movement. A possibility would be that they move as tethered DSEs, thereby maintaining the preference for *cis* repair while still being able to move. This model has in fact become the working model in the field and tethering of DSEs has been proven several times [3,80]. Here, encounter of two DSBs would be random and transient and the probability of *trans* repair (so the formation of a translocation) would be limited.
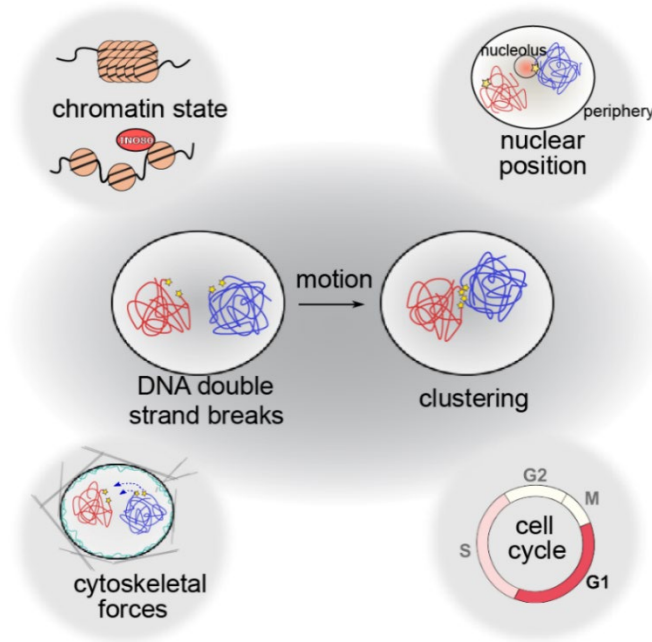
Figure 7: Factors influencing DSB mobility and motion. Certain chromatin signatures have been shown to influence the motion of a DSB as well as the spatial position of a DSB in the nucleus and the cell cycle state. More recently, also cytoskeletal forces have been described to influence and even facilitate the motion of DSBs. (adapted from [88])

An alternative to random motion of DSEs could be that their movement is directed - and recent reports have suggested the existence of this directed motion during DNA repair and imply the involvement of F-Actin and nuclear myosins [90]. While nuclear Actin itself interacts directly with DDR proteins and histone modifiers [91], it has been shown that myosins (myosin I and myosin V in *D. melanogaster* and myosin II in human cells) can move DSBs to the nuclear periphery along nuclear actin filaments, which are induced upon DNA damage [90,92]. Combined with an intrinsic attraction towards each other, this could also be the mechanism of DSB clustering, which would therefore follow a partially active and directed motion perhaps driven by phase separation of DSB repair assemblies [93,94]. What really determines the frequency of DSB encounters in the nucleus remains to be determined; but it probably involves several processes.

3.3.3 DSB fusion

As the formation of a translocation requires the fusion of two broken chromosomes, the DNA repair machinery, which prevents the formation of translocations by rapidly repairing lesions, is, paradoxically, also a key player in the formation of any chromosome translocation or other rearragengments [3]. It is therefore a demanding question whether distinct pathways that mediate DSB repair or specific proteins of the repair machinery influence the frequency of translocations.

It has been shown that HR-mediated strand invasion or HR-mediated break-induced replication can copy a part of a homologous sequence and can thereby for example transfer a stop codon from a (pseudo-)gene to a homeologous but coding sequence, resulting in its loss of function. Furthermore, crossovers between repetitive sequences can result in genomic rearrangements such as translocations, deletions, amplifications and inversions [95,96]. In addition, in cancer cells, 50% of recurrent deletions are localized in CFS associated with large genes, indicating an involvement of replication-transcription conflicts and thereby potentially HR [62,97].

It has however, already been demonstrated that homologous recombination does not contribute to translocation formation between heterologous sequences [98] and furthermore, sequence analysis of translocation junctions derived from patients shows characteristics of NHEJ [99]. Most studies analysing the formation of translocations and identifying involved factors have been performed in mouse lymphoid cells upon programmed DSBs during antibody diversification or mouse embryonic stem cells using site specific endonucleases or zinc finger nucleases [34,36,100]. These studies demonstrate higher translocation frequencies in the absence of cNHEJ factors, concluding that the cNHEJ pathway in mouse cells suppresses translocations. Furthermore, in the absence of factors involved in the aEJ pathway a decrease in translocation frequency and in microhomology usage was observed [36,100]. This suggests that in mouse cells, translocations typically arise by aEJ. In contrast to that, a recent study using TALENs and CRISPR/Cas9 to induce DSBs in human cell lines states a decrease in translocation frequency in the absence of the cNHEJ factor Lig4; proposing that in human cells, translocations are generated by cNHEJ [101]. Taken together, the current model of how the different repair pathways contribute to the formation of translocations suggests a species-specific dependency on the different EJ pathways.

In general, detecting and quantifying oncogenic translocations has been difficult as they occur rarely and then often undergo a positive selection throughout tumorigenesis. Therefore, translocation frequencies have mainly been studied using population-based methods like different PCR approaches. DSBs were most commonly induced by site specific endonucleases (e. g. ISceI), zinc finger or TALEN nucleases and lately CRISPR/Cas9 [36,80,102]. However, these types of breaks are far from physiological and their induced breaks present different DSB features, which may therefore account for some of the observed discrepancies between studies. Different number and complexity of DSBs may account for different necessities of end-processing and repair time and may even involve the use of distinct repair pathways [103]. In our lab, we have recently established a methodology that is able to detect rare translocation events between recurrent translocation partners frequently found in patients on a single-cell level. We use FISH in

interphase cells in combination with high-throughput imaging. This allows the quantification of translocations in frequencies as low as 10^{-3} to 10^{-4} on a single cell level. In addition, this methodology does not require the knowledge of the exact breakpoint and is therefore compatible with different ways of DSB induction, such as site-specific endonucleases, but also ionizing radiation or chemotherapeutic drugs.

3.4 Top2-poison induced chromosome rearrangements

Due to the highly compacted nature of the chromosomal content, every mechanism and machinery that acts on the DNA or slides along the double helix, has an impact on its structure [69,71,104]. Replication and transcription machinery e. g. have been shown to lead to super-coiling of the helix ahead of them and that they in turn leave behind a trail of under-wound DNA (positive vs. negative super-coiling) [69,105]. This kind of torsional stress can lead to the disruption of chromosome integrity if it is not properly resolved. Topoisomerases are enzymes, which can release this torsional stress by breaking and re-ligation of the DNA backbone.

Type I topoisomerases work as monomers and induce a SSB during their catalytic cycle and come in two flavours in humans: type IA enzymes (human Top3) covalently bind via a phospho-tyrosine linkage to the 5' end of the DNA, whereas type IB enzymes (human Top1) covalently bind to the 3' end of the DNA (also via a phospho-tyrosine bond) [106].

Type II topoisomerases (Top2A and Top2B in humans) act as homo-dimers and cleave both strands of DNA in a single reaction that can involve ATP-binding and -hydrolysis [106,107]. After cleaving one DNA duplex, a second duplex is transported through the DSB that the homo-dimer initiated and covers. The cleaved double strand is finally re-ligated. In order to cleave the first DNA duplex, a pair of tyrosine residues in the catalytic centre of Top2 attacks the opposite strands of the DNA helix and covalently binds to the DNA through a 5'-phosphotyrosine link ("Top2 covalent/cleavage complex", Top2cc; see Figure 8).
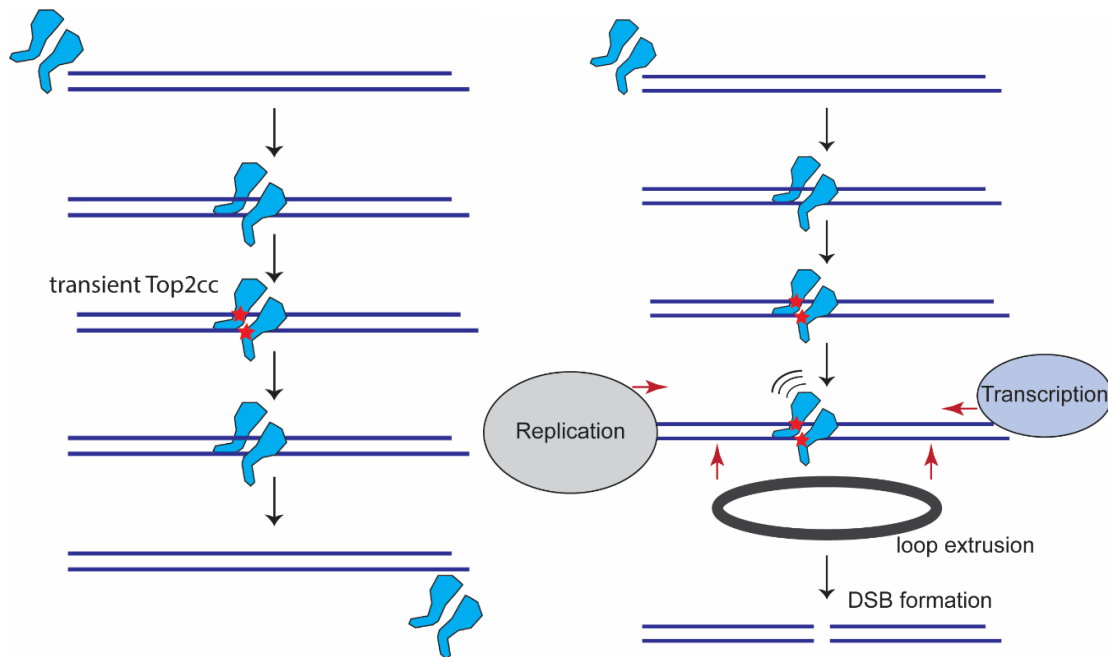
Figure 8: Top2 action and mechanisms of Top2cc to DSB conversion. Left: Catalytic cycle of Top2s. **Right:** Conversion of transient Top2cc to DSBs after encounter with transcription or replication machinery or during loop extrusion.

The process of letting one DNA helix pass while another one is being held open is also an essential process during mitosis as it ensures the de-catenation of sister chromatids which may be necessary when two replication forks converge at the end of DNA replication and the daughter molecules are intertwined [108]. To account for this increased need of type II topoisomerases, also type II topoisomerases like type I topoisomerases come in two flavours in eukaryotic cells. Top2A is only found in proliferating cell types and is expressed almost exclusively in G2- and M phase of the cell cycle, whereas Top2B is active in all cell types and during all cell cycle stages [109].

3.4.1 Regulation and repair of Top2ccs

If Top2ccs do not resolve but persist and are thereafter not repaired, this can lead to the formation of an open DSB, which poses a threat to the genomic integrity. In fact, chromosome translocations resulting from persistent Top2ccs (e. g. through a Top2 poison like etoposide) often lead to leukaemia and it is estimated that up to 3% of patients, who receive the Top2 poison etoposide as chemotherapy, will develop acute myeloid leukaemia (AML → therapy-related AML, tAML), which, are driven by translocations within the *MLL* gene (see 3.4.2).

How Top2ccs are converted into DSBs, is not entirely clear. It has been shown, that encounters with replication or transcription machinery and trapped Top2 can induce the proteasomal

degradation of the protein part of this DNA-protein crosslink (DPC), thereby revealing an open DSB (Figure 8 [110]). Since it has been found that Top2-dependent fragile sites are also located at chromatin loop anchors, it is proposed that loop extrusion induces a similar mechanism [69,111]. Since the consequences of unrepaired or incorrectly repaired Top2ccs are rather detrimental to genome integrity, cells have evolved several, at least partially redundant pathways to protect the genome by facilitating faithful removal of Top2ccs. Some of these pathways are specific for Top2ccs; other pathways are more diverse and work on different kinds of DPCs.

The most prominent Top2cc specific repair enzyme is the 5′ Tyrosyl-DNA phosphodiesterase 2 (Tdp2) [105,112,113]. Tdp2 consists of an amino-terminal Ubiquitin binding UBA domain and a carboxyl-terminal catalytic domain that presumably exerts endo- and exonuclease activity [114]. Tdp2 can efficiently hydrolyse the 5′-Y DNA bond within Top2ccs and 3'-Y bonds like that of Top1ccs but with a lower efficiency [115,116]. It has also been shown that Tdp2 activity is accelerated on free phosphotyrosyl-modified ends as compared to intact, bulky Top2ccs [117]. Whether Tdp2 can recognize the shielded 5'-Y bond of intact Top2ccs is not clear but it is likely that remodelling of the DPC is necessary to initiate repair, which makes the remodelling process an import regulatory step in Top2cc repair.

A recently discovered way of initiating remodelling works via the E3 SUMO2 (Small Ubiquitin-like Modifier 2) ligase ZATT (Zinc-finger Associated with Top2 and Tdp2, formerly known as ZNF451) [118]. The same study that found the function of ZATT on Top2ccs also found that Tdp2 harbours a non-canonical, split SIM (Sumo Interacting Motif) in its catalytic domain [118] and suggested that Tdp2 activity also depends on SUMOylation of Top2ccs. Furthermore, it showed a delayed turnover of SUMO2-modified Top2ccs in *TDP2*-/- cells, when the proteasome was inhibited, which suggests the implication of an additional proteasomal degradation step of the protein part of the DPC [118].

VCP (Valosin containing protein) or p97 is a well-studied ATPase from the AAA+ family of ATPases (ATPase associated with multiple cellular activities). Six monomers form a homohexameric ring structure; each monomer consists of two ATPase domains and an N-terminal domain via which VCP can interact with multiple cofactors [119,120]. This variability enables VCP to be involved in various cellular processes that usually involve the recognition of ubiquitinated substrates, which are remodelled (using energy from ATP hydrolysis) and segregated from their surroundings, making these substrates accessible to the 26S proteasome and promoting their proteasomal degradation. Nevertheless, not all processes VCP is involved in, lead to the proteasomal degradation of the substrate - it is rather thought to have a chaperone like function

and regulate complexes and their activity by segregating components from each other [120] which is also why it is often referred to being a segregase.
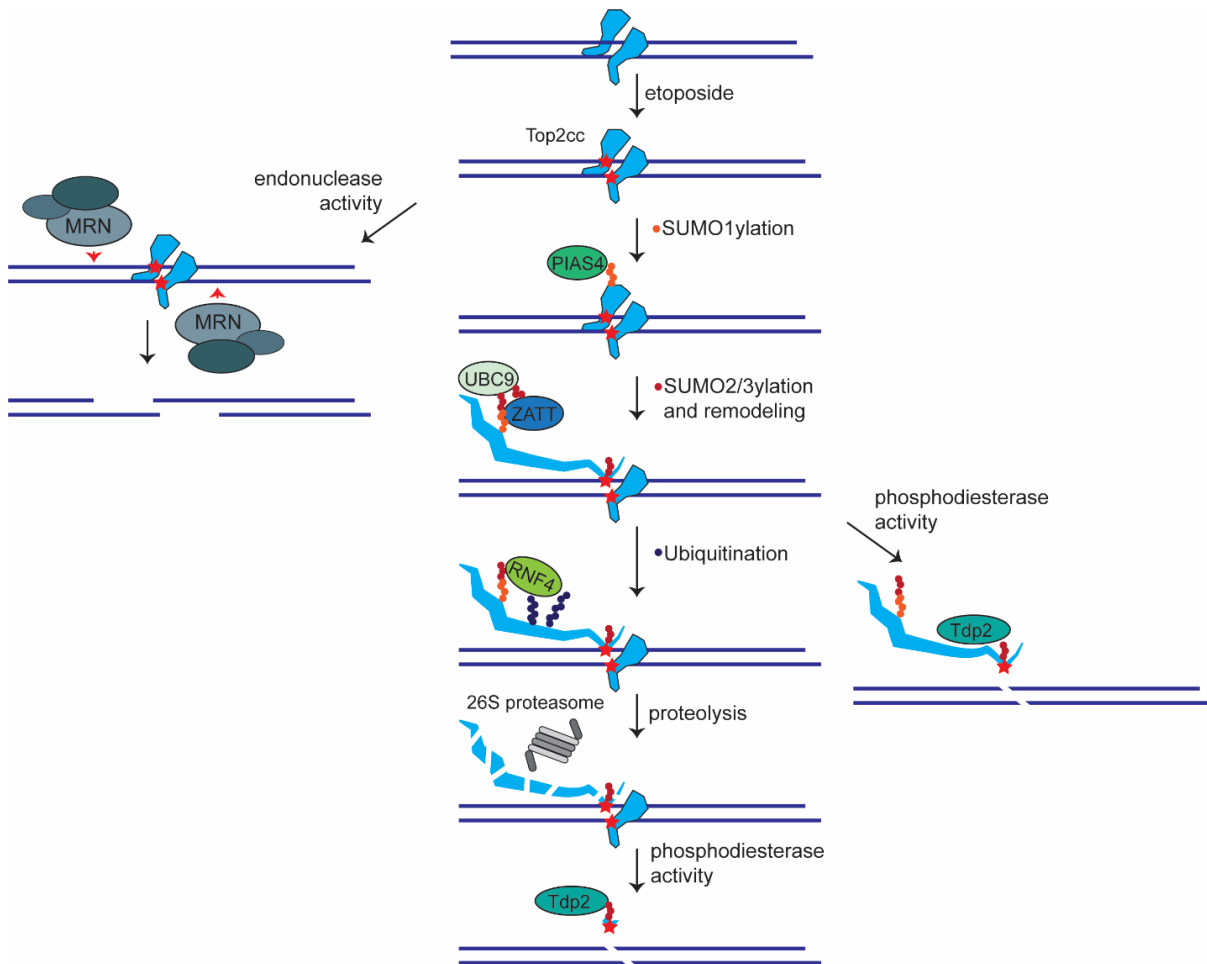

Figure 9: Repair and resolution of Top2ccs. In case a Top2cc persists e.g. because of administration of the Top2 poison etoposide, the DPC can be resolved via different mechanisms involving the MRN complex, the phosphodiesterase Tdp2 and/or the 26S proteasome.

It is proposed that mammalian orthologue VCP mainly acts in one of three core complexes which then determine substrate recognition. Binding of the co-factor p47 to VCP is required for post-mitotic fusion of Golgi membranes and the transitional endoplasmic reticulum (ER). The VCP-Ufd1-Npl4 complex is known to be involved in ER associated degradation (ERAD) and, at least in budding yeast (p97-Ufd1-Npl4), recognizes ubiquitinated as well as sumoylated substrates [121].

Monoubiquitinated substrates and alternative VCP-cofactors, including UBXD1, have been associated with endosomal trafficking and autophagy [120,122]. VCPs function during mitosis where it regulates spindle dynamics, makes the loss of VCP lethal [121].

24

SUMO2/3 modification of Top2ccs is probably mediated via SUMO1ylation through the SUMO1 ligase PIAS4 and triggers ubiquitylation via RNF4, a SUMO-targeted ubiquitin ligase (STUbL) [123]. Since the E2 SUMO2/3 enzyme UBC9 has been shown to be important for Top2cc SUMOylation in mitosis, where it acts together with PIAS4, it may also be the E2 enzyme needed for the signalling of Top2ccs in interphase cells [124].

3.4.2 Top2 poisons in chemotherapy and therapy-related chromosome translocations

There are two ways how Top2 action can be influenced by chemical inhibition. First of all, the binding of ATP can be inhibited, thereby slowing the catalytic reaction of breaking, transition and re-ligation of the DNA helix. This is achieved by administering ATP competitive inhibitors. Second, there are Top2 poisons. Top2 poisons inhibit the re-ligation step of the Top2 catalytic cycle and Top2ccs accumulate. Some Top2 poisons like mitoxantrone intercalate in the DNA and do not allow relegation of the DSEs by changing the structure of the DNA helix. Etoposide and doxorubicin e. g. probably act on the enzyme directly and block re-ligation by a different mechanism [105,125].

Top2 poisons can be from exogenous but also endogenous sources. Endogenous Top2 poisons include abasic sites, ribonucleotides that are accidentally introduced to the DNA during replication or repair and bulky adducts like alkylated bases. Besides being used as therapeutics, exogenous Top2 poisons can be found in our food or in the environment [114]. It is long known, that the treatment of cells with Top2 poisons leads to the induction of apoptosis [126] and there are also some reports of etoposide-induced autophagy whose inhibition potentiates etoposide-induced apoptosis [127], highlighting the presence of a cross-talk between the different cellular survival and programmed death mechanisms [128]. The potent mechanism of Top2 poison induced cell death through apoptosis has made Top2 poisons widely used drugs in anti-cancer therapies.

Nowadays, we often consider cancer to be a chronic genetic disease and the survival of patients steadily improves due to advancements in diagnostics and therapy. However, experience over time has revealed that surviving patients are facing a risk of new cancer diagnosis. This in turn increased the awareness of secondary cancers, which are malignancies that do not originate from a primary cancer or its metastases, but are a consequence of the treatment of the primary malignancy [129]. It is estimated that ~18 % of cancer incidents are secondary cancers and some of those have been clearly identified to result from cancer treatments [130]. Secondary, therapy-related cancers are associated with specific treatments that patients received, such as radiotherapy or chemotherapy, which are moderately carcinogenic themselves as they damage

the genomes of tumour cells. Clinicians and researchers thus became increasingly aware of the consequences that specific cancer therapies can have on patients.

Also the treatment of cancer patients with Top2 poisons can lead to the development of new malignancies directly caused by the treatment [57,131,132]. The therapy related cancers after Top2 poison treatment share certain features: They induce chromosomal aberrations in specific hotspots in the genome, which are often the only gross aberration that is present in these cancers, they show a high mortality rate and a rather short latency after the initial treatment [132]. Interestingly, Top2 poisons create DSBs *in vitro* that map to translocation break points *in vivo* [57,131].

In the following paragraphs, the current knowledge of two Top2 poisons and their involvement in therapy-related malignancies will be described: Etoposide and mitoxantrone, which interestingly do not lead to the same chromosomal aberration.

3.4.2.1 Etoposide induces *MLL* translocations causing t-AML

The mixed lineage leukaemia gene *KMT2A* or *MLL*, coding for the transcription factor MLL1, lies on chromosome 11q23. It is a well-described model for the study of translocation induction in leukaemia after treatment with topoisomerase inhibitors. MLL1 is a methyl-transferase with a role in the regulation of haematopoiesis and the dysregulation of this mechanism leads to the development of leukaemia.
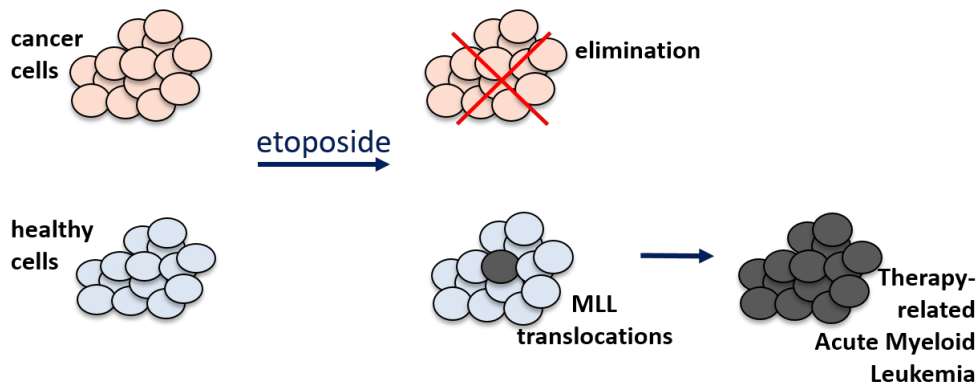

Figure 10: How secondary cancers develop. Cancer therapy (here etoposide) eliminates cancer cells. However, since it also harms healthy cells genomes, they may acquire mutations or rearrangements with oncogenic potential (here *MLL* translocation) which can drive a secondary malignancy (here t-AML).

The demonstration that etoposide can potently induce *MLL* rearrangements in cultured haematopoietic progenitor cells gave the direct link between etoposide exposure and *MLL* translocation [133]. In 2013, a study of t-AML patients with *MLL* translocations found 121 different

MLL rearrangements and characterized 79 translocating partner genes. Interestingly, the vast majority of *MLL* rearrangements (90%) happens between *MLL* and *AF4*, *AF9* or *ENL* and all translocations studied demonstrated deletion of the 3′ part of *MLL* [134]. The residual 5′ part of *MLL* always remained in frame, suggesting that it is important for the transforming potential and that the fusion gene codes for a protein with dominant carcinogenic properties. And indeed, it has been shown that translocated *MLL* has transforming properties in knock-in overexpression experiments of a *MLL*-fusion protein in mice in combination with mutagen treatment [135].

Analysis of the *MLL* break and fusion points in AML shows a high site specificity especially for the fusions that arise after etoposide treatment. Chromosomal breakpoints that result in fusion events of *MLL* lie in a region between exon 8 and exon 12 (referred to as breakpoint cluster region (BCR)) which spans approximately 8 kb [136] with *de novo* leukemic *MLL* breakpoints mapping to the whole BCR whereas the ones inducing t-AML, cluster near exon 12 [132].

3.4.2.2   Mitoxantrone induces *PML-RARA* translocations causing t-PML

The most prominent form of t-AML is therapy-related acute promyelocytic leukaemia (t-APL) [137] which is characterized by the occurrence of a balanced chromosomal translocation between chromosomes 15 and 17 (t(15;17)(q22;q21)). This translocation leads to the expression of a chimeric protein by fusing the genes coding for retinoic acid receptor α (Rarα, *RARA*) and the tumor suppressor promyelocytic leukaemia (Pml, *PML*). Pml has been implicated in a variety of physiological processes including tumour suppression and apoptosis, Rarα is an important mediator for transcription of genes involved in granulocytic differentiation [138]. In APL, the cancerogenic potential does not lie in a loss of function of one of the proteins but rather in a dominant negative effect of the fusion protein itself. The expression of the Pml-Rarα chimeric protein does not allow myeloid precursor cells to differentiate, leading to the evasion of functioning granulocytic cells from blood and bone marrow thereby causing APL [137,139]. Since the initial discovery that the chimeric protein was indicative of APL, four other translocations, all involving *RARA*, were reported in rarer cases of APL, indicating that disruption of Rarα's function leads to the pathogenesis of APL [137]. T-APL induced by Pml-Rarα expression has luckily shown a remarkable response to treatment with all-trans retinoic acid (ATRA) and novel agents such as arsenic trioxide even before the molecular cause of APL was known, but some other fusion proteins remain resistant to ATRA treatment [137,140].

The Top2 poison mitoxantrone has been used for decades mainly to treat primary breast cancer, lymphoma and AML but more recently also in multiple sclerosis (MS) therapy. It intercalates

between DNA bases and thereby stabilizes the Top2cc [141]. Since MS patients do not show any common defects in DNA repair pathways [142,143], mitoxantrone-induced leukaemia are considered to exclusively rely on the formation of Top2ccs [143–145]. A role for Top2 in causing t(15;17) was first based on the observation that an increased use of mitoxantrone in breast cancer therapy was accompanied by an increased frequency of t-APL in patients receiving mitoxantrone [138]. It was reported that breakpoints in t-APL cases after mitoxantrone treatment as breast cancer therapy were found to be limited to an 8bp region of *PML* intron 6 [146]. In *in vitro* cleavage assays, this hotspot was found to correspond to a preferential site of mitoxantrone-induced Top2a-dependent cleavage at *PML* nucleotide position 1484 [131,146]. Interestingly, the induced breakpoints in *PML* and *RARA* depend on the applied Top2 poison as indicated by the finding that in one patient, *PML-RARA* translocations induced by a combination of doxorubicin and etoposide show a different translocation breakpoint as they show after mitoxantrone treatment in the other cases this study investigated [146]. Shared *RARA* breakpoints (nucleotide positions 11569–71 and 14446–49) in patients who received mitoxantrone treatment were identified within a 17kb region in *RARA* intron 2 [144]. The precise mechanisms underlying the formation of *PML-RARA* translocations upon treatment with the Top2 poison mitoxantrone and especially the mechanisms how different Top2 poisons trigger the formation of different but presumably, specific chromosomal rearrangements remain to be determined.

3.5 Methodologies available to study chromosomal rearrangements

The rare occurrence of chromosomal rearrangements paired with their oncogenic potential, makes it difficult to study their formation and the underlying mechanisms. To detect chromosome rearrangement, different tools have been developed and used in the past years. Since every methodology has certain disadvantages and advantages compared to others, the choice of method to study rearrangements depends on the research question and experimental system.

To test patient tumour samples for fusions, low throughput methods can be applied as the frequency of the fusion within the sample is usually already high due to the shared clonal origin. In case that information about the genetic sequence is required or desired, whole genome sequencing techniques are applied, which can detect chromosome rearrangements in an unbiased way at a high resolution and additionally provide information about the exact underlying sequence changes. In both cases, translocations are already present in a cell population. To study the biogenesis of chromosome translocations however, techniques with high sensitivity are required.

One of the longest used techniques is the detection of fusion genes or transcripts via amplification in PCR, which can detect specific chromosome rearrangements on a molecular level. In order to do so, primers have to flank the expected fusion junction on DNA or mRNA level. To obtain information about the frequency of a specific translocation in a population of cells, the serial dilution of input genomic DNA can give an estimate [36,147]. The translocation frequency of *NPM1* with *ALK* (t(2;5)(p23;q35)) upon induction of DSBs within *NPM1* and *ALK* using TALENs was for example found to be as low as 1 in 1000 by 96-well fusion screening and by serial dilution PCRs of genomic DNA [148]. More precise is the use of quantitative PCR approaches such as reverse transcription quantitative PCR (RT-qPCR) or digital droplet PCR (ddPCR, discussed later) [147,149,150]. PCR-based techniques are sensitive and precise and can yield information about the genomic sequence surrounding the fusion, but importantly they require the exact knowledge of the fusion junction in order for proper primer binding and assay design.

An inverse PCR can partially overcome this limitation if at least one fusion site is known. It can be used to detect translocation partners of the known site in a unbiased way but does not yield information about the frequency of the different fusions [151]. Another unbiased approach towards the genome-wide detection of fusion partners is based on linear amplification and combines it with high-throughput genome-wide sequencing [152]. Linear-amplification mediated high-throughput genome-wide sequencing (LAM-HTGTS) uses PCR amplification of fusions with a "bait" DSE combined with the detection of fusion partners by next generation sequencing (NGS). Sequences that are fused to the bait ("prey") are amplified, sequenced and thereby identified. Like PCR approaches, LAM-HTGTS is very sensitive and can detect rare fusions but it is still limited due to the requirement of a specific DSE as bait. Due to the fast evolving temper of high-throughput sequencing techniques, approaches where neither one of the fusion partners has to be known, will probably soon become available for translocation detection but also their quantification.

Besides nucleic-acid-based approaches for translocation detection, the before-mentioned imaging techniques involving FISH and chromosome banding are still used in the clinics for diagnostics but also to study chromosomal rearrangement and their underlying mechanisms.

A more advanced way to image chromosome breaks by microscopy is to tether fluorescently labelled proteins to two sites of an artificially introduced site of enzymatic cleavage [80], which gives the advantage of being able to study loci movement and dynamics or the dynamics of DSB repair but remains an artificially introduced system.

3.6 Aims

Chromosome translocations are drivers of oncogenesis. Yet, mechanistic insights of their biogenesis remains uncertain in large parts. In order to find the mechanisms underlying the formation of chromosome rearrangements, we set out during my PhD studies to assess:

3.6.1 How can we improve detection and quantification of chromosome rearrangements by interphase FISH in combination with high-throughput microscopy and automated image analysis?

Due to their rareness, the mechanisms underlying the formation of genome rearrangements are difficult to study. In order to have methods available to detect and quantify rearrangements in a population of interphase cells, we slightly changed an assay described before [153] where FISH is performed using differently coloured probes labelling regions of the genome where chromosomes are expected to break. This method can be used independently of the DSB inducing agent to be studied and can be performed in a high throughput manner including automated, unbiased image analysis. My main goals here were to find out if the frequencies of chromosome rearrangements that we obtain with this new methodology are comparable to frequencies obtained with a newly established ddPCR approach for the direct quantification of chromosomal rearrangements, and to improve specificity as well as sensitivity of the image analysis pipeline following image acquisition. The improved methodology is called qCRI-3D.

3.6.2 Which EJ pathway fuses broken chromosomes? Are there differences depending on the type of DNA damage or the specific rearrangement that we look at?

The field of translocation research has encountered a discrepancy in the last years: Previously, it seemed to be clear that the rapid action of cNHEJ protects cells from translocation formation [36,100,154,155]. More recently however, contradictory findings have accumulated, suggesting that cNHEJ is the pathway responsible for translocation formation [80,101,156] - possibly specifically in human cells. In order to shed light onto this discrepancy, we followed a strategic approach and used qCRI-3D to study changes of chromosome translocation frequency in human cells null for factors from either cNHEJ or aEJ. qCRI-3D also allows to use different kinds of DNA damage with varying amounts and nature of DSBs and compare the results in the same isogenic cell lines to investigate the influence of DSB nature on the reliance on different repair mechanisms.

3.6.3 Why does etoposide favour *MLL* translocations while mitoxantrone favours translocations between *PML* and *RARA*?

While mitoxantrone and etoposide are both considered Top2 poisons, are both widely used in clinics as therapies and have been shown to trap Top2 on DNA and prevent the relegation of the Top2-induced DSB as well, they seem to induce different chromosomal rearrangements. In clinics, treatment of patients with etoposide comes with an up to 5% risk of developing chromosomal translocations involving the *MLL* gene whereas mitoxantrone treatment triggers the development of *PML-RARA* translocations. During my PhD studies, we set out to investigate why these Top2 poisons show the specificity for one or the other rearrangement and explore initial hints towards where the difference in outcome between treatments with one or the other Top2 poison could result from.

3.6.4 Which role does the Ubiquitin-proteasome system play in the resolution and conversion of Top2ccs to DSBs?

So far, the conversion of Top2ccs to DSBs remains poorly understood. It is known that the protein-part of Top2ccs can be degraded by proteolysis, involving the proteasome and/or specific metalloproteases (such as SPRTN) [71,123,157]. How a cell senses a Top2cc that is not in the regular intermittent state of the catalytic cycle but is stuck on the DNA, how the cell signals the poised Top2 and if Top2cc-to-DSB-conversion is a wanted or unwanted outcome of this process is largely unclear. More recently, it has been shown that trapped Top2 becomes decorated with SUMO and Ubiquitin chains, which may then trigger proteolytic processing. Moreover, since the AAA+ ATPase VCP has often been shown to act upstream of the 26S proteasome also in nuclear processes [119,158], we wanted to explore the possible involvement of VCP in Top2cc remodelling or extraction from the DNA.

4 Results

4.1 Optimizing a FISH-based high-throughput imaging approach to study the formation of chromosome rearrangements

In order to be able to study mechanisms involved in translocation formation, the methodology of choice has to be very sensitive, as they occur rarely. Therefore, high-throughput approaches are a good choice. For my PhD studies, we decided to employ a methodology that combines FISH in interphase cells with high-throughput imaging and unbiased automated image-analysis. We adapted a previously described approach [153] where FISH probes are designed to bind to flanking regions of potential or expected breakage. The FISH probes on both sides of the regions of interest are labelled with different fluorescent dyes and can thereby be discriminated using a fluorescence microscope. Under unperturbed conditions, the two spots resulting from the fluorescently labelled probes on both sides of a region of interest are very close or overlapping. If a DSB occurs between them and the two DSE separate in the nuclear space, this can be detected by image analysis as the spatial distance between the spots changes.

By implementing a fourth fluorescently labelled FISH probe and the possibility of a 3D analysis of the distance between the fluorescently labelled spots (see Figure Results 1, work done by H. J. Gothe & O. Drechsel) we are able to efficiently detect 1 in 10,000 cells that harbours a specific chromosome rearrangement and can finally investigate the mechanisms underlying genome rearrangement formation. We named this improved methodology qCRI-3D, short for quantitative chromosome rearrangement imaging in 3D. In qCRI-3D Alexa488- and Alexa568-labelled FISH probes label the two ends of one breakpoint and Alexa647- and CF405S-labelled probes the other one. These probe pairs are referred to as "break-apart-probes" as they separate if a DSB occurs in the region between them. Break-apart-probes usually bind 50 – 200kBp apart on a genomic scale, which results in an average spatial distance of approximately 1.2-1.4µm.

After high-throughput image acquisition in 3D on an Opera Phenix HCS system (PerkinElmer), the Harmony software (PerkinElmer) can segment the images for nuclei and within these nuclei, the differently coloured spots resulting from the differently labelled FISH probes can be detected. The software calculates the Euclidean spot-to-spot distances between the differently coloured spots (i.e. the spot maxima) in 3D thanks to custom-built integrated analysis blocks. Depending on the kind of assay, between 500 and 10,000 nuclei are analysed and while we started using coverslips for the FISH assay, we later went on to multi-well plates where up to 384 different conditions can be analysed in the same experiment, allowing for unbiased screening approaches.
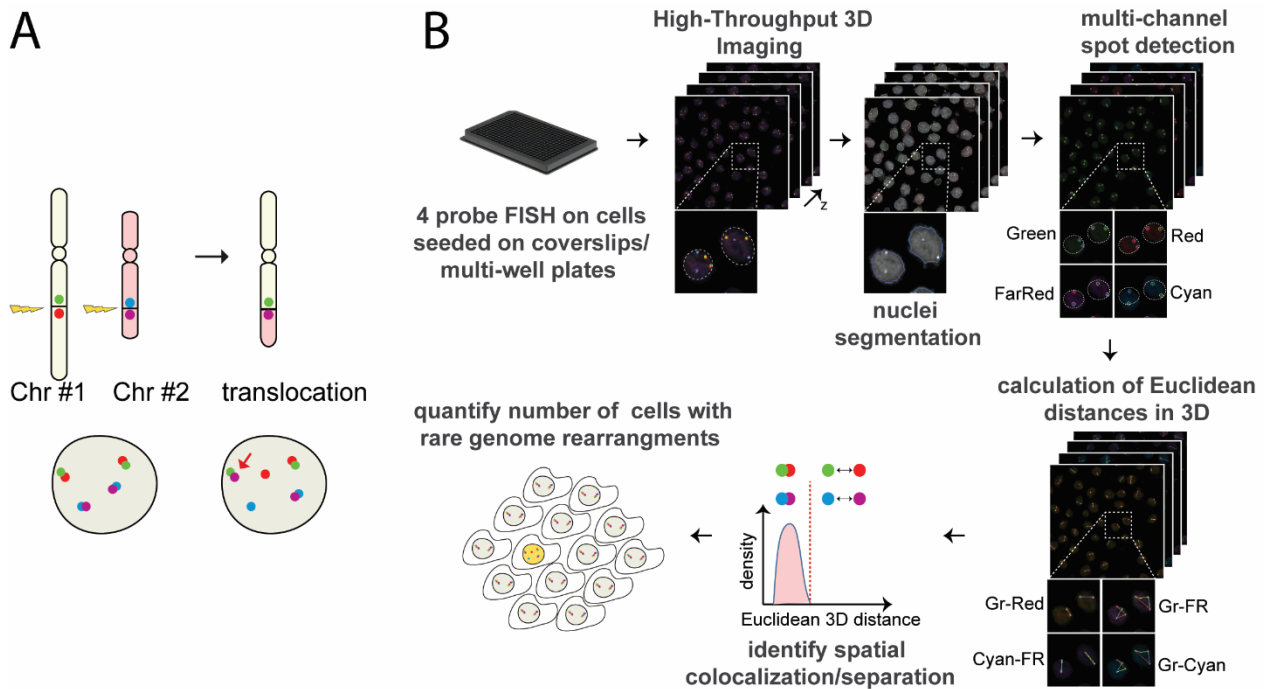
Figure Results 1: Introducing qCRI-3D, a combination of multi-colour FISH in interphase cells, high-throughput imaging and automated image analysis. A) Schematic of the FISH based chromosome break and fusion probe setup. **B)** Schematic of the qCRI-3D imaging and image analysis pipeline.

Using custom-built R Markdown scripts (O. Drechsel), a spot-to-spot distance threshold to distinguish between broken and intact loci is defined. Here, the break-apart probe distance in unperturbed control cells is taken to account and at least 99% of break-apart probes have to be closer than the threshold. This threshold depends on the cell lines and the break-apart probes used as the spatial distance between the probes varies. The definition of chromosome breakage calls for two break-apart probes being separated further than the threshold that can be set manually (usually 4pxs or 1.2µm, for more details, see 4.1.1). In case of a chromosome translocation, one of the break apart probes (e.g. Alexa488, "green) is further away than the threshold from its partner probe (e.g. Alexa568, "red") and closer to the probe labelling the potential translocation partner (e.g. Alexa647, "farred") than the threshold. When adding the fourth colour to the translocation partner, the probe labelling the other DSE (e.g. CF405S, "blue") also has to be further away from the potential acceptor probe than the threshold (see Figure Results 1 A). The R Markdown script produces an html file that holds the information of total number of analysed nuclei, the number of chromosome breaks and translocations and the resulting ratio within the cell population in several tables. Furthermore, the html file includes information on spot-to-spot distances in the different cell populations and on how an implemented 3D-correction (work done by H. J. Gothe and O. Drechsel) affects the measured spatial spot position within the nucleus in 3D.

4.1.1 Implementing a co-localization threshold improves comparability of chromosome rearrangement frequencies obtained by ddPCR and qCRI-3D

Since many previous reports on mechanisms influencing genome rearrangement frequencies relied on PCR approaches, we were interested in how comparable the results that we obtain by qCRI-3D are to frequencies obtained by a PCR-based approach. In order to compare the direct quantification of chromosome rearrangements by qCRI-3D with a directly quantitative PCR approach, we decided to develop a translocation specific assay for digital droplet PCR. Here, only the product of a translocation will amplify and give a positive droplet in the final droplet read-out (see Figure Results 2 B).
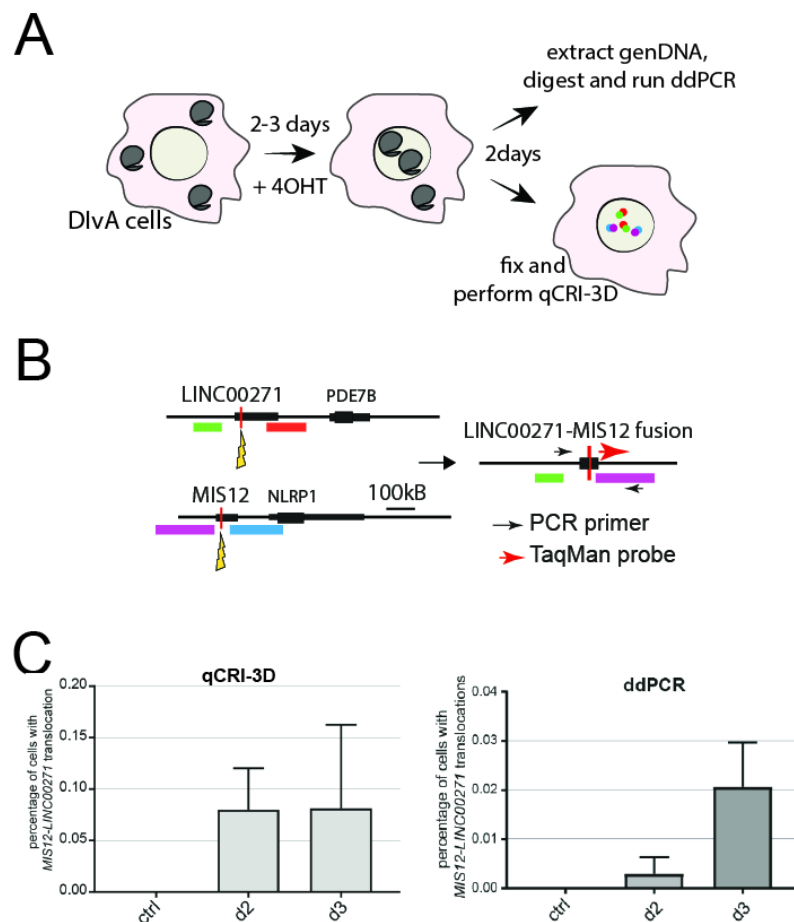
Figure Results 2: Investigating genome instability and genome rearrangements using DIvA cells and qCRI-3D. A) Schematic of DIvA system. AsiSI-ER is transferred to the nucleus upon addition of 4OH-Tamoxifen. 2-3 days later, samples are taken for further assays. **B)** Schematic of FISH probe binding flanking the AsiSI sites (red lines) in the *LINC00271* and *MIS12* genes and resulting pairing in the AsiSI induced *LINC00271-MIS12* translocations. For the *LINC00271-MIS12* translocation, the primer and TaqMan binding sites are schematically presented on the right side by black and red arrows, respectively. **C)** Comparison of results from qCRI-3D and ddPCR.

In order to study translocation formation using a PCR-based approach, we needed to use a cellular system where we could induce site-specific DSBs to study chromosome breakage and fusions frequencies using either methodology. For this purpose, we employed the well-studied U-2-OS-based DIvA cell line (DSBs inducible via AsiSI, [159]) and designed FISH probes flanking the restriction sites of AsiSI in the genes *LINC00271,* coding for a long non-coding RNA (lncRNA), and *MIS12* (see Figure Results 2 B).
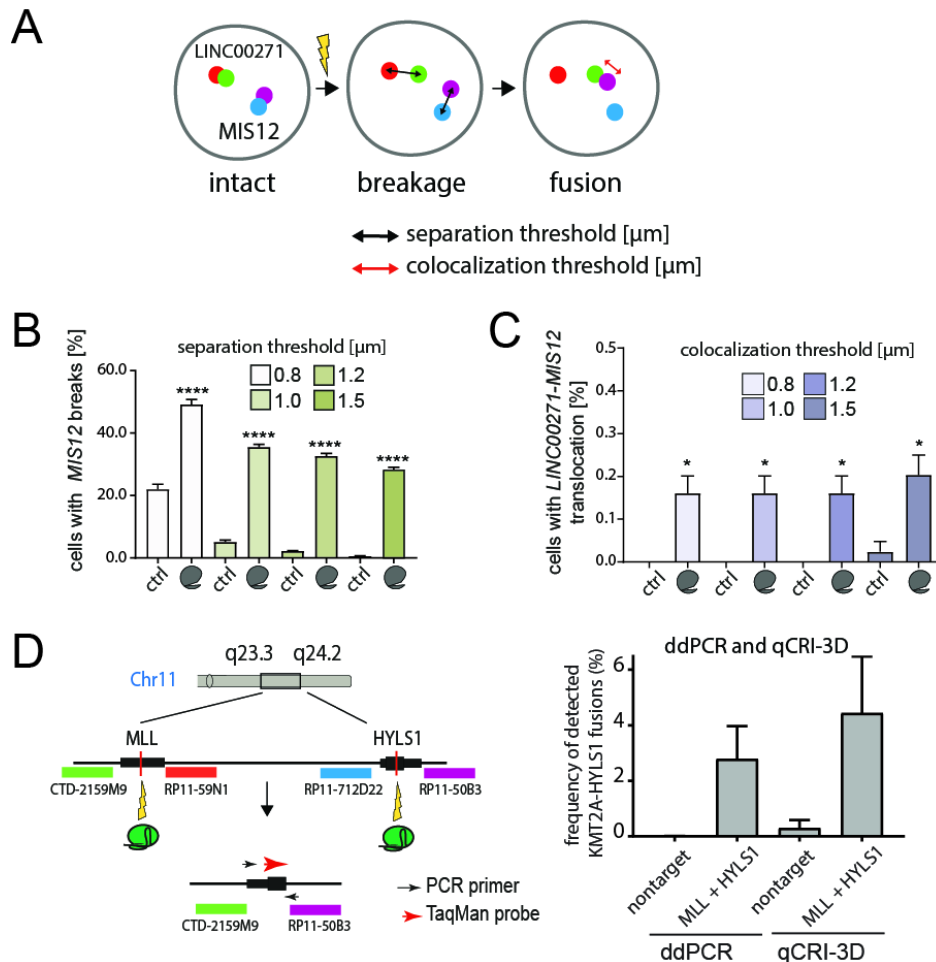
Figure Results 3: Improving the specificity of qCRI-3D by incorporation of an additional threshold in the analysis pipeline. **A)** Schematic of cells where *LINC00271* and *MIS12* are labelled with FISH probes flanking the AsiSI sites and are intact, broken or fused. The two different thresholds are depicted with black ("separation threshold") and red ("colocalisation threshold"). **B)** Analysing the same measurements with a different separation threshold and the resulting quantified percentage of cells with breaks in *MIS12*. **C)** Analysing the same measurements with a constants separation threshold (1.5µm) but changing colocalisation threshold and the resulting quantified frequency of translocations between *LINC00271* and *MIS12*. **D)** left: Schematic of FISH probes flanking the CRISPR sites (red lines) in the *MLL* and *HYLS1* genes and resulting pairing in the CRISPR/Cas9 induced *MLL-HYLS1* rearrangement. For the *MLL-HYLS1* fusion, the primer and TaqMan binding sites are schematically presented on the by black and red arrows, respectively. Right: Comparison of results from 4 independent experiments from qCRI-3D and ddPCR.

Importantly, the number of translocations quantified by ddPCR is almost 10x less than by qCRI-3D (see Figure Results 2 C). This could either be due to false-positive detections using qCRI-3D e. g. through random colocalisation of the FISH probes without actual fusion of the DSEs, or due to false-negative detections by ddPCR e.g. if the PCR reaction failed to amplify a template. Therefore and in order to increase the specificity of qCRI-3D, we incorporated a second threshold to the image analysis pipeline in R, which lowers the risk of false positive detections: By distinguishing between a separation and new colocalisation threshold, we can make our assay more stringent.

Usually, the single threshold we use to distinguish between separation and colocalisation of two FISH probes is around 1.3μm or 4pxs. Now, we can choose a separation threshold that will only detect broken loci when the two FISH probes are far away from each other (saturation at 1.5μm). On the other hand, we can also decrease the required colocalisation threshold (saturation at 1.2μm). To summarize, only break-apart loci that are truly broken are detected as broken and only potential translocations that are truly overlapping are considered to be fused.

Using this more stringent analysis for qCRI-3D (separation threshold 1.5μm, colocalisation threshold 1.2μm), we can quantify chromosome rearrangements in the same order of magnitude as by ddPCR (Figure Results 3; ~4% vs ~2.5%, respectively; here in a different experimental setup: TK6 Cas9 cells).

4.1.2 Enabling the detection of intra-chromosomal deletions, inversions or the deletion of a chromosome arm

Since chromosome translocations are only a subtype of potential oncogenic chromosome rearrangements, we decided to try to also quantify intra-chromosomal rearrangements like inversions, deletions or the partial loss of a chromosome arm. In order to be able to model these rearrangements, we created and used stably Cas9 expressing cell lines, which allow to induce targeted DSBs in only a few specific locations in the genome at a time. Cas9 is part of an adaptive bacterial immune mechanism [160,161] and works on viral but also foreign bacterial plasmid DNA that is integrated in specialized clustered regularly interspaced short palindromic repeat (CRISPR) regions of the bacterial genome. These regions are transcribed into crRNA, which bind to and guides the endonuclease Cas9 to the respective homologous DNA sequence for degradation. The idea that the CRISPR/Cas9 system could be used to specifically guide Cas9 to a locus of interest, thereby leading to its disruption, has greatly transformed the possibilities of genome engineering

in the recent years. For my PhD studies we were however not so much interested in gene transformation but rather in the induction of targeted DSBs in a region of interest.
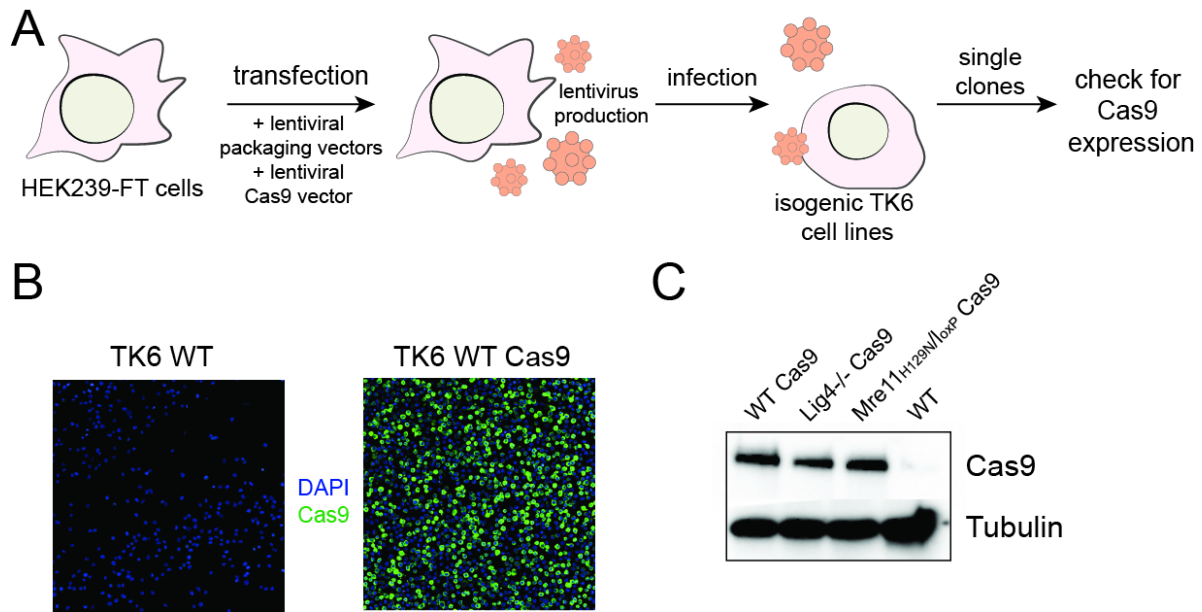
Figure Results 4: Creation of stably Cas9 expressing TK6 Cas9 cell lines. A) Creation of isogenic stable Cas9 expressing TK6 cell lines. **B)** Immunofluorescence image from final TK6 WT Cas9 clone. **C)** Immunoblot against Cas9 in final clonal TK6 Cas9 cell lines used in this study.

In order to create cell lines that stably express Cas9, we used lentiviral transduction. Briefly HEK293-FT or HEK293-T cells, which can produce a high viral titer [162], were transfected with 3rd generation lentiviral packaging plasmids (Addgene) and a lentiviral vector coding for Cas9 (Addgene) and a resistance to blasticidin using FuGENE (Promega). Culture media was changed the following day, virus-containing supernatant was harvested on two consecutive days and concentrated using Lenti-X concentrator (TaKaRa) before being added to the receiving cell lines. In order to increase the transduction efficiency, TK6 cells were "spinfected" by centrifugation (300xg) in the viral supernatant for 30 minutes. The day after transduction, antibiotic selection was added to the media and one week later, and replenished every day thereafter. Single clones were diluted in 96-well plates and checked for Cas9 expression levels by immunofluorescence and high-throughput microscopy (example in Figure Results 4 B). In order to compare Cas9 expression levels between different isogenic cell lines, immunoblots were performed (Figure Results 4 C). Finally, we obtained Cas9 expressing TK6 WT, TK6 Lig4-/-, TK6 Tdp2-/-, TK6 Mre11H129N/loxP, HEK-293 and HeLa cell lines. Unfortunately, in HCT116 and U-2-OS cells Cas9 expression was lost over time.
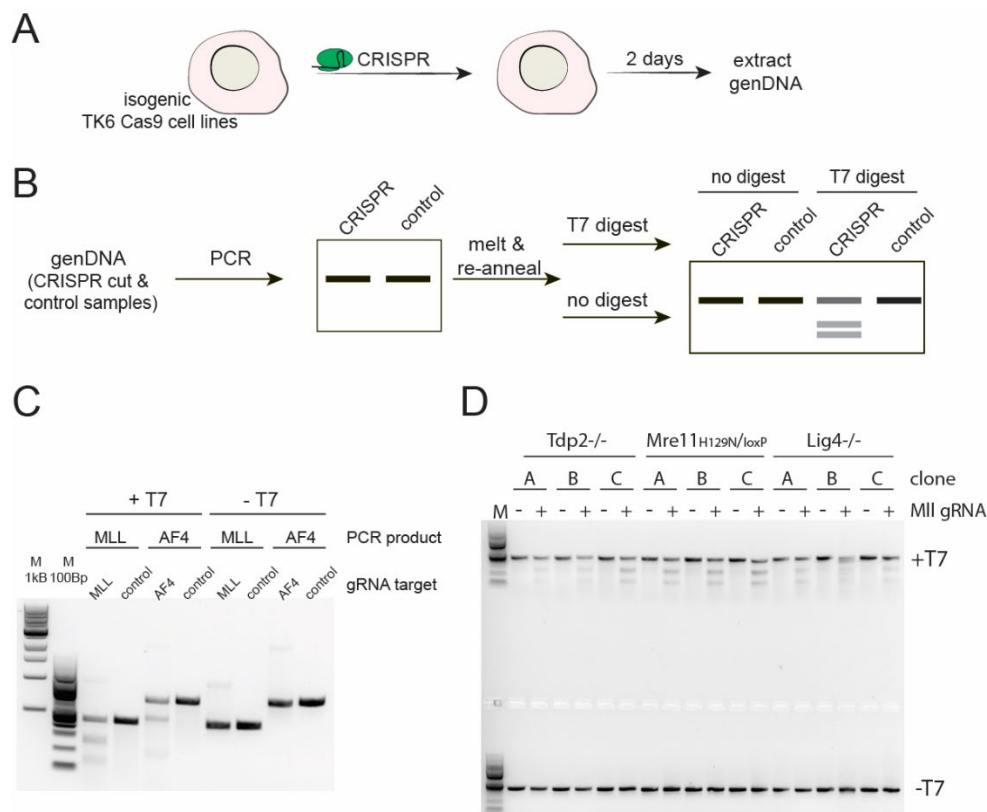
Figure Results 5: Checking Cas9 activity by T7 endonuclease assay. A) Schematic of experimental pipeline. TK6 Cas9 cells were electroporated with the targeting and non-targeting crRNA complexes and genDNA was extracted 2 days later. **B)** Schematic of experimental pipeline for T7 assay. Region surrounding the Cas9 cut site is amplified by PCR and after melting and random re-annealing of amplicons either digested by T7 or not. This results in a characteristic digestion pattern for amplicons where Cas9 had introduced small mutations which were then detected by T7 as mismatches. **C)** T7 endonuclease assay to confirm Cas9 activity in TK6 WT Cas9 clone around *MLL* CRISPR and *AF4* CRISPR sites (expected PCR product size *MLL*: 500Bp, *AF4*: 800Bp). **D)** T7 endonuclease assay to confirm Cas9 activity in TK6 *TDP2-/-*, *MRE11*H129N/loxP and *LIG4-/-* Cas9 clones around MLL CRISPR site (expected PCR product size: 500Bp).

The T7 endonuclease assay is widely used to check for Cas9 activity [163]. To check Cas9 activity in the TK6 Cas9 cell lines, we electroporated them (Lonza) with a mix of sgRNA and trcRNA (Horizon Genomics/Dharmacon, for specific sequences see section 6.3) which, when aligned, resemble the crRNA that Cas9 uses to detect its target sequence. A non-target sgRNA was always added as a control condition. Two days after electroporation, we extracted genomic DNA (genDNA) and performed a regular PCR over the CRISPR site with a high-fidelity DNA polymerase (Phusion High-Fidelity DNA Polymerase, Thermo Scientific, or in-house high-fidelity DNA polymerase as supplied by the protein production core facility at IMB).

In cells where targeted crRNA was added, active Cas9 will introduce a DSB and during DSB repair, small nucleotide changes will occur in some instances. If the PCR amplicons are melted and allowed to randomly anneal to each other, these nucleotide changes will lead to mismatches

at the specific site between different amplicons. The T7 endonuclease detects these mismatches and cleaves the amplicons at the mismatch site. This leads to two distinct populations of cut amplicon species with specific sizes (see Figure Results 5 B). If the DNA has not been cut by Cas9 and therefore not been modified in sequence, mismatches do not occur. T7 assay analysis shows that TK6 WT, *LIG4-/-*, *MRE11*H129N/loxP and *TDP2-/-* Cas9 show efficient activity of Cas9 (see Figure Results 5 C-D) and can be used to efficiently induce inter- as well as intra-chromosomal rearrangements.

In order to detect and quantify these rearrangements, we adapted the R Markdown image analysis scripts to not only quantify inter-chromosomal translocations but also intra-chromosomal changes such as inversions, deletions of a part of a chromosome or the loss of an entire chromosome arm.

If we choose the probes and their labelling as seen in Figure Results 6 A, this means that in order for an inversion to be present, Alexa488 ("green") and Alexa568 ("red") have to be apart, while green should be close to C405S ("blue") but apart from Alexa647 ("farred"). The number of spots of each color in the nucleus should however not be altered.
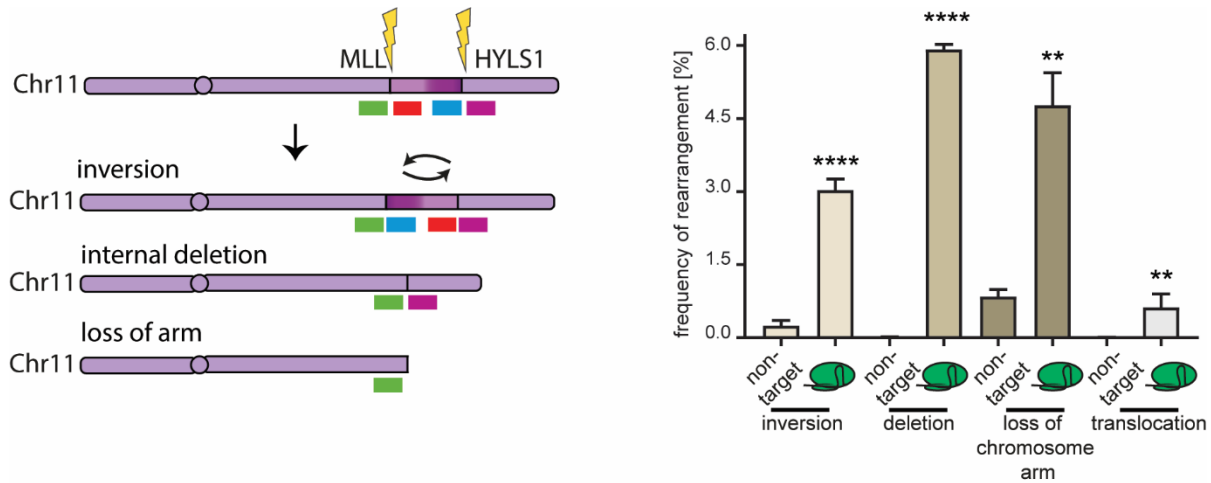
Figure Results 6: Modelling intra-chromosomal rearrangements. A) Schematic of FISH setup to quantify different intra-chromosomal rearrangements between *MLL* and *HYLS1* on chromosome 11. **B)** The resulting CRISPR induced genome rearrangement frequencies as quantified by qCRI-3D. Results from three independent experiments, according to student's t-test. ** p < 0.01, **** p < 0.0001

In a deletion, the nucleus would lack one blue and red spot each as they are aligning to the part of the chromosome that is lost, green would be close to purple and distal to all other colours. In order to be able to analyse this, the script has to be run twice selecting a different population of cells. For diploid cells, only nuclei that have two spots of each colour are considered when analysing translocations or inversions. In case of deletions, the number of green and purple spots will remain two, while the number of red and blue spots will eventually decrease to one spot each.

The first time the script is run to quantify deletions, we select cells with two green and purple spots (==2) and at least one blue and red spot (>=1). This way, we receive the number of total cells in the images, which we want to include in our population. The second time the script is run, we analyse cells with two green and purple (==2) and with exactly one red and blue spot (==1). The ratio between the quantified number of deletions and the total population of cells from the first run, then results in the frequency of the specific chromosomal rearrangement.

In case that a chromosome arm is lost after CRISPR/Cas9 induced breakage, cells will remain with two green spots (==2) and one spot of the other colours. The analysis has to be repeated similarly as for deletions described above (first red, farred, blue >=1, second ==1).

Interestingly, these intra-chromosomal rearrangements do not occur at the same frequency in the same sample. We induced Cas9 mediated breaks in *MLL* and the *HYLS1* locus, which lies about 4kBb downstream of *MLL* on the same chromosome (chr11). In the final population, two days after DSB induction, we could quantify inversions in 3.0 ± 0.1% of cells and deletions and partial chromosome arm losses in 5.9 ± 0.1% to 4.7 ± 0.4% of cells, respectively (see Figure Results 6 B). Importantly, the frequencies of all intra-chromosomal rearrangements we analysed is higher than that of inter-chromosomal Cas9 induced translocations between *MLL* and *AF9* even though all loci show a similar breakage frequency (not shown).

4.2 Studying the involvement of DSB repair pathways in the formation of chromosomal rearrangements

The mechanisms underlying the formation of oncogenic chromosome rearrangements have been studied for a long time but have also been proven a difficult field of research. The rare occurrence of chromosome rearrangements and the positive selection they undergo as drivers of oncogenesis, exacerbate the study of the involved pathways. For a long time it was believed that chromosome translocations are formed by aEJ as in the absence of aEJ, less translocations have been detected [36]. This model has however recently been challenged in human cells, where the opposite was observed, meaning that the absence of cNHEJ led to a decrease in translocation formation [101]. In order to shed light on this question, we decided to use qCRI-3D and induce different genome rearrangements in different isogenic human cell lines by different DSB-inducing agents.

Results

4.2.1   Cell lines null for EJ factors

To be able to study the influence of the absence of factors from either aEJ or cNHEJ pathways, we made use of isogenic human colorectal carcinoma cells (HCT116) null for either Lig4 or XLF as cNHEJ factors, or nuclear Lig3 or Parp1 which are playing a role in aEJ. Most HCT116 cell lines have been purchased (*LIG4*-/- and *XLF*-/-, Dharmacon Horizon) or were kindly given to us by Eric Hendrickson (*nucLIG3*-/- [164]).
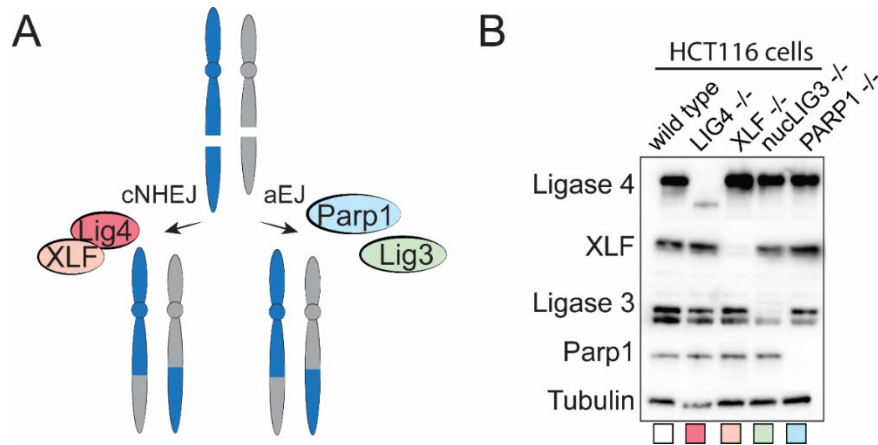
Figure Results 7: Cell lines used in this study. A) Broken chromosomes can be fused by two different EJ pathways. cNHEJ involves DNA Ligase 4 in a complex with XLF. aEJ involves the actions of Parp1 and DNA Ligase 3. **B)** Western Blot against EJ factors in isogenic HCT116 cell lines used later in the study.

For the generation of a *PARP1-/-* HCT116 cell line, we transduced HCT116 wild type cells with lentiviral particles containing a plasmid coding for Cas9 and a gRNA targeting the first exon of Parp1 (the resulting clonal cell line has been further validated and characterized here [165]).

Using these HCT116 cell lines allowed me to compare the influence of presence vs. absence of the different factors on chromosome break and rearrangement formation in human HCT116 cells after irradiation or after treatment with the Top2 poison etoposide.

Irradiation and etoposide treatment resemble physiological ways of DSB induction. Many of the previous, partially contradictory studies have however made use of non-physiological DSB induction by site-specific endonucleases, TALENs or Cas9. In order to be able to compare the influence of the nature of DSBs and their quantity, we also made use of the before described TK6 wild type and *LIG4-/-* Cas9 cell lines and compared the frequency of irradiation, etoposide or CRISPR/Cas9 induced chromosome translocations in these cells.

41

4.2.2 The absence of cNHEJ factors leads to persistent DNA damage and higher chromosome translocation frequencies

A first and commonly used proxy of DSB formation is the presence of γH2AX, a histone H2A variant that is phosphorylated on Serine 139 upon DSB detection by ATM [166]. In order to see how well the different isogenic HCT116 cell lines can resolve DNA damage, we irradiated them or treated them with etoposide and performed immunofluorescence analysis in a recovery time course afterwards.

Cells null for nuclear DNA ligase 3, did not show a delayed resolution of γH2AX, but cNHEJ deficient cells presented high levels of γH2AX even three days after irradiation with 20 Gy (see Figure Results 8 B and C). Furthermore, we tested the activity of the checkpoint kinases Chk1 and Chk2 in response to irradiation. Chk1 is thought to be phosphorylated in an ATR dependent manner and relies on ssDNA coated by phosphorylated RPA [126] whereas Chk2 is phosphorylated and activated by ATM in the presence of γH2AX. More recently, a cross talk of the checkpoint kinases has softened this view to a certain extent [167]. Chk2 is expressed throughout the cell cycle but remains inactive in the absence of DNA damage [168]. Chk1 on the other hand is restricted to S and G2 phase and is active even under unperturbed cell cycle conditions, with increased activity in response to DNA damage or stalled replication. Interestingly, HCT116 wild type and cNHEJ deficient cells still showed high abundance of phosphorylated Chk2, as analysed by Immunoblot, even three days after irradiation but *nucLIG3-/-* cells did not. On the other hand, phosphorylated Chk1 seemed to be more abundant in HCT116 *nucLIG3-/-* cells compared to wild type and cNHEJ deficient ones three days after irradiation. Importantly, *XLF-/-* HCT116 cells presented a baseline phosphorylation of Chk1, indicating that the checkpoint is constantly active at a low level or in a subset of cells (see Figure Results 8 B). Therefore, there seems to be a difference in DDR signalling in the absence of factors from either pathway.

In order to find out how this influences chromosomal fusions, we irradiated the HCT116 cells with 20Gy and quantified chromosome breakage in *MLL* and *AF9* and translocations resulting from these chromosome breaks using qCRI-3D two and three days after irradiation. In all studied cell lines, irradiation leads to chromosome breaks and fusions. Two days after irradiation, wild type cells present 2-5% breakage (2.0 ± 0.1% - 4.9 ± 0.2%) whereas this reaches up to 4.9 ± 0.1% in *LIG4-/-* HCT116 cells and 6.2 ± 0.3% in the absence of Parp1. Interestingly, the number of cells with chromosome breaks increases in all cell lines from day two to day three after irradiation but not in *nucLIG3-/-* cells (2.0 ± 0.2% on day two, 1.5 ± 0.3% on day three). We could observe that both cNHEJ deficient cell lines as well as *PARP1-/-* cells have high levels of broken chromosomes remaining even three days after irradiation (see Figure Results 8 D). This, together with the

remaining high γH2AX signalling described before, could indicate that DSBs, which remain unrepaired for a long time, loose the contact between their two DSEs, which in turn could be reflected in the higher translocation frequency detected in the later time point - especially in cNHEJ deficient cells.
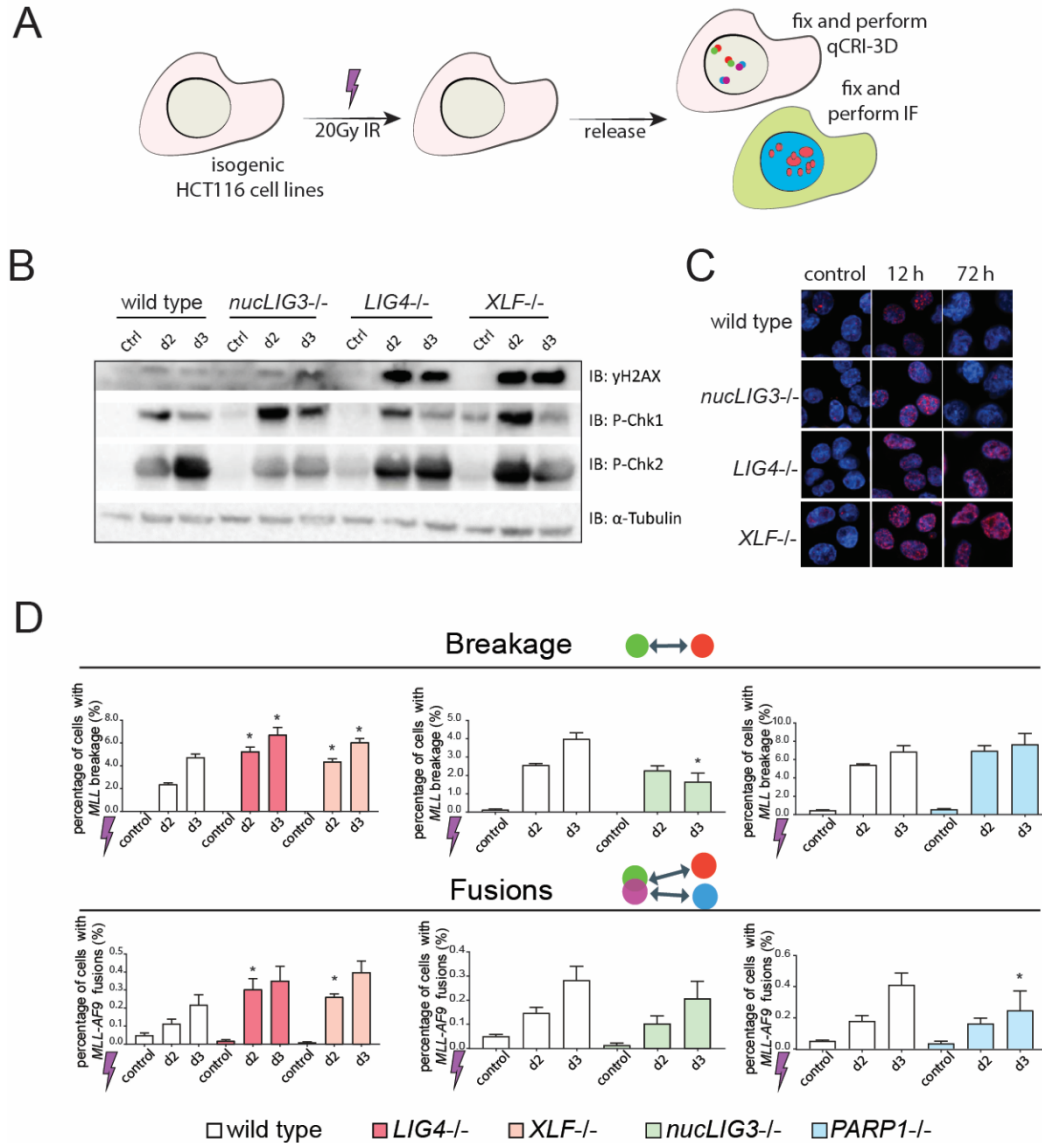
Figure Results 8: The absence of cNHEJ factors leads to persistent DSBs and a higher translocation frequency after irradiation. A) Experimental setup: Isogenic HCT116 cell lines were seeded the day before treatment. After irradiation with 20Gy, cells were washed twice with PBS and released into fresh media. Two days after, cells were fixed and stained for γH2AX or prepared for qCRI-3D analysis. **B)** Immunoblot of remaining γH2AX, Chk1 and Chk2 phosphorylation up to three days after irradiation in HCT116 cell lines. **C)** Example images of γH2AX immunofluorescence in isogenic HCT116 cell lines at indicated time points after irradiation with 20Gy and release into fresh medium. **D)** Quantification of *MLL* breaks and *MLL-AF9* translocations using 3-end qCRI-3D in isogenic HCT116 cell lines released for the indicated time from 20Gy irradiation.* $p<0.05$ according to student's t-test, n = 4

cNHEJ deficient cell lines show a higher number of translocations (wild type cells 0.2-0.4 ± 0.08%, cNHEJ deficient cells 0.4 ± 0.08% (p < 0.05)), whereas aEJ deficient cells show even a slight

decrease compared to wild type cells*(PARP1-/- cells <0.2 ± 0.07% (p < 0.05), nucLIG3-/- cells <0.2 ± 0.07% (p > 0.05)).*

Potentially, the absence of aEJ makes cNHEJ more efficient and DSBs are repaired faster. On the other hand, in the absence of cNHEJ, breaks remain unrepaired longer, can dissociate and two DSEs can be fused illegitimately. In some cases, the remaining DSEs on day three may have been fused to a DSE, which we do not detect in the assay setup.

This could mean that the cell lines null for factors from the cNHEJ and those null for factors from the aEJ pathway may be able to handle different kinds of DNA damage with a different efficiency. In order to compare their response to irradiation to the behaviour after treatment with the Top2 poison etoposide, we also performed a DNA damage recovery assay in the HCT116 cell lines deficient for cNHEJ or aEJ.
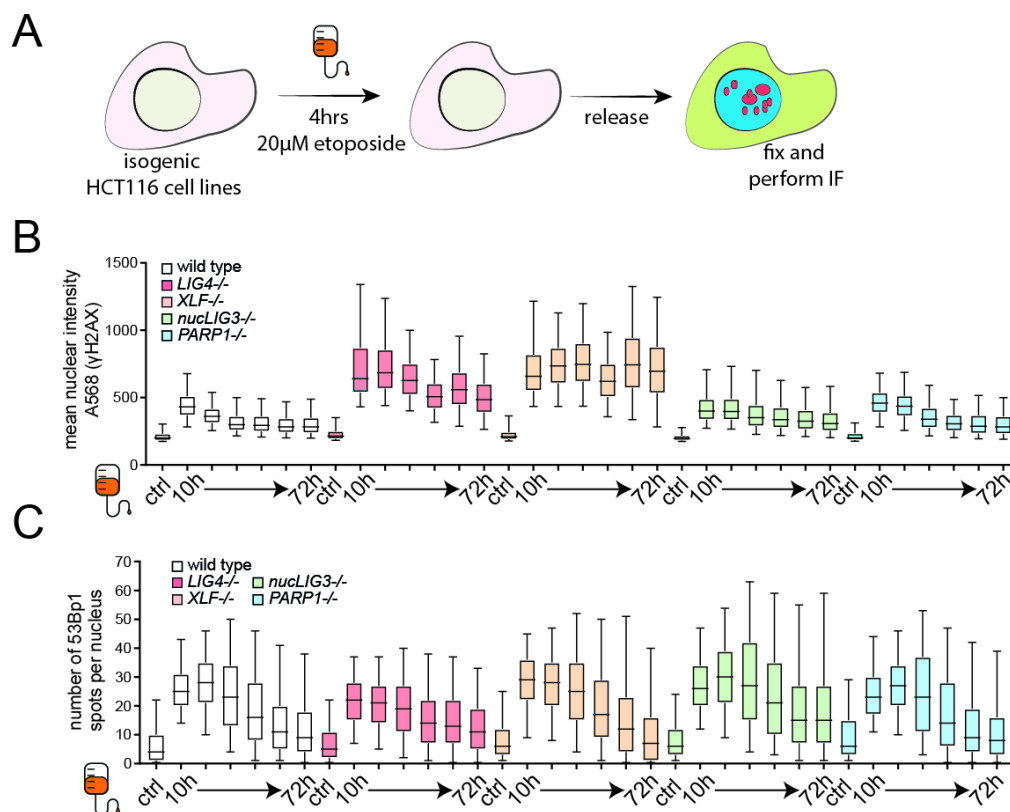
Figure Results 9: The absence of cNHEJ factors leads to persistent DDR signals after treatment with etoposide. A) Isogenic HCT116 cell lines were treated with 20μM eto for 4hrs before being released into fresh media and fixed for downstream analysis by immunofluorescence at different time points thereafter. **B)** Quantification of mean nuclear γH2AX intensity at indicated time points after eto treatment in indicated HCT116 cell lines. **C)** Quantification of the number of 53BP1 foci per nucleus in indicated HCT116 cell lines at indicated time points after eto treatment.

After treatment with 20μM etoposide for 4hrs and release into fresh media, these cells were sampled for immunofluorescence and analysis for changes in the DDR. As for irradiation, cNHEJ

deficient cells were not able to resolve γH2AX as efficiently as wild type cells, meaning that presumably they are not able to repair the DNA damage even three days after etoposide treatment. Cells deficient for aEJ factors did not show a delayed decrease of γH2AX signal (see Figure Results 9 B). Besides γH2AX, also 53BP1 has been shown to be recruited to DSBs and form clusters due to phase separation [93]. However, comparing the number of 53Bp1 foci in the nuclei of the different cell lines after etoposide treatment reveals no striking difference (see Figure Results 9 C).
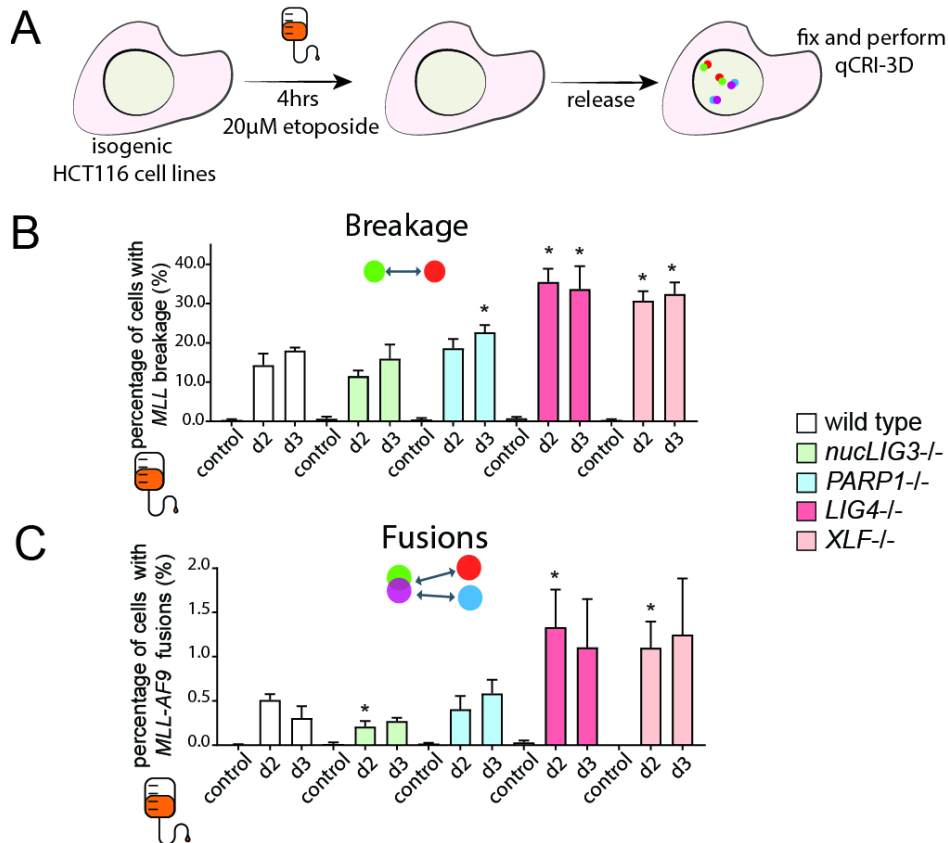
Figure Results 10: The absence of cNHEJ factors increases the frequency of chromosomal translocations after treatment with etoposide. A) Experimental setup: Isogenic HCT116 cell lines null for EJ factors were seeded the day before treatment with 20µM etoposide for 4hrs. After treatment, cells were washed and released into fresh media. Two days later, cells were fixed and qCRI-3D was performed. **B)** Quantification of *MLL* breaks using 4-end qCRI-3D in isogenic HCT116 cell lines released for the indicated time from 4hrs of 20µM etoposide treatment. **C)** Quantification of *MLL-AF9* translocations using 4-end qCRI-3D in isogenic HCT116 cell lines released for the indicated time from 4hrs of 20µM etoposide treatment. * $p < 0.05$ as determined using student's t-test

In order to find out if the decreased resolution of γH2AX goes along with an increased frequency of chromosome breakage and translocation formation, as it is the case for cells after irradiation, we performed qCRI-3D using the same experimental setup as for DDR analysis by immunofluorescence. As for irradiation, both cNHEJ deficient cell lines (HCT116 *LIG4*-/- and HCT116 *XLF*-/-) show an increased frequency of chromosome breaks and translocations when

compared to wild type cells (translocations on day 3: wild type 0.3 ± 0.1%, *LIG4*-/- 1.0 ± 0.5% (p > 0.05), *XLF*-/- 1.1 ± 0.5% (p > 0.05)). On the other hand, there is only a slight difference between the frequencies observed in wild type cells and the aEJ deficient cell lines. HCT116 *PARP1*-/- cells show an increased chromosome breakage at the *MLL* locus compared to wild type cells (breaks on day 3: wild type 18 ± 1%, *PARP1*-/- 22 ± 1% (p < 0.05)), three days after eto treatment but this does not result in an increase in *MLL-AF9* translocation formation (translocations on day 3: wild type 0.3 ± 0.2%, *PARP1*-/- 0.5 ± 0.2% (p > 0.05)). HCT116 *nucLIG3*-/- cells on the other hand present no difference in breakage frequency (breaks on day 2: wild type 15 ± 2%, *nucLIG3*-/- 10 ± 1% (p > 0.05)) but a slightly lower frequency of resulting *MLL-AF9* translocations two days after etoposide treatment (wild type 0.5 ± 0.1%, *nucLIG3*-/- 0.3 ± 0.1% (p < 0.05)). These results indicate once more that the absence of aEJ may make cNHEJ mechanisms more efficient as the two pathways are not competing for DSB repair. If this is a direct effect of the absence of one pathway or a consequence of adaptation to the knockout in these cell lines remains unclear. The results could furthermore indicate that even if the frequency of translocations is increased in the absence of cNHEJ, translocations in wild type cells are formed through cNHEJ mechanisms as the frequency of translocation formation in wild type and aEJ deficient cells is not altered. Importantly, the results so far do not support reports of a lower translocation frequency in human cells in the absence of cNHEJ, which have however been obtained using non-physiological, site-directed DSB induction methods [80,101].

4.2.3 In the absence of DNA Ligase 4, CRISPR-induced DSBs undergo end resection resulting in a lower PCR-based detection frequencies of rearrangements

In order to see if the discrepancy between the above described results and those of previously published studies looking at chromosome translocation frequencies in human cells is due to the nature of the DSBs, we made use of the before described human lymphoid TK6 Cas9 cells.

TK6 Cas9 cells allow the comparison of translocation frequencies after irradiation, etoposide treatment or CRISPR induced DBSs in qCRI-3D directly. Furthermore, as CRISPR-induced breaks are site-specific, the resulting chromosomal rearrangements allow quantification of translocation frequency by ddPCR, therefore making our results comparable to previous studies where translocation frequencies were studied using PCR approaches.

Importantly, the absence of DNA ligase 4 leads to a higher frequency of chromosome breaks and translocations two days after inducing DSBs independently of the DSB inducing method (*MLL* breaks after irradiation: wild type 2.5 ± 0.0%, *LIG4*-/- 5.0 ± 0.1% (p < 0.05). *MLL* breaks after

etoposide: wild type 5.0 ± 0.0%, *LIG4*-/- 12.5 ± 0.3% (p < 0.05). *MLL* breaks after CRISPR: 2.0 ± 0.0%, *LIG4*-/- 5.0 ± 0.1% (p < 0.05). *MLL-AF9* translocations after irradiation: wild type 0.01 ± 0.00%, *LIG4*-/- 0.02 ± 0.01% (p > 0.05). *MLL-AF9* translocations after etoposide: wild type 0.02 ± 0.05%, *LIG4*-/- 0.25 ± 0.11% (p < 0.05). *MLL-AF9* translocations after CRISPR: wild type 0.10 ± 0.02%, *LIG4*-/- 0.15 ± 0.02% (p < 0.05)).
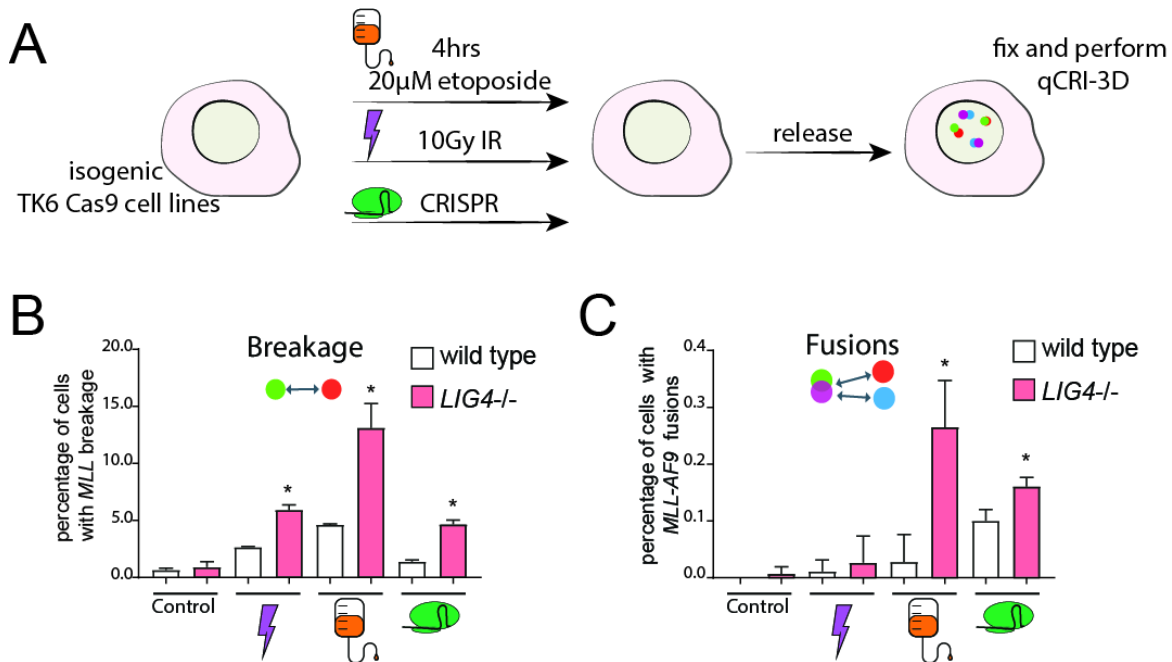
Figure Results 11: The absence of DNA Ligase 4 leads to an increase in DSBs as well as *MLL-AF9* translocations after irradiation, etoposide treatment as well as CRISPR-induced DSBs. A) Experimental setup: TK6 Cas9 cell lines (wild type and *LIG4*-/-) were either irradiated with 10Gy, treated with 20µM etoposide for 4hrs or electroporated with site-specific or non-targeting sgRNAs. After irradiation, etoposide treatment or electroporation, cells were washed and released into fresh medium. Two days later, cells were fixed and qCRI-3D was performed for the same loci in all conditions. **B)** and **C)** Quantification of *MLL* breaks and *MLL-AF9* translocation frequencies respectively, in TK6 Cas9 wild type and *LIG4*-/- cells. Results from five independent experiments, students t-test * p< 0.05

These results indicate that it is not the nature or the amount of induced DSBs that leads to the reported discrepancy. The discrepancy could however still be resulting from the different methodologies used to study chromosome translocation frequencies.

In order to compare our results obtained with qCRI-3D with previous reports using genomic approaches, we quantified their frequencies in parallel using ddPCR as described before. Here, looking at the CRISPR-induced translocation between the genes *RBMXL1* and *MIS12* in TK6 Cas9 cells by qCRI-3D and ddPCR reveals that while we observe more translocations in *LIG4*-/- cells by qCRI-3D, we interestingly observe less by ddPCR. This result supports the previous reports where by PCR-based approaches studying rearrangements after site-specific DSBs, a decrease in translocation frequency was observed in the absence of cNHEJ factors.
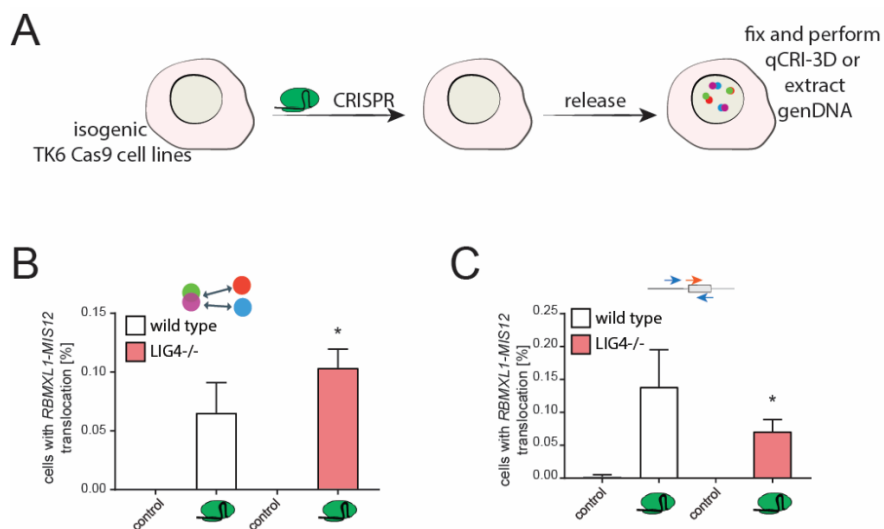
Figure Results 12: qCRI-3D detects higher translocation frequencies in TK6 Cas9 LIG4-/- cells compared to wild-type cells whereas less translocations are quantified by ddPCR. A) Experimental setup. TK6 Cas9 cells (wild type or LIG4-/-) were electroporated with sgRNA-trcrRNA complexes and fixed 2 days later for qCRI-3D or genomic DNA was extracted for ddPCR analysis. **B)** Resulting *RBMXL1-MIS12* translocation frequencies obtained by qCRI-3D. **C)** Resulting *RBMXL1-MIS12* translocation frequencies obtained by ddPCR on HindIII digested genDNA. * p<0.05

When analysing the resulting PCR products on an agarose gel, we realised that for "short" 700Bp PCR products spanning the putative translocation junction, the resulting bands were much fainter when the PCR was run on genDNA from TK6 Cas9 *LIG4*-/- cells than when run on genDNA from TK6 Cas9 wild type cells. However, when extending the size of the PCR product surrounding the translocation junction to 2.4Kbp, these bands ran as a single band at the expected size in wild type cells but the size of the translocation product in *LIG4-/-* cells did not and often ran at lower molecular weights (see Figure Results 13 A).

The lower molecular size of translocation products made me wonder if the DSEs had been resected prior to fusion. In order to investigate this, we designed qPCR primers compatible with a previously described qPCR-basec resection assay [169]. Here, primers are designed to amplify over restriction enzyme sites near a DSE in different proximities (in Figure Results 13 C: 250Bp and 1100Bp away from the Cas9 targeted site). If the DSE is not resected, the restriction site is intact and will be cleaved by the restriction enzyme. If the DSE has been resected and ssDNA present, the restriction site is not recognized by the restriction enzyme, and the ssDNA can therefore serve as template in the following qPCR. The non-resected, digested DSE will not be amplified. Performing the resection assay at different distances to the DSEs allows a good overview over the extent of resection at a certain locus.
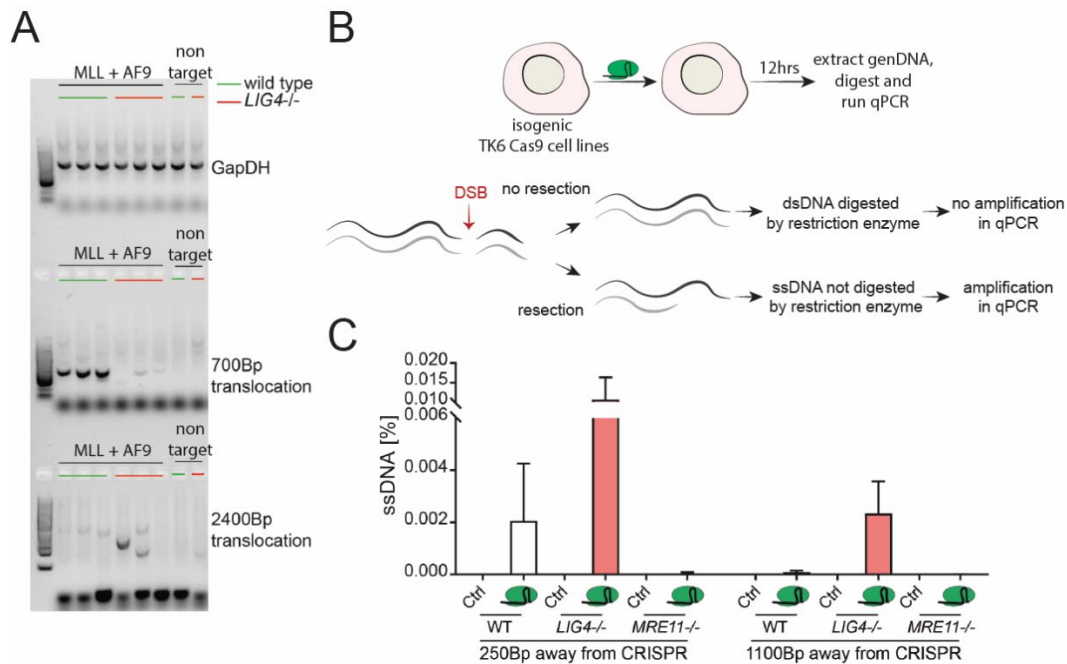
Figure Results 13: The absence of DNA ligase 4 leads to increased DSE resection and therefore a decrease in translocation frequency observed by PCR-based approaches. A) Translocation PCR products in TK6 Cas9 cells after inducing CRISPR mediated *MLL-AF9* translocations for 2 days. GapDH serves as a loading control. 20% of PCR reactions originally containing 100ng genDNA were loaded on a 1.5% agarose gel. **B)** Experimental and methodological setup for the resection assay in TK6 Cas9 cells. TK6 Cas9 cell lines were electroporated with sgRNA-trcrRNA complexes targeting *MLL*. 12hrs later genDNA was extracted and digested with the BsrGI restriction enzyme for 3hrs. If a DSB is resected and the resection extends to the restriction site of BsrGI, the resulting ssDNA cannot be digested but it can therefore be amplified by qPCR. **C)** Resection assay result around *MLL* CRISPR site in TK6 Cas9 wild type, LIG4-/- and MRE11$_{H129N/loxP}$ cells. MRE11$_{H129N/loxP}$ serves as non-resection control.

Twelve hours after electroporation of sgRNA-trcrRNA complexes into TK6 Cas9 cells, we extracted the genomic DNA and digested it with the respective restriction enzyme. Comparison of the percentage of ssDNA present surrounding the CRISPR sites reveals that resection happens 250Bp away from the Cas9 cut but to a greater extent in the absence of Lig4. *LIG4-/-* cells present resection even more than 1Kbp away from the DSB. *MRE11$_{H129N/loxP}$* cells were used as a control as they do not undergo resection.

These results indicate that resection happens to a greater extent in the absence of cNHEJ activity than in unperturbed conditions in wild type cells. This could be due to delayed repair without the rapid cNHEJ activity therefore leaving more time for DSEs to be processed. Largely resected DSEs could result in smaller translocation products by PCR and if the PCR primers bind close to the DSB, the translocation junction may not be amplified, as primer-binding sites may be lost during resection. This would in turn explain the differences in the before observed results where by ddPCR less translocations were detected as by qCRI-3D and it may at least partially explain the discrepancy in the translocation research field.

So far, we could conclude that the absence of aEJ does not largely influence repair kinetics and translocation formation in HCT116 cells. The absence of cNHEJ however, leads to a delayed repair, increased processing of DSBs and a higher probability of translocation formation. Importantly, this does not depend on the kind of DSB-inducing agent. In order to find out if the observed increase in resection after DSB induction in the absence of Lig4 and the accompanying increased risk of translocation formation is cell type specific, we used again the DIvA cell line where DSBs are also introduced in a site-specific way through the restriction enzyme AsiSI thereby allowing comparison of qCRI-3D- and ddPCR-based results.
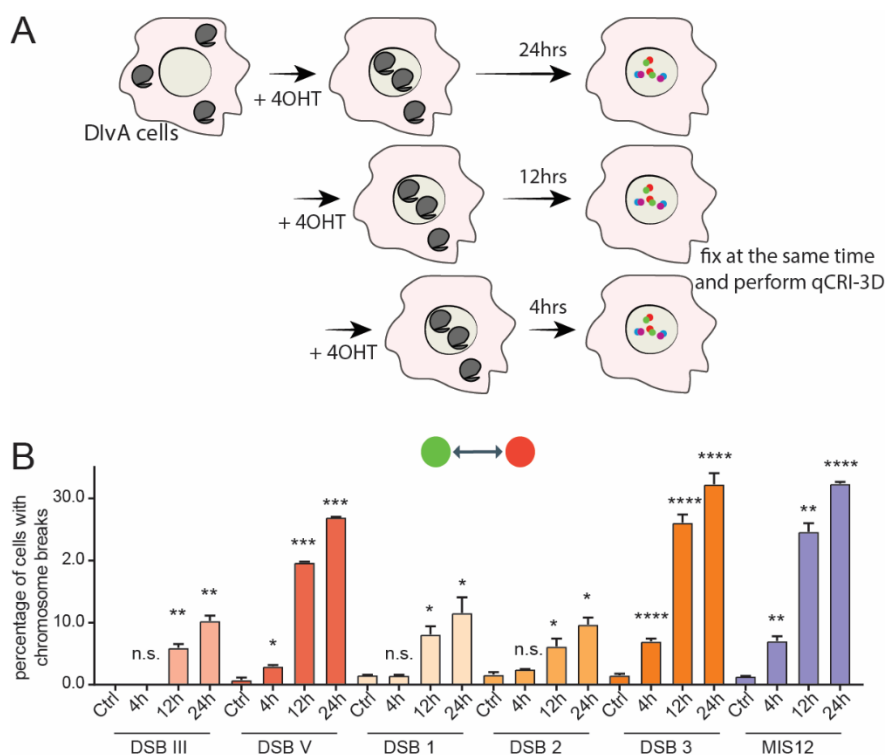
Figure Results 14: Using DIvA cells to efficiently induce chromosome breakage across the genome. A) Experimental setup: DIvA cells were treated with 300nM 4OHT at different time points to induce nuclear transfer of AsiSI and fixed at the same time in order to perform qCRI-3D. **B)** qCRI-3D based quantification of AsiSI induced breakage at different loci and different time points. n ≥ 2. n.s. $p > 0.05$, * $p < 0.05$, ** $p < 0.01$, *** $p < 0.001$, **** $p < 0,001$ according to student's t-test

In DIvA cells, AsiSI is fused to part of the estrogen receptor, which leads to the cytoplasmic localization of AsiSI in the absence of estrogen or its analog 4-Hydroxy-Tamoxifen (4OHT). If 4OHT is added to the culture medium, AsiSI is transported into the nucleus and induces around 80-100 well-studied DSBs residing mostly in promotor regions of actively transcribed genes [159,170]. In order to get an overview of the behavior of these cells and some of the previously studied DSBs, we performed a time course experiment where we added 4OHT to the cells and

fixed them at different time points thereafter to analyze the frequency of chromosome breaks at different AsiSI sites over time.

Since DIvA cells are derivatives of U-2-OS cells, the genome presents multiple duplications and most AsiSI restriction sites studied are present in three copies per nucleus [171]. Some loci however, are still diploid (e.g. *MIS12*; not shown). Previous studies using γH2AX signaling as a read-out of DSB presence have shown that DSBs accumulate in DIvA cells until 4hrs after 4OHT addition and that their frequency decreases thereafter. Using qCRI-3D however, we can only detect chromosome breaks after 4hrs and for some loci even later (see Figure Results 14 B).

Overall, it is noteworthy that the few DSBs we studied in this assay already show a great variability in the speed of DSE separation and the overall frequency of break-apart-probe separation over time (~30% maximum in DSB V, DSB 3 and *MIS12* compared to ~10% in DSB III, DSB 1 and DSB 2, see Figure Results 14 B).
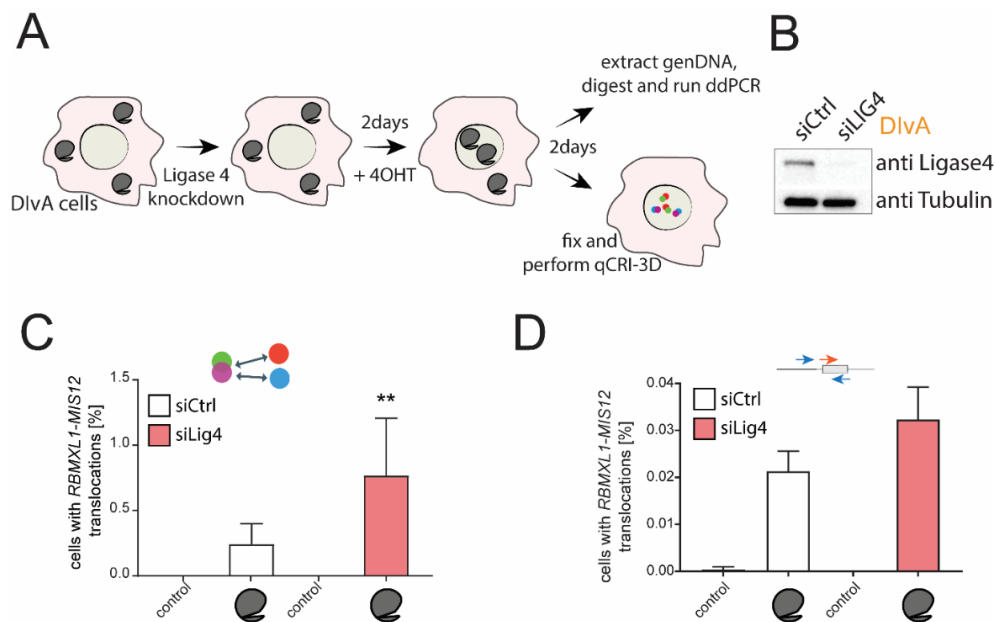
Figure Results 15: Ligase 4 knockdown in HeLa cells leads to an increase in RBMXL1-MIS12 translocations observed by qCRI-3D. A) Experimental setup for DIvA experiments: siRNA mediated knockdown of DNA Ligase 4 was performed two days prior to 4OHT addition. Two days later, cells were fixed for qCRI3D or genomic DNA extracted for ddPCR. **B)** Immunoblot for Ligase 4 two days after siRNA knockdown. **C)** *RBMXL1-MIS12* translocations quantified by qCRI-3D. ** p<0.01 **D)** *RBMXL1-MIS12* translocations quantified by ddPCR.

In order to investigate whether the absence of Lig4 has an influence on AsiSI-induced DSB persistence or resulting chromosomal translocation frequency, we planned to create *LIG4-/-* DIvA cells by lentiviral transduction with a Cas9 encoding vector targeting the first exon of *LIG4* that had successfully been used in the lab before. Unfortunately, we were not successful to obtain a

Lig4 deficient cell line still expressing the AsiSI protein this way and we therefore went for siRNA-mediated knockdown of Lig4.

Luckily, siRNA mediated knockdown of Lig4 worked very well (see Figure Results 15 B) and the absence of Lig4 led to an increased translocation formation frequency obtained by qCRI-3D as it did for other types of DNA damage in the previously used *LIG4-/-* cell lines (see Figure Results 15 C). In order to find out whether the site-specific translocations introduced by AsiSI show similar behaviour as CRISPR-mediated rearrangements, we further also studied translocation frequencies using ddPCR. Surprisingly, when we analysed the translocation frequency by ddPCR, we did not see a decrease as we had seen before in the TK6 Cas9 *LIG4-/-* cells (compare Figure Results 15 D and Figure Results 12 C). This could indicate that either AsiSI-induced DSBs are not resected in the absence of DNA ligase 4 or that the TK6 Cas9 *LIG4-/-* cells adapted to the gene knockout by upregulating resection and this is not the case for the transient absence induced by siRNAs.
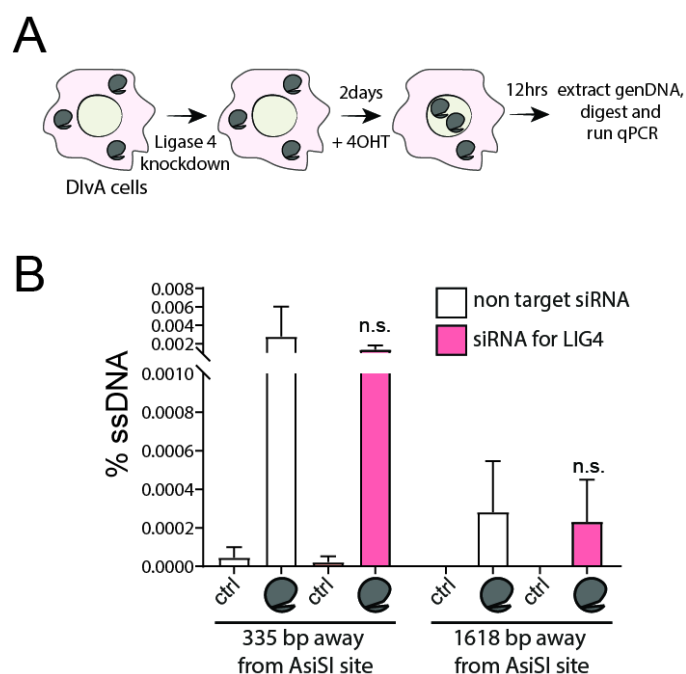
Figure Results 16: Ligase 4 knockdown does not influence the resection at *RBMXL1* in DIvA cells. A) Experimental setup: siRNA mediated knockdown of Ligase 4 was performed two days prior to 4OHT addition. Two days later, genomic DNA was extracted for resection assay. **B)** Resection assay at *RBMXL1* after AsiSI induced cleavage. Results from three independent experiment, significance according to student's t-test. n.s. p > 0.05

Since there is the possible indication of less resection at the DSE, we performed again a resection assay, using previously published primers for the AsiSI site in the *RBMXL1* gene. Interestingly,

we could not detect a difference in resection at this site in the absence of Lig4 (see Figure Results 16 B) which is different to what we had observed in TK6 Cas9 cells.
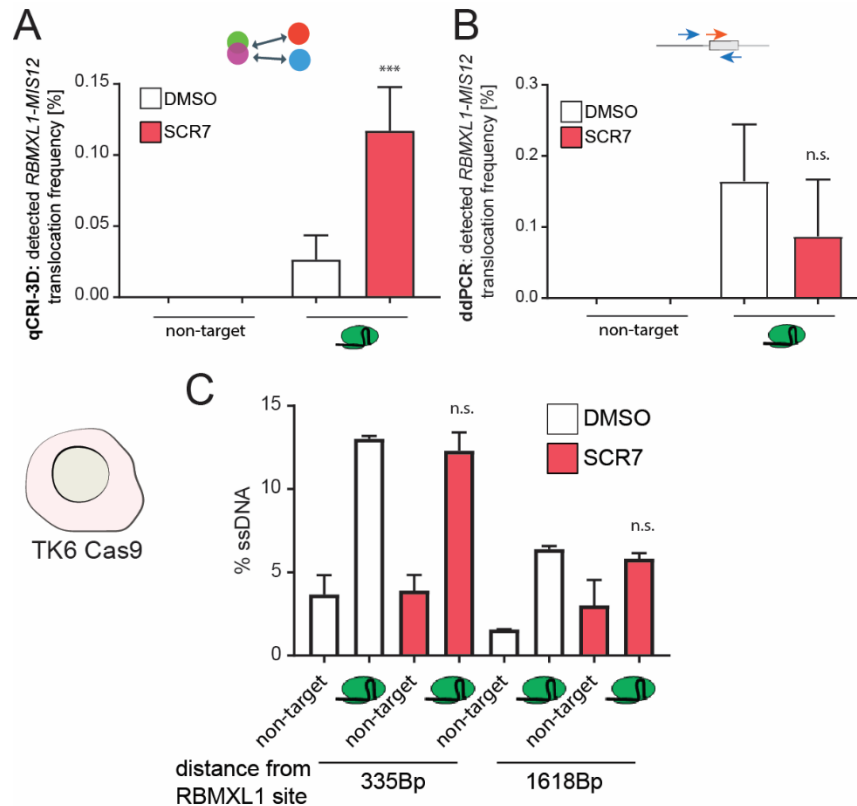
Figure Results 17: Inhibition of Ligase 4 does not influence the frequencies of chromosome breaks or translocations in TK6 Cas9 cells. A) Translocations between *RBMXL1* and *MIS12* as quantified using qCRI-3D. Results from three independent experiments and significance according to student's t-test. *** p < 0.001 **B)** Translocations between RBMXl1 and MIS12 as quantified using ddPCR. Results from three independent experiments and significance according to student's t-test. n.s. p > 0.05 **C)** Resection assay results for *RBMXL1* in HeLa cells. Cells were released into media with 10mM SCR7 or DMSO after electroporation of indicated sgRNA complexes. 12hrs later, genomic DNA was extracted and prepared for resection assay analysis. Results from two independent experiments and significance according to student's t-test. n.s. p > 0.05

After some tests and optimizing sgRNA transfection, we studied the influence of Lig4 knockdown on CRISPR induced chromosome breaks in these cells using qCRI-3D and ddPCR as described before. Importantly, we induced DSBs at the same site in *RBMXL1* as AsiSI does, but could interestingly not see a difference in translocation frequency by ether method between wild type cells and cells deficient in cNHEJ activity. Furthermore, no difference in resection at *RBMXL1* was observed (see Figure Results 16 B).

Since we could not detect a significant difference between samples from DNA Ligase 4 knockdown compared to control samples in DIvA cells, we decided to investigate what happens at the same locus (*RBMXL1*) when using an inhibitor of DNA Ligase 4 and compare the results from the same conditions between TK6 Cas9 and DiVA cells. The Ligase 4 inhibitor SCR7 [172] allows to

circumvent the difficulty of siRNA-mediated knockdown in suspension cells and therefore allows comparable conditions for all cell lines.
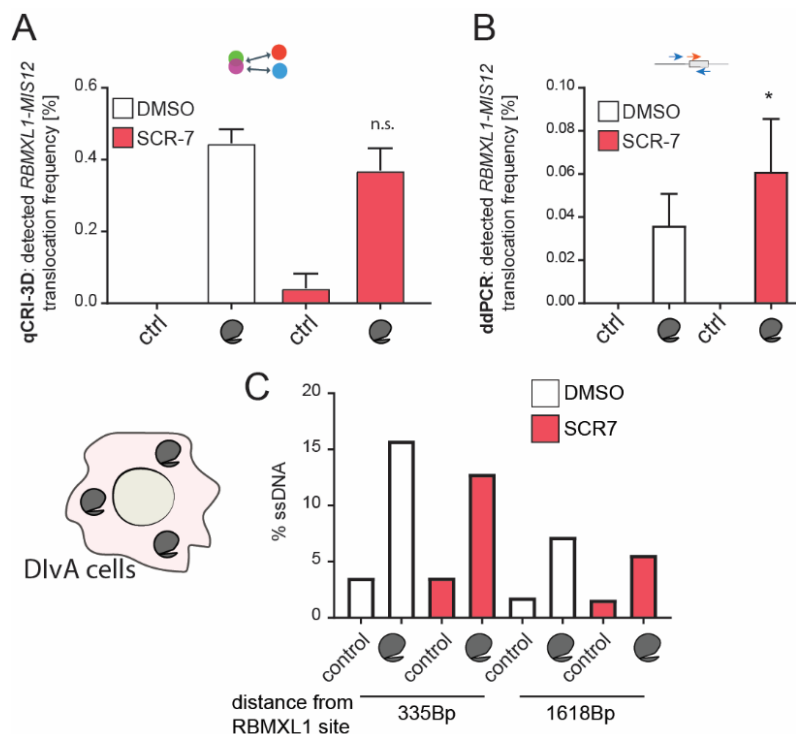
Figure Results 18: Inhibition of Ligase 4 alters the frequency of *RBMXL1-MIS12* translocations obtained by qCRI-3D in DIvA cells. A) Translocations between *RBMXl1* and *MIS12* as quantified using qCRI-3D. Results from three independent experiments and significance according to student's t-test. n.s. p >0.05 **B)** Translocations between *RBMXL1* and *MIS12* as quantified using ddPCR. Results from three independent experiments and significance according to student's t-test. * p < 0.05 **C)** Resection assay results for *RBMXL1* in DIvA cells. Cells were released into media with 10mM SCR7 or DMSO after electroporation of indicated sgRNA complexes. 12hrs later, genomic DNA was extracted and prepared for resection assay analysis. Results from one experiment.

Interestingly, in TK6 Cas9 cells the loss of Ligase 4 activity after addition of SCR7 does not affect resection at *RBMXL1*. As seen previously using *LIG4*-/- cells, Lig4 inhibition leads to an increase in translocation frequency as detected by qCRI-3D but not to a (significant) decrease of detected translocations by ddPCR. Taken together, there is a potential difference in the effect of Lig4 knock out and inhibition on chromosome rearrangement handling after CRISPR-induced breaks in this cell line. Using qCRI-3D, we still detect a higher frequency of translocations after transient Lig4 inhibition using SCR7. However, DSEs are not handled differently compared to control cells (at least in regards to resection), which could explain a lower effect of absence of Lig4 activity on translocation frequencies measured by ddPCR.

Potentially, in the TK6 Cas9 *LIG4*-/- cell line the permanent absence of Lig4 has led to a change in DSB repair dynamics with a higher rate of end resection possibly leading to a higher

dependency on homology-directed-repair-like pathways as e. g. SSA. More tests would however be necessary to prove this.

Inhibition of Lig4 after DSB induction in DIvA cells had no effect on the observed translocation frequency by qCRI-3D (control 0.4 ± 0.03%, SCR7 0.4 ± 0.05% (p > 0.05)) but led to an increased translocation frequency detected by ddPCR (control 0.04 ± 0.02%, SCR7 0.06 ± 0.03% (p < 0.05), Figure Results 18).

Taken together, the CRISPR-based results suggest that in the absence of Lig4, DSB repair in human cells works via different mechanisms than simple joining of DNA ends. Without the rapid cNHEJ-meidated ligation reaction at the DSB, DSBs undergo alterations like resection. Interestingly, the degree of dependency on different pathways seems to increase in cells with a genetic knock out of Lig4 compared to cells that recently and/or transiently lost Lig4 activity. These results seem to be specific for CRISPR-induced DSBs but independent of the site of break induction, as the same results have been observed at different genomic loci and for intra- as well as interchromosomal rearrangements. DSBs induced by the endonuclease AsiSI (DIvA cells) do not show the same reliance on the cNHEJ specific Lig4. However, if this effect results from the cell lines' background or the specific way of DSB induction and the resulting differences in DSB nature and likely in DSE structure remains unclear, as we were not able to study both enzymatic DSB inducing methods in the same cell line.

4.3 Investigating processes involved in chemotherapy-induced chromosome rearrangements

The mammalian Top2 isozymes are involved in many nuclear processes involving the detangling or unwinding of the DNA helix as it forms e.g. ahead and behind the replication or transcription machineries. During their catalytic cycle, Top2 enzymes form a transient covalent complex with the DNA backbone that under normal circumstances is reverted in the same catalytic reaction cycle. Structural abnormalities like TT-dimers in close proximity or an approaching transcription machinery can trap Top2 in the covalently bound state. It remains largely unclear how Top2ccs are converted to DSBs or how cells sense the difference between a regular intermittent Top2cc and one that is permanently stuck on the DNA. Furthermore, it remains to be investigated whether the conversion of a Top2cc to a DSB is a wanted or an unwanted outcome during the resolution of Top2cc.

Why is it that two chemotherapeutic Top2 poisons, mitoxantrone and etoposide have both been shown to trap Top2 on DNA and prevent the relegation of the Top2-intoduced DSB but in the clinic, one (etoposide) leads to a risk of *MLL* translocation whereas the other one (mitoxantrone) to a risk of translocations between *PML* and *RARA*? By exploring the different outcomes from the Top2 poisons on a genomic scale as well as by investigating an involvement of the VCP-Ubiquitin system, we hope to gain insight towards different mechanisms that lead to the conversion of Top2ccs to DSBs, which could potentially have implications in the clinics.

4.3.1 DNA damage induced by the Top2 poisons etoposide and mitoxantrone depends on different cellular processes

Mitoxantrone and etoposide have both been shown to lead to different secondary malignancies (t-APL and t-AML) underlying different genomic rearrangements (*PML-RARA* and *MLL* translocations) following their administration. Since etoposide-induced damage has been shown to mainly depend on Top2A [69], the DDR after mitoxantrone treatment in inducible *TOP2A-/-* and *TOP2B-/-* cells or inducible *TOP2A-/- TOP2B-/-* cells was investigated.
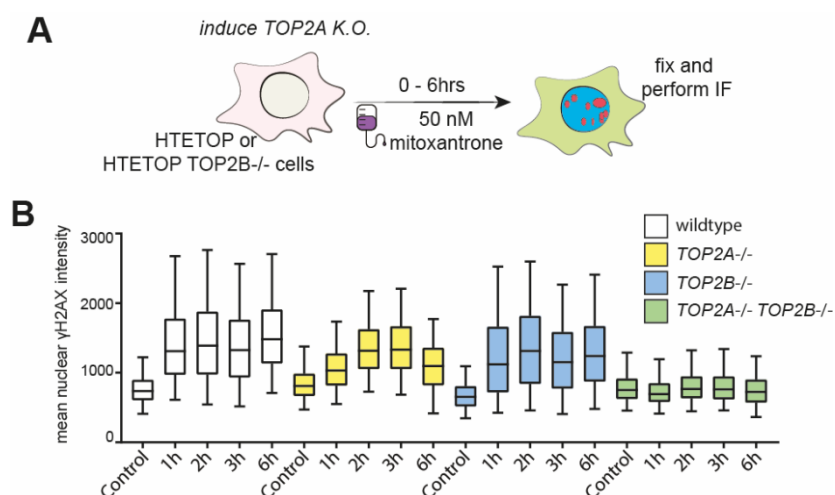
Figure Results 19: Mitoxantrone-induced DNA damage response depends on both TOP2 isozymes. A) Schematic of experimental setup. In order to induce TOP2A-/-, HTETOP cells were treated 1µg/ml doxycycline for 1 hr prior to addition of mitoxantrone for the indicated time before cells were fixed for IF for DDR markers. **B)** Mean nuclear intensity of γH2AX signal after IF in HTETOP cells treated with 100nM mitoxantrone for the indicated amount of time.

In HTETOP cells, the endogenous *TOP2A* alleles were disrupted and the gene coding for the tetracycline transactivator as well as an exogenous *TOP2A* allele controlled by the tetracycline transactivator have been introduced into the genome. This way, by addition of doxycycline more than 99% of Top2A expression can be silenced [173].

Besides the conditional *TOP2A-/-* HTETOP cells, we furthermore introduced a stable *TOP2B-/-* in these cells using lentiviral transduction and CRISPR-based gene knockout (work done by Matthias Rieb, a former B. Sc. student in the lab), which upon addition of doxycycline works as a double knockout cell line for both Top2 isozymes. In order to repress Top2A expression, these cells were kept in media containing tetracycline-free serum.
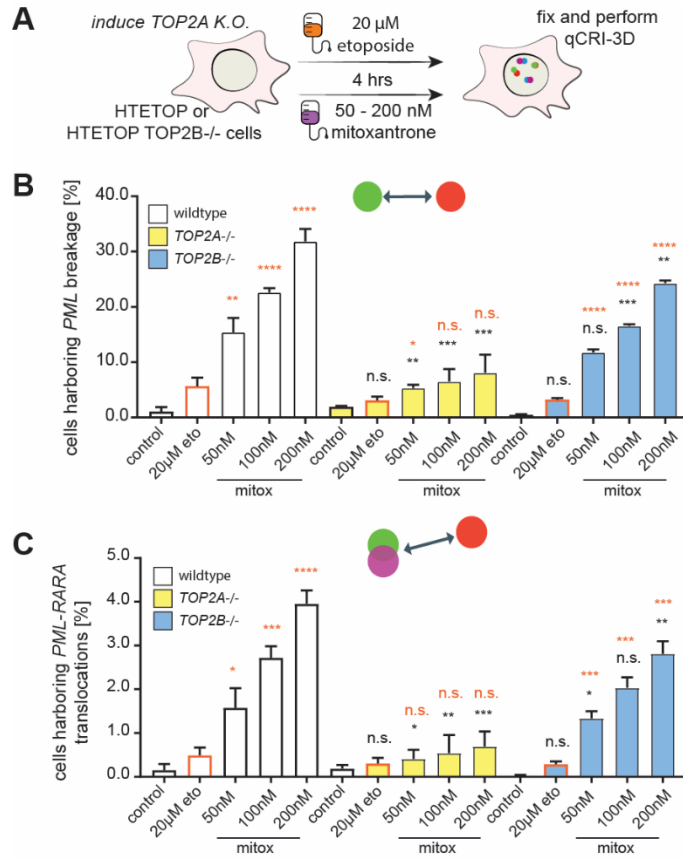
Figure Results 20: Mitoxantrone-induced DSBs and PML-RARA translocations depend on both TOP2 isozymes. A) Schematic of experimental setup. In order to induce TOP2A-/-, HTETOP cells were treated 1µg/ml doxycycline for 1 hr prior to addition of etoposide or mitoxantrone for the indicated time before cells were fixed for qCRI-3D. **B)** DSBs in the *PML* gene as quantified by qCRI-3D (3D analysis) after acute treatment with indicated dose of mitoxantrone or etoposide for 4 hrs and 48 hrs of release. Results from three independent experiments and significance according to student's t-test. n.s. $p > 0.05$, * $p < 0.05$, ** $p < 0.01$, *** $p < 0.001$, **** $p < 0.0001$ **C)** *PML-RARA* translocations as quantified by qCRI-3D (3-end, 3D analysis) after acute treatment with indicated dose of mitoxantrone or etoposide for 4 hrs and 48 hrs of release. Results from three independent experiments and significance according to student's t-test. Orange: significance in comparison to etoposide treatment of the same cell line, black: significance compared to the same treatment in the wild type cell line. n.s. $p > 0.05$, * $p < 0.05$, ** $p < 0.01$, *** $p < 0.001$

In order to investigate whether one of the two Top2 isozymes is preferably trapped when using mitoxantrone, the DRR that would result from Top2ccs was measured by IF analysis for γH2AX intensity. The *TOP2A-/-* was induced prior to treatment of HTETOP cells with 50nM mitoxantrone. Cells were fixed at different time points thereafter for IF analysis. Interestingly, other than etoposide [69], mitoxantrone-induced DNA damage depends on the presence of both isozymes

as only in the inducible double knockout cell lines, no increase in γH2AX intensity was measured after addition of mitoxantrone.

To investigate whether the decrease in γH2AX intensity is also reflected in a decrease of DSBs and eventually chromosome rearrangements, we used qCRI-3D in HTETOP cells and quantified breaks in *PML* and translocations between *PML* and *RARA*. Importantly, in this experiment, other than for the IF analysis described before, cells were kept in culture 48 hrs after 4 hrs of treatment with etoposide or mitoxantrone and the HTETOP double knockout cells were not viable anymore. Therefore, only results from the single-knockout cells were analyzed. While in my hands, the knockout of either isozyme had no significant effect on the resulting breakage frequency in the *PML* gene when treating cells with etoposide, mitoxantrone induced breakage was decreased in the absence of Top2A and Top2B (see Figure Results 20 B, black descriptions on bars). Here, the absence of Top2A had a greater effect than the absence of Top2B and both showed a mitoxantrone dose dependent increase of *PML* breakage. The absence of Top2A decreases the frequency of mitoxantrone-induced breaks in the *PML* gene from around 4.0 ± 0.3% in wild type cells treated with 200 nM mitoxantrone to only 1.0 ± 0.4% (p < 0.001) in *TOP2A-/-* cells treated with the same dose of mitoxantrone. In the absence of Top2B, around 3.0 ± 0.3% (p < 0.01) of cells still harbor a broken *PML* gene when cells were treated with 200 nM mitoxantrone. These results indicate that like etoposide-induced breaks in general, the majority of breaks induced by mitoxantrone depends on Top2A activity, but about a quarter of breaks seems to involve Top2B. This could be due to differences in abundance of the two isozymes – Top2B is only expressed during late G2 and S phase. Nevertheless, more studies would be necessary to shed light on to this phenomenon, e. g. by re-analyzing the experiments and taking into consideration the DAPI signal and thereby the cell cycle stage of the imaged cells [174] or trapping cells in different cell cycle stages prior to mitoxantrone addition.

In order to investigate whether the difference in the induction of a specific chromosome rearrangement, as observed in the clinics, results from different break frequencies in the genes involved, human lymphoblastoid TK6 cells, which are closely related to the blood cell lineages where translocations occur after treatment with mitoxantrone or etoposide, were acutely treated with etoposide or mitoxantrone. After certain time points of release into fresh media, cells were fixed on coverslips and IF for DDR markers or qCRI-3D to probe for DSBs in the specific loci or genomic rearrangements between the specific genes was performed (Figure Results 21 A).

Interestingly, etoposide leads to a faster accumulation of γH2AX in the nucleus whereas with lower molarities of mitoxantrone, the γH2AX signal remains upregulated for longer and only two days

after addition of the drug returns to background levels (Figure Results 21 B). This indicates that etoposide induced DNA damage is resolved faster and that mitoxantrone induced DNA damage accumulates slower, is not resolved as quickly or may be recognized later in general.

In order to find out whether mitoxantrone shows a specificity in the genomic location where breaks are induced, we compared the break frequencies between *PML*, the gene involved in *PML-RARA* translocations and *MLL*, which translocates after etoposide treatment, after mitoxantrone treatment.
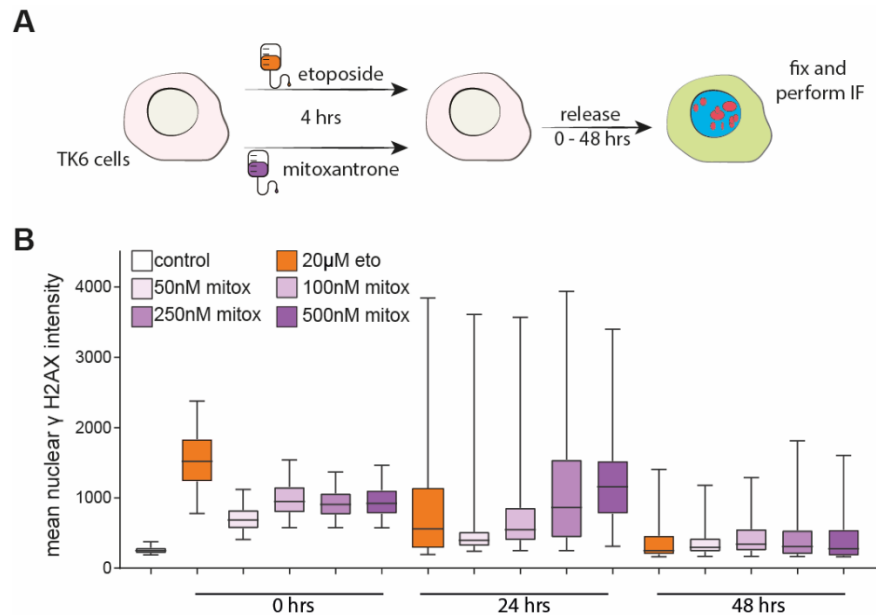
Figure Results 21: Mitoxantrone treatment leads higher levels of γH2AX signaling at lower concentrations than etoposide. **A)** Schematic of experimental setup. TK6 cells were treated with etoposide or mitoxantrone for 4 hrs before 2x wash and release into fresh media. Immediately or 24-48 hrs later, cells were fixed for IF analysis for DDR markers. **B)** Mean nuclear intensity of γH2AX signal after IF in cells treated with different doses of mitoxantrone or 20μM etoposide for 4 hrs and release for indicated time into fresh media.

Importantly, the frequencies of breaks induced by mitoxantrone in *PML* and *MLL* show no significant difference when analysed by qCRI-3D. 24 hrs after treatment release from 100nM mitoxantrone for 4 hrs, in wild type cells *MLL* is broken in around 1.0 ± 0.4% of studied nuclei whereas *PML* is broken in around 2.0 ± 0.5% (p > 0.05) of cells. Interestingly, after 48 hrs the insignificant difference vanishes and both loci show a breakage frequency of around 3.0 ± 1.0% (p > 0.05, see Figure Results 22 B). The same trend is observed for a higher dose of mitoxantrone. This could again indicate that mitoxantrone induced breaks do not occur immediately after treatment. However, a difference in DSB-site preference of mitoxantrone as observed on a nucleotide level [175] cannot be observed by qCRI-3D, potentially because the FISH probes span a very large genomic region (up to 500MB) thereby neglecting nucleotide specific effects.
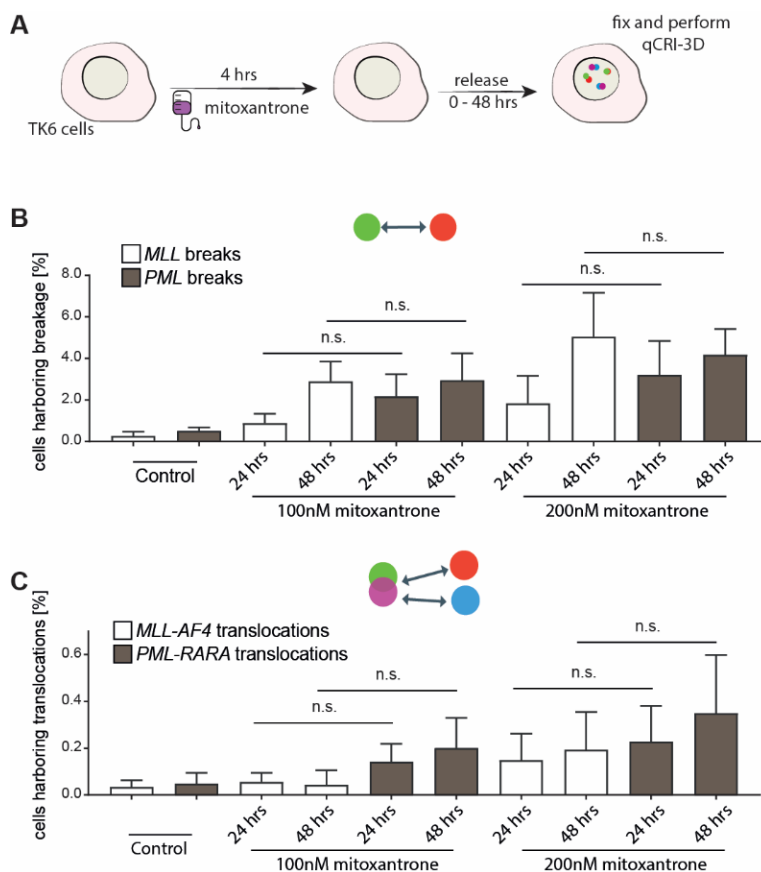
Figure Results 22: Mitoxantrone does not specifically induce *PML-RARA* translocations. A) Schematic of experimental setup. TK6 cells were treated with mitoxantrone for 4 hrs before 2x wash and release into fresh media. 24-48 hrs later, cells were fixed for qCRI-3D. **B)** DSBs at indicated genes as quantified by qCRI-3D (3D analysis) after acute treatment with indicated dose of mitoxantrone for 4 hrs and indicated time of release. Results from three independent experiments and significance according to student's t-test. n.s. $p > 0.05$ **C)** Chromosomal translocations between indicated genes as quantified by qCRI-3D (4-end, 3D analysis) after acute treatment with indicated dose of mitoxantrone for 4 hrs and indicated time of release. Results from three independent experiments and significance according to student's t-test. n.s. $p > 0.05$

Surprisingly, the resulting translocation frequencies differ after all and a higher translocation frequency between *PML* and *RARA* than between *MLL* and *AF4* can be observed after mitoxantrone treatment, even if the difference is again insignificant. Since these experiments were performed using the 3-end approach of qCRI-3D, re-doing the experiments using the 4-end approach with a higher number of imaged and analysed nuclei could potentially give a better resolution here. However, as of now the results do not allow any statement on site-specificity of mitoxantrone action and therefore cannot explain the specificity of the secondary malignancy this treatment induces. Other factors influencing this could be the cellular background where the malignancy occurs. Potentially, a *PML-RARA* translocation only gives rise to oncogenic potential in a certain cellular background in anaplastic precursor cells, which may have already prone the patient to the primary malignancy or disease.

Etoposide-induced DSBs and chromosomal translocations have been shown to rely on transcriptional activity and presumably blocked Top2 is converted to a DSB due to conflicts with the transcriptional machinery [69,71].
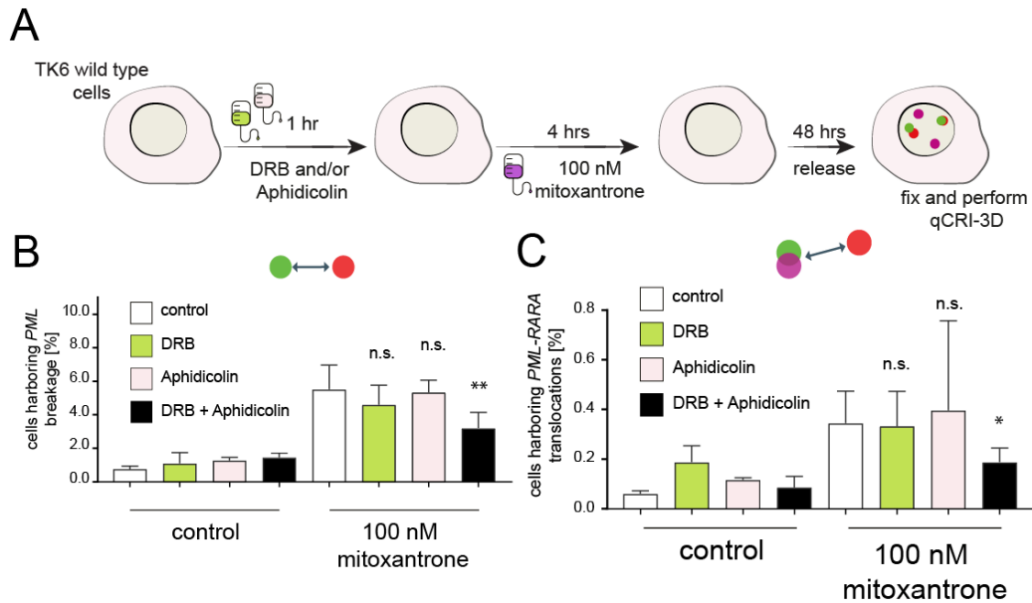
Figure Results 23: Mitoxantrone-induced DSBs and chromosomal rearrangements depend on the activity of replication and transcription. A) Schematic of experimental setup. TK6 wild type cells were treated for 1 hr with either the replication inhibitor Aphidicolin, the transcription inhibitor DRB or a combination of both. Then, 100 nM mitoxantrone were added and cells were released into fresh media following 4 hrs of incubation and two washes with PBS. 48 hrs later, cells were fixed in multi-well imaging plates and qCRI-3D was performed for the *PML* and *RARA* loci break-apart probes. **B)** DSBs in the *PML* gene as quantified by qCRI-3D (3D analysis). Results from three independent experiments and significance according to student's t-test. n. s. $p > 0.05$, ** $p < 0.01$ **C)** *PML-RARA* translocations as quantified by qCRI-3D (3-end, 3D analysis). Results from three independent experiments and significance according to student's t-test. n.s. $p > 0.05$, * $p < 0.05$

In order to investigate whether this is the case for mitoxantrone-induced genomic instability as well, TK6 cells were pre-treated with the replication inhibitor Aphidicolin [176], the inhibitor 5,6-dichloro-1-β-D-ribofuranosylbenzimidazole (DRB), which inhibits transcriptional elongation [177] or both inhibitors. Following 1 hr of pre-treatment, 100 nM mitoxantrone was added to the cells for 4 hrs. Cells were washed twice thereafter, transferred into new flasks with fresh media and fixed for analysis by qCRI-3D two days later (Figure Results 23 A). Here, we performed a 3-end qCRI-3D experiment where red and green FISH probes were flanking the *PML* gene and the farred probe the 5'end of the *RARA* gene. The distances between the resulting spot maxima were analysed in 3D and only cells were included in the analysis that had exactly two spots of each colour. Interestingly, pre-treatment with DRB or Aphidicolin alone had no significant influence on the resulting frequency of chromosome breaks at the *PML* locus or the formation frequency of *PML-RARA* translocations. Only a pre-treatment with a combination of both inhibitors led to a 50%

decrease in chromosome breakage and therefore translocations to a similar extent (Figure Results 23 B and C).

4.3.2 The absence of the VCP-proteasome system reduces etoposide induced DNA damage and cytotoxicity

It was shown in 2014 by Stingele et al. [157,178], that in budding yeast Top1 is extracted from DNA in a mechanism involving the newly characterized metalloprotease Wss1 (Sprtn in human cells) and Cdc48 (VCP in human cells). In recent years, VCP has been shown to play a role as a segregase in more and more processes within the nucleus, including DNA replication and repair [119,179–181]. In order to study whether VCP's function is needed in the resolution of Top2ccs or the transition of Top2ccs into DSBs, VCP can only be depleted from cells or its activity can be inhibited as it it's absence is lethal.

Known VCP inhibitors act allosterically (NMS-873) or by competing with ATP and inhibiting ATPase activity. CB-5083 is a potent and highly selective inhibitor of the D2 ATPase domain of VCP and has recently entered initial clinical trials as a chemotherapeutic drug [182,183].

Importantly, the effect is specific for etoposide and cannot be observed when inducing DSBs via the endonuclease AsiSI in DIvA cells but the VCP inhibitor NMS-873 alone induces low levels of γH2AX and pRPA in these cells as well as in regular U2OS cells treated with 4OHT (Figure Results 25). MG-132 has no such effect. In order to distinguish a signaling effect from a true reduction in genome instability, qCRI-3D was performed on the known etoposide-induced chromosome break points MLL (*KMT2A*), *AF4*, *AF9* and a locus on Chromosome 13 (Chr. 13-52-1) in Cal51 (Figure Results 26) and U2OS cells (not shown) was studied in presence and absence of VCP and proteasome activity.
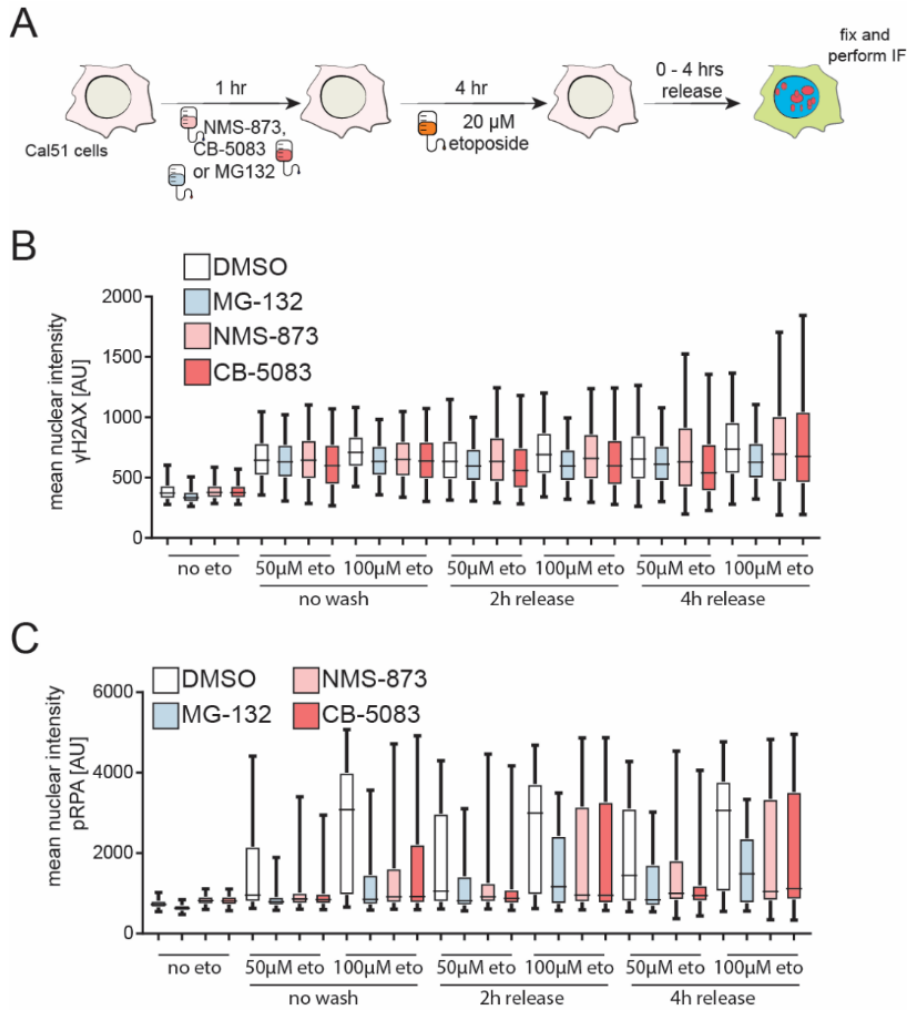
Figure Results 24: The absence of VCP or proteasome activity abolishes DDR signaling after etoposide treatment in Cal51 cells. A) Schematic of experimental setup. Cal51 cells were pre-treated with the proteasome inhibitor MG-132 (10µM) or the VCP inhibitors NMS-873 (5µM) or CB-5083 (1µM) before treatment with 50µM etoposide for 4 hours. Cells were fixed immediately thereafter or after 2 or 4 hours of release into media with the same inhibitor of the pre-treatment for immunofluorescence analysis for γH2AX and phospho-RPA (Ser4/Ser8) and the mean nuclear intensity of either signals is plotted here in **B)** and **C)** respectively.

Strikingly, the absence of VCP or proteasomal activity leads to an almost absolute ablation of chromosome breaks as detected by qCRI-3D. This effect is neither site-specific and nor cell line specific (Figure Results 26).
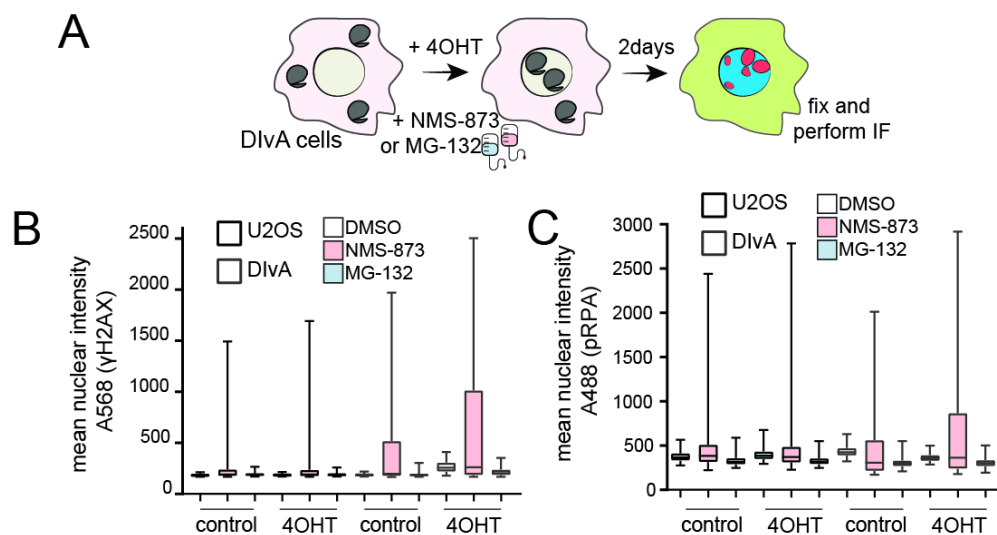
Figure Results 25: The absence of VCP or proteasome activity does not alter DDR signaling in DIvA cells. A) Experimental setup: DIvA cells were plated the day before treatment. 5µM NMS-873 or 10µM MG-132 were added to the cells in order to inhibit VCP or proteasome activity respectively. Nuclear transfer of AsiSI was induced by addition of 300nM 4OHT. Two days later, cells were fixed and stained for γH2AX and pRPA (Ser4/Ser8). The mean nuclear intensity of either signal is plotted in **B)** and **C)** respectively.

In the gene coding for MLL, Cal51 cells present a breakage frequency of around 3% directly after an acute treatment with 50µM etoposide for four hours. This is reduced to almost background levels of less than 2% in the absence of either proteasome or VCP activity when cells were pre-treated with specific inhibitors. Four hours after the wash-out of etoposide, the breakage frequency increased in etoposide-only conditions to 10 ± 7%, whereas it only reached around 3-4 ± ~2% under the conditions of pre-treatment with proteasome or VCP inhibitors. The effect is similar in the other loci studied here (see Figure Results 26C) as well as in U2OS and TK6 cells (not shown).

Since Top2-induced DSBs have been shown to rely on replication and transcription activity (among other processes), we studied the incorporation of EU or EdU depending on VCP or proteasome activity in the presence or absence of etoposide to eliminate the absence of these processes as the cause of absence of chromosomal breaks. Therefore, Cal51 cells were pre-treated with MG-132 or one of the before used VCP inhibitors and 30 minutes thereafter, EU was added to the cells for 30 minutes before addition of 20µM etoposide and fixation of cells 30 to 60 minutes thereafter. The Click-iT reaction was performed according to the manufacturer's protocol (Click-iT™ RNA Alexa Fluor™ 488 Imaging Kit, Invitrogen™).
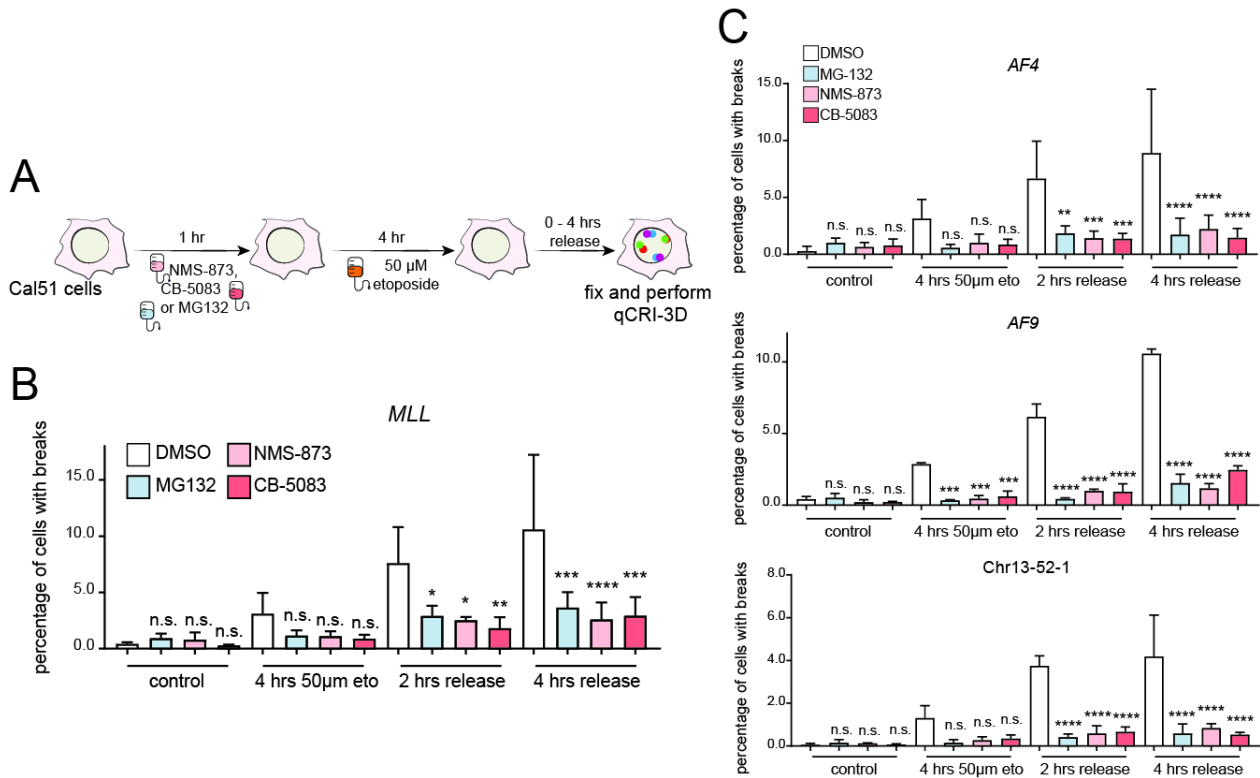
Figure Results 26: The absence of VCP or proteasome activity abolishes chromosome breakage after etoposide treatment. A) Schematic of experimental setup. Cal51 cells were pre-treated with the proteasome inhibitor MG-132 (10µM) or the VCP inhibitors NMS-873 (5µM) or CB-5083 (1µM) before treatment with 50µM etoposide for 4 hours. Cells were fixed immediately thereafter or after 2 or 4 hours of release into media with the same inhibitor of the pre-treatment for immunofluorescence analysis or for analysis of chromosomal breaks at *MLL* or *AF4*, *AF8* or a locus on Chr. 13. **B)** DSBs in the *MLL* gene as quantified by qCRI-3D (3D analysis). Results from three independent experiments and significance according to student's t-test. n. s. $p > 0.05$, * $p < 0.05$, ** $p < 0.01$, *** $p < 0.001$, **** $p < 0.0001$ **C)** DSBs in the indicated genes as quantified by qCRI-3D (3D analysis). Results from two (AF9) to three independent experiments and significance according to student's t-test. n. s. $p > 0.05$, * $p < 0.05$, ** $p < 0.01$, *** $p < 0.001$, **** $p < 0.0001$

Etoposide treatment alone leads to a decrease in EU incorporation but does not abolish it entirely as indicated by the slight increase of EU incorporation between 30 min and 1 hr of etoposide treatment. However, both proteasome inhibitors significantly decreased almost abolished the incorporation of the ribonucleotide analogue whereas both inhibitors of VCP had a less drastic effect. These results could indicate that proteasomal activity is needed for transcriptional activity or that protein accumulation due to a lack of proteasomal degradation stops transcriptional activity to prevent further protein accumulation in some kind of feedback-loop. The absence of transcriptional activity in the absence of proteasomal activity may therefore explain the lack of genome instability after treatment with etoposide.
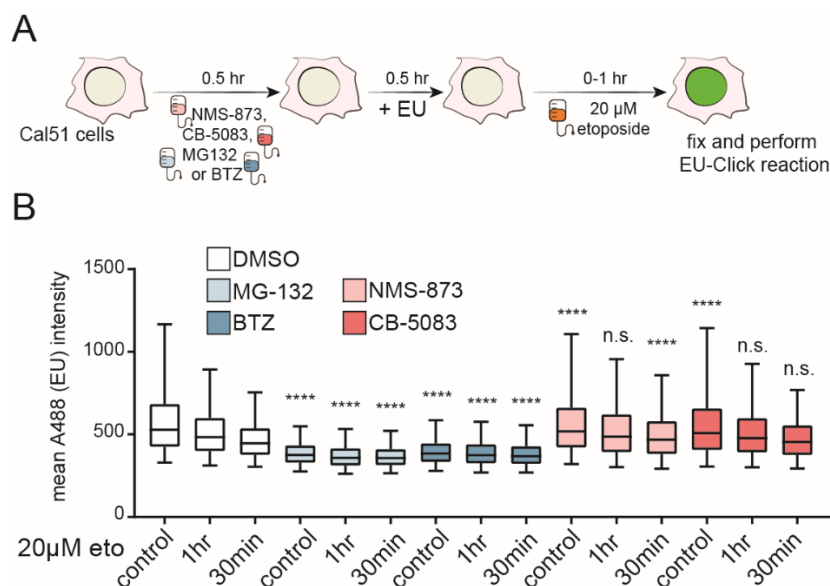
Figure Results 27: The absence of proteasomal activity abolishes transcriptional activity whereas the absence of VCP activity only has a minor effect. A) Schematic of experimental setup. Cal51 cells were pre-treated with 10μM MG-132, 1μM BTZ, 5μM NMS-873 or 1μM CB-5083 for 30 minutes prior to addition of EU. 30 minutes thereafter, 20μM etoposide was added to the cells, which were then fixed 30 to 60 minutes later for Click-iT reaction and analysis of nuclear EU signal by high-throughput imaging. **B)** Mean nuclear A488 [a.u.] signal as acquired by high-throughput imaging on an Opera Phenix HCS microscope and analyzed using Harmony image analysis software.

VCP inhibition on the other hand, does not alter transcriptional activity to the same extent as proteasome inhibition and could therefore act via a different pathway. If not by preventing the transcriptional machinery to collide with and Top2ccs, maybe by acting on the resolution of Top2ccs.

As it has been shown before that Top2 levels drop after addition of etoposide[110] and that this degradation relies on proteasomal activity [123,185], we went on to test if also the inhibition of VCP would decrease the degradation of Top2 after etoposide treatment. In order to do so, U2OS cells were plated evenly on 6 cm dishes a day before the experiment so they would reach 50% confluence the next day. Cells were then pre-treated with the proteasome inhibitor MG-132 (10μM), the VCP inhibitor NMS-873 (5μM) or the VCP inhibitor CB-5083 (1μM) for 30 minutes prior to the addition of 100μM etoposide for 1 hr. Cells were then rapidly harvested and whole cell extracts enriched for the nuclear protein fraction were collected.

The resulting immunoblot against Top2A and Top2B (see Figure Results 28) shows the degradation of both isozymes upon addition of etoposide. Furthermore, we were able to also see the rescue of Top2A and Top2B presence in the absence of proteasomal activity in the samples from cells pre-treated with MG-132. For the samples from cells pre-treated with either of the

studied VCP inhibitors, a small decrease in Top2B degradation can be observed, but it remains unclear whether also Top2A degradation is reduced.
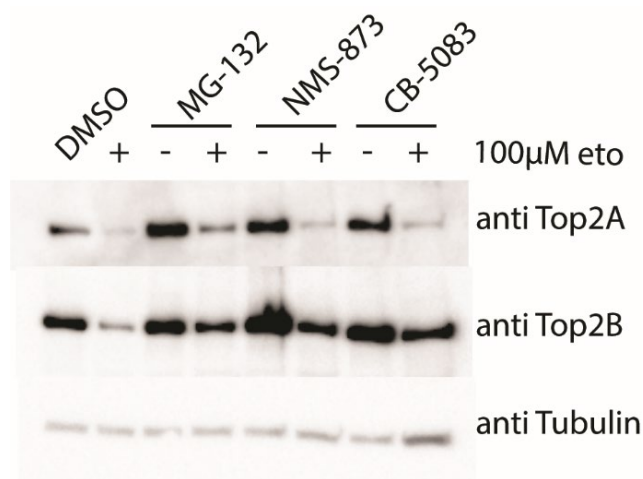
Figure Results 28: Top2 is stabilized after etoposide treatment in the absence of proteasome or VCP activity.

Taken together, these results suggest that Top2ccs are modified by both the proteasome and VCP activity and that this processing allows the cell to identify the Top2cc as a source of DNA damage. If this process is connected to the activity of the transcription machinery or if transcription machinery and Top2cc need to collide in order to activate VCP or the proteasome remains to be determined. Additionally, it remains unclear whether VCP acts downstream of the proteasome as it does in many other cellular processes, and whether VCP modification necessarily leads to the degradation of the protein part of Top2ccs by the proteasome.

5 Discussion and Conclusions

5.1 Implementing a co-localization threshold improves comparability of chromosome rearrangement frequencies obtained by ddPCR and qCRI-3D

While the rare occurrence of chromosomal rearrangements is good news in general, this fact on the other hand makes it difficult to study how they form. If a chromosomal rearrangement gives a growth advantage to a certain cell, the cell has the potential to eventually overgrow the rest of the cell population. This in turn can be the start of tumour growth.

Therefore, during my PhD we set out to improve an available, population-based method that is compatible with high-throughput approaches and results in unbiased observations. qCRI-3D has improved in specificity compared to the previously used method [153] through the addition of a fourth FISH probe and the possibility to incorporate a second spot-to-spot distance threshold. Furthermore, we now calculate spot-to-spot distances as Euclidean distances in 3D, which allows us to also detect probe separation along the z-axis, meaning chromosome breaks, and less false positive colocalisation events, meaning falsely detected chromosomal rearrangements. Detected chromosomal rearrangement frequencies by qCRI-3D thereby reach the same order of magnitude as frequencies observed by a PCR-based approach, while before qCRI-3D detected up to 10-times more translocation events than the applied ddPCR.

One of the main benefits of qCRI-3D is the fact that it is based on high-throughput imaging. This allows the deployment of different DSB-inducing methods studying the formation of the same chromosomal rearrangement or changes in DSB-susceptibility. As we wanted to understand which EJ pathway is responsible to translocation formation in human cells, we compared break and translocation frequencies between different isogenic cell types. In order to state which EJ factor changes the formation of chromosome rearrangements in one way or the other, it was not necessary to employ the most accurate version of qCRI-3D (4-ends, 3D analysis, two distinct thresholds). It was sufficient to make these observations by using the simplest setup with three FISH probes and an analysis in 2D with only one threshold that separated fused from broken loci. In fact, in the case of irradiation with X-rays, where we used a dosage of up to 30 Gy, the cellular genomes were shattered and ploidy was altered. Therefore, we had to use less restrictive thresholds and filters, e .g. by not only including cells with exactly two spots of each colour in the analysis but also those that had at least two of each colour. This way, a higher number of false positive cells will be admitted in the analysis as can be seen by the higher frequencies in control

conditions. qCRI-3D seems to overestimate the frequencies of illegitimately fused chromosomes as it cannot distinguish between random co-localisation and real fusions. However, it still allows comparing the influence of the absence of a certain factor on the changes on detected translocation frequencies.

The accumulation of absolute numbers of rearrangement events requires the use of the most specific and sensitive approach of qCRI-3D: 4-ends, 3D analysis and two separate thresholds and works best in conditions when the number of alleles of the studied loci does not change.

5.2 The absence of DNA ligase 4 leads to increased DSE resection partially explaining a controversy in the translocation research field

If a DSB is formed, it is usually rapidly repaired via the cNHEJ pathway, which re-ligates the broken ends and sometimes incorporates single nucleotide changes or deletions [4]. If cNHEJ is inhibited, aEJ can act. This competition is most likely tilted towards an over-representation of cNHEJ by the sheer abundance of its factors [22]. My studies underline the fact that cNHEJ is needed to resolve DSB quickly and correctly. In the absence of cNHEJ, DSEs can undergo alterations such as resection, leading on one hand to larger deletions in the region of the DSB and on the other hand, leaving the DSB unrepaired for a long time, increases the chance that the two DSEs dissociate and cannot be fused directly. This in turn increases the risk of chromosomal rearrangements.

Which of the two EJ pathways is responsible for the formation of oncogenic chromosome rearrangements has been studied in the past years using different cellular model-systems and different methodologies as read-out. A number of studies made use of tailor-made, site-specific endonucleases or incorporated site-specific restriction enzymes into the cellular genome [36,147,186–188] while others made use of physiological but random ways of DSB-induction [189,190]. Methodologies used as read-out of the formation of chromosomal translocations and their frequency include imaging [80,153], population PCR for fusion genes [102] and proof of presence of resulting fusion transcripts [189].

While for a long time, the studies in cells from murine origin showed consistently that translocations increase in the absence of cNHEJ, indicating that aEJ would be the pathway responsible for their formation [33,36,191,192], more recent studies in human cells using PCR-based approaches to quantify translocation formation showed the opposite [101].

qCRI-3D gives the advantage that it can be used using any kind of DSB-inducing method to study specific chromosome translocations. Using it in a combination of isogenic HCT116 cell lines null

for different factors from either cNHEJ or aEJ, we could show that independently of the method used to induce DSBs (Top2 poison or irradiation), the absence of cNHEJ factors led to an increase in break appearance and persistence as well as chromosome translocation formation. The same is true for TK6 cells where we compared wild type and *LIG4*-/- cells. This suggests that cNHEJ is needed to protect cells from translocation formation.

However, using ddPCR to quantify chromosome translocation frequency, we were surprised to detect less translocations in TK6 Cas9 *LIG4*-/- cells as in wild type cells after CRISPR induction. Interestingly, using a resection assay, we could show that the DSEs in TK6 Cas9 *LIG4*-/- cells were resected to a great extent partially as far as 1.3 kB away from the CRISPR site. We could not observe similar trends in any other condition we studied using cell lines with site-specific DSB induction. Importantly, this suggests that using PCR-based approaches to detect and quantify chromosome rearrangements could underestimate their formation due to resection or other alterations of the DSEs involved.

The extended resection could be a result of the cells adaptation towards the genomic deletion of *LIG4* as using the DNA Ligase 4 inhibitor SCR-7 did not have a similar effect in TK6 Cas9 cells. In order to investigate this further, it would be necessary to either study several isogenic TK6 Cas9 *LIG4*-/- cell lines and ideally, to further extent the analysis towards either DIvA *LIG4*-/- cells, HeLa Cas9 *LIG4*-/- cells or TK6 AsiSI-ER cells (as comparison to DIvA cells). We were however not able to obtain either of these cell lines during my studies.
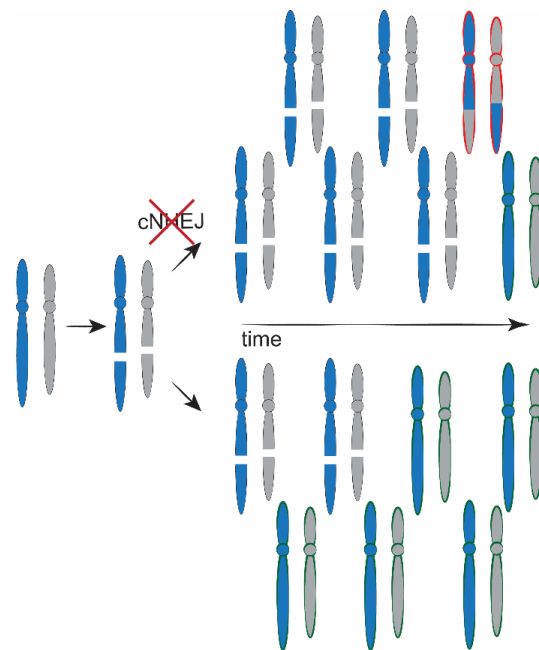
Figure Discussion 1: Working model of the influence of and dependency on cNHEJ in the formation on chromosomal rearrangements.

In the end, the results obtained in this part of my studies suggest, that cNHEJ is probably causing genomic rearrangements under wild type conditions, as it is the fastest pathway to act. Nevertheless, in the absence of cNHEJ, DSEs remain unrepaired for a longer time, which increases the probability of them being fused to an incorrect partner DSE.

The above-described results should however also make us aware that the effect of a genomic deletion of a certain gene in a clonal cell population should be studied extensively by using several different clones before making conclusions about the effect of this deletion on cellular processes the absent protein is directly involved in. In our case, the deletion of LIG4 could have altered the dependency on the other DSB repair pathways and potentially increased resection rates to unveil larger stretches of homology that these pathways rely on.

5.3 Mitoxantrone-induced DSBs and chromosomal translocations depend on different cellular processes than the ones induced by etoposide

Mitoxantrone and etoposide are both widely used in the clinics as therapeutic or, in the case of mitoxantrone, therapy against multiple sclerosis. Both chemicals are so-called Topoisomerase-2-poisons which means that they disrupt the catalytic cycle of Top2 and both come with a risk of inducing secondary malignancies involving chromosome translocations. While etoposide induces translocations involving the *KMT2A* gene (*MLL*) that codes for the methyl-transferase MLL1, mitoxantrone induces translocations between the genes *PML* and *RARA*, which encodes the retinoid-receptor alpha.

MLL translocations can lead to the development of acute myeloid leukaemia (AML) whereas *PML-RARA* translocations are pre-dominantly responsible for anaplastic promyelocytic leukaemia (APL), a sub-type of AML. Previous studies have shown that both Top2 poisons show mechanistic differences [107,110,138] and importantly, mitoxantrone shows a very significant breakage pattern in *PML* where breaks cluster within a region of only 8 bases of intron 6 [193].

In my studies using both Top2 poisons and investigating the differences in the frequency of either *MLL* or *PML-RARA* translocations, we could not see a striking difference in the formation of one translocation over the other. However, we observed differences in the cellular mechanism underlying the genomic instability upon addition of mitoxantrone or etoposide. While in both cases transcriptional activity coincides with genomic instability, mitoxantrone (other than etoposide) leads to genomic instability even in the absence of transcriptional activity and genomic instability after mitoxantrone treatment is only abolished if replication is disrupted as well.

This also goes along with the finding that, mitoxantrone induced breaks depend on the presence of both Top2 isozymes whereas etoposide-induced breaks rely largely on the presence of Top2A, which is active throughout the cell cycle unlike Top2B that is expressed in late G2- and S-phase only.

To finally understand why one chemotherapeutic drug favours one chromosome translocation over the other, further studies will be needed studying e.g. differences in binding affinity and mechanism of drug action on activity of the two Top2 isozymes. While it has been shown that mitoxantrone intercalates in the major groove of the DNA double helix [194], this was not observed for etoposide, prompting towards one difference in action. The precise site-specificity of the 8 Bp breakpoint cluster region in *PML* intron 6 can however not fully be explained by this.

5.4 The absence of VCP or proteasome activity abolish chromosome breakage after etoposide treatment

How Top2ccs are eventually converted to DSBs is only partially understood. While collisions with transcription machinery and loop extrusion have been shown to lead to DSBs after etoposide treatment [69], the proteasome has furthermore been shown to be involved in the resolution of Top2ccs [71]. The hexameric AAA+ enzyme VCP has been shown to be involved in many cellular processes where protein remodelling is needed, often to hand the remodelled, segregates protein to proteasomal degradation. In order to find out whether VCP lie the proteasome is as well involved in Top2 segregation following treatment with a Top2 poison, we investigated DDR signalling and DSB induction using qCRI3D. During my PhD studies we could further show, that the inhibition of the proteasome not only abolishes the DDR signalling after etoposide treatment but that VCP inhibition has a similar effect. Importantly, inhibiting either enzymatic complex also abolishes the dissociation of the DSEs as detected by qCRI-3D and this effect is specific for etoposide-induced DSBs as it has no effect on break induction in DIvA cells, but can be observed after etoposide treatment in several different cell lines.

Since etoposide-induced breaks largely depend on the presence of transcription activity, we studied whether transcription was perturbed under VCP inhibition. Interestingly, transcription is running un-perturbed in conditions of VCP inhibition whereas it slows down during inhibition of the proteasome. The absence of transcriptional activity is therefore likely not the cause for the remaining genome stability after etoposide treatment following pre-treatment with a VCP inhibitor.

Very recently, it was proposed that inhibition of the proteasome stopped Top2ccs from being resolved in the presence of etoposide. When etoposide was washed out, the remaining Top2ccs were able to fulfil their enzymatic cycle and detached from the previously re-ligated DNA strand [185]. Top2 was not degraded in the absence of proteasomal activity. During my studies, we could show that the inhibition of VCP had a similar effect on Top2 degradation as the levels of both Top2 isozymes were stabilized after etoposide treatment in conditions of VCP inhibition. If VCP inhibition also allows Top2 to fulfil its catalytic cycle when etoposide is washed out remains however to be investigated – as does the influence on cell cytotoxicity. Since VCP is an essential enzyme in human cells especially during late S-phase, where it is involved in the separation of sister chromatids [181], inhibition of VCP leads to cell death and it is currently under investigation in clinical trials as a chemotherapeutic target. If inhibition of VCP would lower the effect of Top2 poisons as chemotherapeutic drugs, a combination of both therapies should carefully be studied.

Taken together, the results from literature and my studies indicate that the protein part of Top2ccs is degraded in the presence of VCP and the proteasome, which opens up a free DSB. Why this mechanism evolved and why it is useful for cell remains unclear to me. One explanation could be that a persistent Top2cc is more dangerous to the cellular genome integrity than an open, re-ligatable DSB.

6 Materials and Methods

6.1 Culturing of cell lines

TK6 cell lines and derivatives were maintained at 37°C and 5% CO_2 in RPMI-1640 with 5% horse serum (Gibco), 2mM L-glutamine, 100U/ml penicillin, 100µg/ml streptomycin, and 100µM sodium-pyruvate. HCT116 and Cal51 cell lines were maintained at 37°C and 5% CO_2, in RPMI-1640 with 10% fetal bovine serum (Gibco), 2mM L-glutamine, 100U/ml penicillin, and 100µg/ml streptomycin. U2-O-S derived cell lines as well as HeLa and HEK293T cells were maintained at 37°C and 5% CO_2 in DMEM with 10% fetal bovine serum (Gibco), 2mM L-glutamine, 100U/ml penicillin, and 100µg/ml streptomycin.

6.1.1 Irradiation of cells

Irradiation dependent DNA breaks and translocations were generated by irradiation of cells using a CellRad irradiation device (Faxitron, 0.5mm aluminum filter, turntable on, 130kV, 5mA) with an accumulated dosage of 5 to 20Gy for HCT116 wild type cells to model *NPM-ALK* translocations. An accumulated dosage of 10Gy was used to irradiate TK6 Cas9 wild type and *LIG4-/-* cells and 20Gy to irradiate isogenic HCT116 cell lines (wild type, *LIG4-/-*, *XLF-/-*, *nucLIG3-/-*, *PARP1-/-*) in order to compare *MLL-AF9* translocation frequencies between mutant cell lines. Media was changed immediately after irradiation and cells were fixed two to three days later on coverslips. C-Fusion 3D was performed using the break-apart probes for *NPM* and *ALK* (HCT116 wild type translocation modelling, in 3D), *MLL* break-apart and an additional *AF9* probe (isogenic HCT116 cell lines, in 2D) or break apart probes of both genes of interest (TK6 Cas9 cell lines, in 3D).

6.1.2 Mitoxantrone treatment

In order to induce DNA damage by the Top2 poison mitoxantrone, TK6 cells were treated with 50 to 200nM mitoxantrone (in DMSO, SigmaAldrich, M2305000) for 4hrs followed by immediate two washes and release into fresh media in fresh flaks. Cells were fixed two days later and C-Fusion 3D was performed with the break-apart probes for *PML* and *RARA* in 3D or as a 3-end version with only the 5'probe for *RARA*.

6.1.3 Etoposide treatment

Etoposide dependent DNA damage was induced by treating TK6 wild type cells with 20 to 30µM etoposide for 4hrs, washed and released into fresh media before fixation two days later. *MLL-AF9* translocations were induced in TK6 Cas9 wild type and *LIG4-/-* cells using 20µM etoposide for 4hrs in order to compare resulting translocation frequencies. Etoposide was washed out and cells released into fresh media before fixation two days later. C-Fusion 3D was performed using *MLL*

and *AF9* break-apart probes in 2D and 3D in order to compare both analysis pipelines. *MLL-AF9* translocation frequencies were compared in isogenic HCT116 cell lines (wild type, *LIG4-/-*, *XLF-/-*, *nucLIG3-/-*, *PARP1-/-*) by treating cells with 50µM etoposide for 4hrs, wash out and release into fresh media. Cells were fixed on coverslips two days later and C-Fusion 3D was performed in 2D using the *MLL* break-apart and an additional *AF9* probe.

6.1.4   DSB induction via AsiSI

Endonuclease induced translocations were studied using the previously described DIvA system [170]. Briefly, DIvA cells are derived from U-2-OS and stably express the sequence specific endonuclease AsiSI fused to an estrogen-receptor tag. In order to induce nuclear localization of the enzyme, 300nM 4-Hydroxy-Tamoxifen (4OHT) was added to the cells for two days following fixation on coverslips or in multi-well plates with 4%PFA or extraction of genomic DNA (Qiagen DNeasy kit). In order to compare translocation frequencies between wild type and DNA ligase 4 deficient cells, siRNA mediated knockdown (ThermoFisher Silencer® Select, s8181, 40nM) was performed using Lipofectamine RNAiMAX (Thermo Fisher) three days prior to 4OHT addition. For 3D translocation quantification via qCRI-3D, break-apart probes of two loci at a time were used.

6.2   Generating Cas9 expressing TK6 and HeLa cell lines

Mre11loxP/H129N, TDP2-/-, and LigIV-/- lymphoblastoid TK6 cells have been previously characterized [20,195]. In order to generate stably Cas9 expressing TK6 or HeLa cell lines, these cell lines were virally transduced with a Cas9 lentiviral expression vector (pLenti-Cas9 Blast, Addgene #52962, kind gift from Feng Zhang). In brief, lentiviral particles were produced in HEK293T cells by transfection with 4µg of the Cas9 lentiviral expression vector and 1µg of each third generation lentiviral packaging plasmids pMDLg/pRRE, pRSV-REV, pMD2.G (Addgene plasmids #12251, #12253 and #12259 respectively, all kind gifts from Didier Trono) using X-tremeGENE™ HP DNA Transfection Reagent (Roche). Virus containing supernatant was pooled on two consecutive days from two transfected HEK293T dishes transfected with the same plasmids and 100x concentrated using Lenti-X™ Concentrator (TaKaRa). The concentrated virus was then added to 10,000 TK6 wild type, LIG4-/- or MRE11loxP/H129N cells or 1 million HeLa cells together with 8µg/ml Polybrene. One day after infection, media was changed and 5µg/ml Blasticidin was added for selection. Clones from single cell dilutions in 96-well plates were checked for Cas9 expression and activity by immunoblotting, immunofluorescence microscopy (Cas9 antibody, ActiveMotif, #61577) and T7 endonuclease assay following electroporation of cells with specific gRNAs.

6.3 CRISPR mediated induction of chromosome breaks

TK6 and HeLa Cas9 cells were electroporated using the Neon electroporation device (Thermo Fisher) according to manufacturer's protocol with crRNA-tracrRNA complexes 12 hrs to two days before fixation of cells on coverslips with 4% PFA or extraction of genomic DNA (DNeasy kit, Qiagen). In order to model chromosome rearrangements between *MLL* and *AF9*, *ENL* or *HYLS1*, cells were electroporated with 8μl of each specific gRNA complex or 16μl of non-target gRNA complex. In order to study resection at a specific locus (*MLL* or *RBMXL1*), cells were electroporated with 16μl of the specific or the non-target gRNA complex.

6.3.1 Electroporation of TK6 or HeLa Cas9 cells with crRNA-tracrRNA complexes

For crRNA-tracrRNA complex (gRNA complex) formation, equal amounts of both RNAs (100μM in 10mM Tris, pH7.4) were mixed, heated to 95°C for 5 minutes and cooled down to room temperature.

Per electroporation reaction, 1Mio. TK6 Cas9 cells were washed in warm PBS and suspended in 100μl buffer R before addition of a total of 16μl gRNA complexes. If more than one locus was targeted at a time, 8μl of each gRNA complex were added. Electroporation with the 100μl Neon pipet tip was performed in three pulses at 1350V for 10msec each and cells were released in 5ml fresh and pre-warmed medium.

Per electroporation reaction, 5Mio. HeLa Cas9 cells were washed in warm PBS and suspended in 100μl buffer R before addition of a total of 16μl gRNA complexes. If more than one locus was targeted at a time, 8μl of each gRNA complex were added. Electroporation with the 100μl Neon pipet tip was performed in two pulses at 1,005V for 35msec each and cells were released in 10cm dishes with 10ml fresh and pre-warmed medium.

If more than cells were needed per experiment, cells undergoing the electroporation procedure with the same gRNA complexes were pooled immediately after electroporation.

6.4 Immunofluorescence

For immunofluorescence, adherent cells were grown in 96- or 384- well plates (Perkin Elmer 6005550, 6007550, 6055302 or 6057300) that were coated with poly-L-lysine (PLL, Sigma-Aldrich), were fixed in 4% formaldehyde for 15 min and washed three times with PBS. Suspension cells were gently spun down on multi-well plates and mixed with PFA at a final concentration of

4% for 15 min. Cells were permeabilized with 0.3% TritonX-100 in PBS and washed three times with PBS. Cells were treated with blocking buffer (3% BSA in PBS) for 1 hour before incubation with primary antibodies in blocking buffer overnight. Cells were then washed three times in PBS and incubated for 1h with fluorescently labeled secondary antibodies. After three PBS washes, DNA was stained with Hoechst 33342 (Sigma-Aldrich) and cells were washed three times with PBS before imaging.

Primary antibodies used in this study: γH2AX (Millipore 05-636, 1:1000), Phospho-RPA32(S4/S8) (Bethyl A30-245A, 1:2000), Cas9 (Active Motif 61577, 1:1000), 53BP1 (Novus Biologicals NB100-304, 1:5000). Secondary antibodies used in this study: Alexa Fluor 568 anti-mouse IgG (Invitrogen A10037, 1:1000), Alexa Fluor 488 anti-rabbit IgG (Invitrogen A11034, 1:1000), Alexa Fluor 568 anti-rabbit IgG (Invitrogen A11011, 1:1000) , Alexa Fluor 488 anti-mouse IgG (Invitrogen A-21202, 1:1000).

Images were acquired using the "Opera Phenix High Content Screening System" (PerkinElmer) and were analysed by automated "Harmony High Content Imaging and Analysis Software" (PerkinElmer) as indicated below.

6.5   Western blotting

Total cell lysates were either prepared by directly lysing cell pellets in SDS-page loading buffer or, for comparative analysis, prepared by lysis in RIPA buffer followed by extraction of proteins from chromatin by sonication (BioRuptor, 30sec, 7 cycles) and addition of 1/10th volume of 5M NaCl. Protein concentration was determined using Bradford reagent (Bio-Rad 5000205). Samples were subjected to electrophoresis on pre-cast 4%–15% gels (Bio-Rad 4561086, 4561085DC) and transferred to PVDF membranes (Merck, IPFL00010) as previously shown (Roukos et al., 2007; Stathopoulou et al., 2012). After blocking in blocking buffer (PBS-T with 5% milk, Sigma-Aldrich, 70166), immunodetection was performed by incubating the membranes overnight at 4°C with primary antibodies diluted in blocking buffer. Membranes were incubated with secondary peroxidase-coupled antibodies in blocking buffer at room temperature for 1 hr. ECL-based chemiluminescence was detected with WesternBright chemiluminescence substrate Sirius (Biozym Biotech, 541021) following manufacturer's instructions.

Primary antibodies were used at the indicated dilutions: TOP2A (Santa Cruz sc-166934, 1:500), TOP2B (Santa Cruz sc-365071, 1:500), DNA Ligase 4 (Abcam 193353, 1:1000), Tdp2 (Bethyl A302-737A, 1:2000), Mre11 (Cell Signaling Technologies 4895, 1:1000), Alpha-Tubulin (Sigma Aldrich T5168, 1:2000), DNA Ligase 1 (Santa Cruz 271678, 1:500), UFD1L (Novus Biologicals

NBP2-61829, 1:500), ZFAND2B (Novus Biologicals NBP1-89174, 1:500), NPLOC4 (Novus Biologicals NBP1-82166, 1: 500), PLAA (Sigma Aldrich HPA020996, 1:1000), VCP (Cell Signaling Technologies 2648, 1:500), DNA Ligase 3 (GeneTex 70145, 1:1000), XLF (Abcam 33499, 1:500), Parp1 (Cell Signaling Technologies 9532, 1:1000).

Secondary antibodies were used as follows: anti-mouse IgG HRP-linked (Cell Signaling Technologies 7076, 1:1000), anti-rabbit IgG HRP-linked (Cell Signaling Technologies 7074, 1:1000), anti-goat IgG HRP-linked (Santa Cruz 2354, 1:1000).

6.6 Chromosome break and rearrangement quantification using fluorescent *in-situ* hybridisation

6.6.1 Fluorescent *in-situ* hybridization with probes from BACs

Three-dimensional FISH probes were generated from bacterial artificial chromosomes (BACs, from BACPAC Resources Center or Thermo Fisher Scientific) complementary to the genomic region of interest by direct labeling via nick translation with fluorescently labeled dUTPs (Chromatide AlexaFluor A488-5-dUTP, A647-5-dUTP and A568-5-dUTP from Life Technologies; CF405S-dUTP from Gentaur) using a nick translation kit according to manufacturers protocol (Abbott Molecular). Sequence specificity of all probes was verified by PCR. For 3D FISH in suspension cells, cells were plated on poly-L-lysine (PLL) coated glass coverslips (22×22mm, 150µm thick, Neuvitro) in 24-well plates (one million cells/well) or in PLL-coated multi-well plates (PerkinElmer 96- or 384-well CellCarrier or CellCarrier Ultra) and centrifuged at 1000-400rpm for 20s. Adherent cells were grown on PLL-coated coverslips or in PLL-coated multi-well plates (PerkinElmer 96- or 384-well CellCarrier or CellCarrier Ultra; 6005550, 6007550, 6055302, 6057300) for at least 12 hours before fixation. After fixation in 4% paraformaldehyde/phosphate-buffered saline (PBS) for 15min, cells were permeabilized (20min in 0.5% Saponin (Sigma Aldrich)/0.5% Triton X-100 (Sigma Aldrich) in PBS) and incubated in 0.1N HCl (15min) with PBS washes between steps. Cells were washed in 2× SSC and incubated in 50% formamide/2× SSC buffer at least 30min. The probe mix (40ng of A488 and A568 and 60ng of A647 and CF405 probe, 3µg human COT-1 DNA (Roche) and 20µg yeast tRNA (Ambion) per sample) was ethanol precipitated, suspended in hybridization buffer (10% dextran sulfate (Sigma Aldrich), 50 % Formamide (Sigma Aldrich), 2× SSC, and 1% Tween-20 (Sigma Aldrich)) and added to each coverslip or well (7µl for coverslips, 15µl for 384-well plates or 30µl for 96-well plates).

Denaturation of cellular DNA and probes was performed at 85°C for five (coverslips on glass slides) or ten (multi-well plates) minutes and hybridization in a humidified chamber overnight at 37°C. Excess probe was removed by three 5-minute washes in 1× SSC at 45°C, followed by three 5-minute washes in 0.1× SSC at 45°C. Coverslips were mounted on glass slides (Tekdon, Myakka City, FL, USA) using Vectashield (Vector, Burlingame, CA, USA; H-1000 or H-1200 with DAPI) and sealed with picodent twinsil (Picodent 1300 1000).

If FISH was performed in multi-well plates and DNA needed to be stained, cells were washed three times with PBS after SSC washes followed by 15 minutes incubation with 1:3000 HOECHST in PBS and additional three PBS washes. Cells in multi-well plates remained in PBS for imaging.

6.6.2   High-throughput imaging

Imaging of mounted coverslips or multi-well plates was performed on an OperaPhenix high content screening confocal microscope (PerkinElmer, Waltham, MA, USA) running Harmony 4.7 or 4.8 software, equipped with a slide holder adaptor using a Planar Apochromatic 40× water immersion lens (Olympus, NA = 0.8) and 1.3 MegaPixel CCD cameras with pixel binning of 2, corresponding to a pixel size of 299nm. DAPI, Alexa488, Alexa568 and Cy5 images were sequentially acquired in more than 50 fields per coverslips in separate exposures using 9 to 15 z-planes (0.5-0.8µm apart). Typically, at least 8000 TK6 derived cells and at least 2000 HCT116 or U2OS derived cells were imaged per experimental condition.

6.6.3   Automated image analysis

6.6.3.1   Image analysis in Harmony

Image analysis was performed using custom-made building blocks in the Harmony software (modified from [153]). In brief, nuclei were segmented based on the DAPI or fluorescent background signal in maximally projected images. Images are analysed in a fully automated fashion to detect cell nuclei and FISH signals. FISH spots in all four channels are identified based on detection of local signal maxima in each probe channel. Image analysis exports spot-to-spot Euclidian distances by using the image x and y coordinates of each FISH spot in the maximally projected images whereas the plane in z with the local signal maxima of each spot is also exported as independent text files.

6.6.3.2   Derivation of Euclidean 3D distances between spot pairs

To determine 3D distances between spots, the Euclidean distances of spot distances from maximum projections and distances between z-planes were calculated. Distances between z planes of spots of different color were corrected for shifts due to chromatic aberration in z. This is due to the fact that fluorophore of different colors are shifted in the third dimension (Finn et al., 2017). To determine the z-shift, a genomic locus was marked with a BAC probe that was labelled with all different colour fluorophores. From this, the pairwise shifts in z between the different channels were measured and a correction value was calculated (Green: –0.768, FarRed: 0.255, Blue: –0.146). For 3D evaluations, the z-plane of spots that had the maximum pixel intensity was changed according to the defined correction value for each colour-combination, whereby each spot in every channel was corrected according the identified shift between the different channels in z. The following formula was used to determine z-correction values:

$$\left(1 - \frac{top.count}{top1 + 2.count}\right) \times \Delta distance + top.distance$$

top.distance = the distance most often observed
top.count = the count of top.distance
top1 + 2.count = the count of the two most often observed distances
Δdistance = the difference of the top two distances

For the determination of proximity or separation of spot pairs, only the minimal distance of one pot to spots of other channels was considered. This is necessary as in in diploid cells for example each Green spot has two distances to both Red spots. Taking the smaller of the two distances secures with high probability that the distance to the spot on the same chromosome is analysed.

6.6.3.3   Chromosome breakage and analysis of chromosome rearrangements

To discern chromosome loci that experienced damage and breakage from intact loci, we established a thresholds of physical separation and proximity (Burman et al., 2015). The distribution of intrachromosomal distances was evaluated in non-damaged control cells by evaluating Green-Red and FarRed-Blue distances. We defined a threshold of 1.2 μm to 1.4 μm (corresponds to 4.0 to 4.7 pixels) for separation or proximity, where distances smaller or equal the threshold were considered intact and distances of more than 1.2 to 1.4 μm were seen as separations.

For detection of chromosome breaks, inversions and translocations, To eliminate cases of falsely identified or missed spots, only cells with the same number of Green and Red spots, or FarRed

and Blue spots respectively, were considered in the analysis to eliminate cases of falsely identified or missed spots. The number of spot pairs was defined based on the ploidy of cells. For TK6 Cas9 cells, only cells with two signals in all channels were considered in the analysis whereas for K562 HCT116 cells or TK6 after irradiation, for example, cells with more than two but equal spot number were also analyzed. A cell was considered positive of a chromosome breakage event, when at least one Green FISH spot that had a minimum Green-Red distance of more than the 1.2 µm threshold or when a FarRed FISH spot had a corresponding minimum FarRed -Blue distance of more than the threshold. Cells were assigned positive for synapsis when Green-FarRed FISH spot distances were less or equal than the threshold. For 4-color FISH, a cell was considered positive of a chromosome translocation when three conditions were met concomitantly in one cell:

    1) a Green FISH spot had a Green-Red distance of more than the threshold

    2) the same Green FISH spot had a minimum Green-Blue distance of more than the threshold

    3) the same Green FISH spot had a minimum Green-FarRed distance of less than the threshold

In a 3-color C-Fusion 3D approach, a cell with a translocation was assigned when the first and third criteria were met, i.e. at least one Green FISH signal had a minimal Green-Red distance of more than the threshold and a concomitant Green-FarRed distance of fewer than the threshold.

A cell was considered to have acquired an inversion after CRISPR induced breaks, if the following criteria were matched:

    1) a Green FISH spot had a Green-Red distance of more than the threshold

    2) the same Green FISH spot had a minimum Green-FarRed distance of more than the threshold

    3) the same Green FISH spot had a minimum Green-Blue distance of less than the threshold

In order to quantify the frequency of CRISPR-induced intra-chromosomal deletions or the loss of a chromosome arm, a change in the number of FISH spots had to be considered as well. If a deletion occurred, the cell would present with one Red and one FarRed FISH probe less than control cells, whereas the number of Green and Blue FISH spots would remain the same. A nucleus would also have to meet the following criteria to be detected as having an intra-chromosomal deletion:

    1) a Green FISH spot had a Green-Red distance of more than the threshold

2) the same Green FISH spot had a minimum Green-FarRed distance of less than the threshold

3) the same Green FISH spot had a minimum Green-Blue distance of more than the threshold

In case that the part of the chromosome arm that lies telomeric to the most centromeric CRISPR site was lost, the number of Red, FarRed and Blue FISH spots would be decreased by 1. Furthermore, a cell would have to meet these criteria:

1) a Green FISH spot had a Green-Red distance of more than the threshold

2) the same Green FISH spot had a minimum Green-FarRed distance of more than the threshold

3) the same Green FISH spot had a minimum Green-Blue distance of more than the threshold

Frequencies of chromosome synapsis, breakage and rearrangements were calculated in R and exported as HTML files, plots were generated in GraphPad Prism. Values were visualized as bar plots of mean plus standard deviation and statistical significance was tested by two-tailed student's t test unless stated otherwise.

6.7 ddPCR to directly quantify CRISPR or endonuclease induced chromosome translocations

For efficient PCR amplification, genDNA concentration was measured (Qubit dsDNA HS assay) and digested over night with HindIII. PCR primers and probes (IDT) were designed to only give a signal when a translocation is present. In order to quantify genDNA copy numbers, specific primers and probes for GapDH were included in the same reactions with 50ng of digested DNA. For translocation quantification, the ratio between GapDH positive droplets and translocation positive droplets was calculated.

oligo	sequence
ddPCR probe GapDH HEX	/5-HEX/CTCCCACTC/ZEN/CTGATTTCTGGAAAAGAGC/3-IABkFQ/
ddPCR primer GapDH fw	CTCTCTCCCATCCCTTCTCC
ddPCR primer GapDH rv	GCCCACCCCTTCTCTAAGTC
ddPCR probe LINC00217-/RBMXL1-MIS12 FAM	/56-FAM/CGCCCGCGC/ZEN/TGCATGCTGGGA/3-IABkFQ/
ddPCR primer MIS12	GACTGGCATAAGCGTCTTCG
ddPCR primer LINC00217	GGAAGCCGCCCAGAATAAGA
ddPCR primer RBMXL1	TCCCTGAGTCCACACCCATAG
ddPCR probe MLL-AF9/-HYLS1 FAM	/56-FAM/TGGTGTCTC/ZEN/AGCCTGCATCCAGAAGCC/3-IABkFQ/
ddPCR primer AF9	TGCCACCATCCCTGATTCTGA
ddPCR primer HYLS1	TGCACAGATGTGGGTAAAAGC
ddPCR primer MLL1	AGGACAAACCAGACCTTACAACT
ddPCR primer MLL2	CCACTCTTAGGTCACTTAGCATGT

6.8 Resection assay

Resection at CRISPR- or endonuclease-induced DSBs was quantified as described elsewhere [169]. Briefly, genDNA was digested using DraI or BsrgI and resection was measured on 50ng of digested genomic DNA by qPCR (2x ssoFast qPCR mix, BioRad; QX1000 thermocycler, BioRad). Using the following formula:

$$ssDNA\,[\%] = \frac{1}{2^{(\Delta Ct - 1)} + 0.5} \cdot 100$$

Primers are designed to bind up- or downstream an *in vivo* induced DSB at varying distances of a few hundred base pairs and up to 2kB away from the in vivo DSB. The PCR product furthermore spans across a restriction enzyme site. Genomic DNA was digested in vitro using the specific restriction enzyme, leading to the digestion of DNA up- or downstream of the DSB if the dsDNA is intact. If resection occurred after the *in vivo* DSB, the restriction enzyme will not cut and the DNA template remains intact and susceptible for qPCR amplification.

oligo	sequence
MLL DraI 1100 fw	TGGGTGAGGGGTACTTAGAATTCT
MLL DraI 1100 rv	TGCTTTGCACCCATATATATGCCAC
MLL DraI 250 fw	AGGACAAACCAGACCTTACAACT
MLL DraI 250 rv	AGTATTGGACACTGCGGGAGAT
RBMXL1 Bsrgl 335Bp fw	GAATCGGATGTATGCGACTGATC
RBMXL1 Bsrgl 335Bp rv	TTCCAAAGTTATTCCAACCCGAT
RBMXL1 Bsrgl 1618Bp fw	TGAGGAGGTGACATTAGAACTCAGA
RBMXL1 Bsrgl 1618Bp rv	AGGACTCACTTACACGGCCTTT

6.9 Software used in this study

Software	Resource	Link
GraphPad Prism (version 7.02)	GraphPad	https://www.graphpad.com/scientific -software/prism
R (version 3.4.3)	R Development Core Team	https://www.r-project.org
Harmony (version 4.4)	Perkin-Elmer	http://www.perkinelmer.de/product/ harmony-4-8-office-hh17000001
QuantaSoft™ Analysis Pro (version 1.0.596.0525)	BioRad	https://www.bio-rad.com/de-de/life-science/digital-pcr/qx200-droplet-digital-pcr-system/quantasoft-software-regulatory-edition
BioRad CFX Manager 3.1	BioRad	https://www.bio-rad.com/de-de/sku/1845000-cfx-manager-software?ID=1845000
Image Lab 5.2.1	BioRad	https://www.bio-rad.com/de-de/product/image-lab-software?ID=KRE6P5E8Z

7 References

1. So, A., Le Guen, T., Lopez, B.S., and Guirouilh-Barbat, J. (2017). Genomic rearrangements induced by unscheduled DNA double strand breaks in somatic mammalian cells. FEBS J. *284*, 2324–2344.

2. Lieber, M.R. (2010). The mechanism of double-strand DNA break repair by the nonhomologous DNA end-joining pathway. Annu. Rev. Biochem. *79*, 181–211. Available at: http://www.pubmedcentral.nih.gov/articlerender.fcgi?artid=3079308&tool=pmcentrez&rendertype=abstract.

3. Roukos, V., and Misteli, T. (2014). The biogenesis of chromosome translocations. Nat. Cell Biol. *16*, 293–300. Available at: http://www.ncbi.nlm.nih.gov/pubmed/24691255.

4. Pannunzio, N.R., Watanabe, G., and Lieber, M.R. (2018). Nonhomologous DNA end-joining for repair of DNA double-strand breaks. J. Biol. Chem. *293*, 10512–10523. Available at: https://pubmed.ncbi.nlm.nih.gov/29247009/ [Accessed January 26, 2021].

5. Cottarel, J., Frit, P., Bombarde, O., Salles, B., Négrel, A., Bernard, S., Jeggo, P.A., Lieber, M.R., Modesti, M., and Calsou, P. (2013). A noncatalytic function of the ligation complex during nonhomologous end joining. J. Cell Biol. *200*, 173–186.

6. Jiang, W., Crowe, J.L., Liu, X., Nakajima, S., Wang, Y., Li, C., Lee, B.J., Dubois, R.L., Liu, C., Yu, X., *et al.* (2015). Differential phosphorylation of DNA-PKcs regulates the interplay between end-processing and end-ligation during nonhomologous end-joining. Mol. Cell *58*, 172–185. Available at: http://dx.doi.org/10.1016/j.molcel.2015.02.024.

7. Dominski, Z. (2007). Nucleases of the metallo-β-lactamase family and their role in DNA and RNA metabolism. Crit. Rev. Biochem. Mol. Biol. *42*, 67–93. Available at: https://pubmed.ncbi.nlm.nih.gov/17453916/ [Accessed May 29, 2022].

8. Moon, A.F., Pryor, J.M., Ramsden, D.A., Kunkel, T.A., Bebenek, K., and Pedersen, L.C. (2014). Sustained active site rigidity during synthesis by human DNA polymerase μ. Nat. Struct. Mol. Biol. *21*, 253–260. Available at: https://www.nature.com/articles/nsmb.2766 [Accessed May 29, 2022].

9. Bebenek, K., Pedersen, L.C., and Kunkel, T.A. (2014). Structure-function studies of DNA polymerase λ. Biochemistry *53*, 2781–2792. Available at: https://pubs.acs.org/sharingguidelines [Accessed May 29, 2022].

10. Ma, Y., Lu, H., Tippin, B., Goodman, M.F., Shimazaki, N., Koiwai, O., Hsieh, C.L., Schwarz, K., and Lieber, M.R. (2004). A biochemically defined system for mammalian nonhomologous DNA end joining. Mol. Cell *16*, 701–713.

11. Bertocci, B., De Smet, A., Weill, J.C., and Reynaud, C.A. (2006). Nonoverlapping Functions of DNA Polymerases Mu, Lambda, and Terminal Deoxynucleotidyltransferase during Immunoglobulin V(D)J Recombination In Vivo. Immunity *25*, 31–41.

12. Lieber, M.R. (2008). The mechanism of human nonhomologous DNA End joining. J. Biol. Chem. *283*.

13. Frit, P., Barboule, N., Yuan, Y., Gomez, D., and Calsou, P. (2014). Alternative end-joining pathway(s): Bricolage at DNA breaks. DNA Repair (Amst). *17*, 81–97. Available at: http://dx.doi.org/10.1016/j.dnarep.2014.02.007.

14. Downs, J. a, and Jackson, S.P. (2004). A means to a DNA end: the many roles of Ku. Nat. Rev. Mol. Cell Biol. *5*, 367–378. Available at: http://dx.doi.org/10.1038/nrm1367.

15. Kabotyanski, E.B., Gomelsky, L., Han, J., Stamato, T.D., and Roth, D.B. (1998). Double-strand break repair in Ku86- and XRCC4-deficient cells. Nucleic Acids Res. *26*, 27–31.

16. Guirouilh-Barbat, J., Huck, S., Bertrand, P., Pirzio, L., Desmaze, C., Sabatier, L., and Lopez, B.S. (2004). Impact of the KU80 pathway on NHEJ-induced genome rearrangements in mammalian cells. Mol. Cell *14*, 611–623. Available at: https://pubmed.ncbi.nlm.nih.gov/15175156/ [Accessed February 8, 2021].

17. Le Guen, T., Ragu, S., Guirouilh-Barbat, J., and Lopez, B.S. (2015). Role of the double-strand break repair pathway in the maintenance of genomic stability. Mol. Cell. Oncol. *2*. Available at: https://doi.org/10.4161/23723548.2014.968020.

18. Guirouilh-Barbat, J., Huck, S., and Lopez, B.S. (2008). S-phase progression stimulates both the mutagenic KU-independent pathway and mutagenic processing of KU-dependent intermediates, for nonhomologous end joining. Oncogene *27*, 1726–1736. Available at: www.nature.com/onc.

19. Shibata, A. (2017). Regulation of repair pathway choice at two-ended DNA double-strand breaks. Mutat. Res. - Fundam. Mol. Mech. Mutagen. *803–805*, 51–55.

20. Hoa, N.N., Akagawa, R., Yamasaki, T., Hirota, K., Sasa, K., Natsume, T., Kobayashi, J., Sakuma, T., Yamamoto, T., Komatsu, K., *et al.* (2015). Relative contribution of four nucleases, CtIP, Dna2, Exo1 and Mre11, to the initial step of DNA double-strand break repair by homologous recombination in both the chicken DT40 and human TK6 cell lines. Genes to Cells *20*, 1059–1076. Available at: https://onlinelibrary.wiley.com/doi/10.1111/gtc.12310 [Accessed January 16, 2022].

21. Kakarougkas, A., and Jeggo, P.A. (2014). DNA DSB repair pathway choice: An orchestrated handover mechanism. Br. J. Radiol. *87*. Available at: https://pubmed.ncbi.nlm.nih.gov/24363387/ [Accessed January 26, 2021].

22. Fattah, F., Lee, E., Weisensel, N., Wang, Y., Lichter, N., and Hendrickson, E. (2010). Ku Regulates the Non-Homologous End Joining Pathway Choice of DNA Double-Strand Break Repair in Human Somatic Cells. PLoS Genet *6*, e1000855. Available at: citeulike-article-id:8450638%5Cnhttp://dx.doi.org/10.1371/journal.pgen.1000855.

23. Yu, A.M., and McVey, M. (2010). Synthesis-dependent microhomology-mediated end joining accounts for multiple types of repair junctions. Nucleic Acids Res. *38*, 5706–5717. Available at: https://academic.oup.com/nar/article/38/17/5706/1032738 [Accessed June 12, 2022].

24. Kent, T., Chandramouly, G., McDevitt, S.M., Ozdemir, A.Y., and Pomerantz, R.T. (2015). Mechanism of microhomology-mediated end-joining promoted by human DNA polymerase theta. Nat Struct Mol Biol *22*, 230–237. Available at: http://www.ncbi.nlm.nih.gov/pubmed/25643323.

25. Shima, N., Munroe, R.J., and Schimenti, J.C. (2004). The Mouse Genomic Instability Mutation chaos1 Is an Allele of Polq That Exhibits Genetic Interaction with Atm . Mol. Cell. Biol. *24*, 10381–10389. Available at: http://jaxmice.jax.org/index.html. [Accessed June 12, 2022].

26. Roerink, S.F., Schendel, R., and Tijsterman, M. (2014). Polymerase theta-mediated end joining of replication-associated DNA breaks in C. elegans. Genome Res. *24*, 954–962. Available at: http://www.genome.org/cgi/doi/10.1101/gr.170431.113. [Accessed June 12, 2022].

27. Ceccaldi, R., Liu, J.C., Amunugama, R., Hajdu, I., Primack, B., Petalcorin, M.I.R., O'Connor, K.W., Konstantinopoulos, P.A., Elledge, S.J., Boulton, S.J., *et al.* (2015).

Homologous-recombination-deficient tumours are dependent on Polθ -mediated repair. Nature *518*, 258–262. Available at: https://www.nature.com/articles/nature14184 [Accessed June 12, 2022].

28. Audebert, M., Salles, B., and Calsou, P. (2004). Involvement of poly(ADP-ribose) polymerase-1 and XRCC1/DNA ligase III in an alternative route for DNA double-strand breaks rejoining. J. Biol. Chem. *279*, 55117–55126.

29. Wang, H., Rosidi, B., Perrault, R., Wang, M., Zhang, L., Windhofer, F., and Iliakis, G. (2005). DNA ligase III as a candidate component of backup pathways of nonhomologous end joining. Cancer Res. *65*, 4020–4030. Available at: http://aacrjournals.org/cancerres/article-pdf/65/10/4020/2530694/4020-4030.pdf [Accessed June 12, 2022].

30. Tomkinson, A.E., and Sallmyr, A. (2013). Structure and function of the DNA ligases encoded by the mammalian LIG3 gene. Gene *531*, 150–157.

31. Dutta, A., Eckelmann, B., Adhikari, S., Ahmed, K.M., Sengupta, S., Pandey, A., Hegde, P.M., Tsai, M.S., Tainer, J.A., Weinfeld, M., *et al.* (2017). Microhomology-mediated end joining is activated in irradiated human cells due to phosphorylation-dependent formation of the XRCC1 repair complex. Nucleic Acids Res. *45*, 2585–2599. Available at: https://academic.oup.com/nar/article/45/5/2585/2716523 [Accessed June 12, 2022].

32. Della-Maria, J., Zhou, Y., Tsai, M.S., Kuhnlein, J., Carney, J.P., Paull, T.T., and Tomkinson, A.E. (2011). Human Mre11/human Rad50/Nbs1 and DNA ligase IIIα/XRCC1 protein complexes act together in an alternative nonhomologous end joining pathway. J. Biol. Chem. *286*, 33845–33853.

33. Boboila, C., Jankovic, M., Yan, C.T., Wang, J.H., Wesemann, D.R., Zhang, T., Fazeli, A., Feldman, L., Nussenzweig, A., Nussenzweig, M., *et al.* (2010). Alternative end-joining catalyzes robust IgH locus deletions and translocations in the combined absence of ligase 4 and Ku70. Proc. Natl. Acad. Sci. U. S. A. *107*, 3034–3039. Available at: www.pnas.org/cgi/doi/10.1073/pnas.0915067107 [Accessed June 12, 2022].

34. Soni, A., Siemann, M., Grabos, M., Murmann, T., Pantelias, G.E., and Iliakis, G. (2014). Requirement for Parp-1 and DNA ligases 1 or 3 but not of Xrcc1 in chromosomal translocation formation by backup end joining. Nucleic Acids Res. *42*, 6380–6392.

35. Caldecott, K.W., Tucker, J.D., Stanker, L.H., and Thompson, L.H. (1995). Characterization of the XRCC1-DNA ligase III complex in vitro and its absence from mutant hamster cells. Nucleic Acids Res. *23*, 4836–4843. Available at: https://academic.oup.com/nar/article/23/23/4836/2400732 [Accessed June 12, 2022].

36. Simsek, D., Brunet, E., Wong, S.Y.W., Katyal, S., Gao, Y., McKinnon, P.J., Lou, J., Zhang, L., Li, J., Rebar, E.J., *et al.* (2011). DNA ligase III promotes alternative nonhomologous end-joining during chromosomal translocation formation. PLoS Genet. *7*, 1–11.

37. Manchester, K.L. (1995). Theodor Boveri and the origin of malignant tumours. Trends Cell Biol. *5*, 384–387.

38. Nowell, P.C. (2007). Discovery of the Philadelphia chromosome: A personal perspective. J. Clin. Invest. *117*, 2033–2035. Available at: http://www.jci.org [Accessed April 3, 2022].

39. Nowell, C. (1962). The minute chromosome (Ph1) in chronic granulocytic leukemia. Blut Zeitschrift für die Gesamte Blutforsch. *8*, 65–66. Available at: https://pubmed.ncbi.nlm.nih.gov/14480647/ [Accessed March 28, 2021].

40. Hanahan, D., and Weinberg, R.A. (2011). Hallmarks of cancer: The next generation. Cell *144*, 646–674. Available at: http://dx.doi.org/10.1016/j.cell.2011.02.013.

41. Hnisz, D., Weintraub, A.S., Day, D.S., Valton, A., Bak, R.O., Li, C.H., Goldmann, J., Lajoie, B.R., Fan, Z.P., Sigova, A. a, *et al.* (2016). Activation of proto-oncogenes by disruption of chromosome neighborhoods. Science (80-.). *351*, 1454–1458. Available at: http://science.sciencemag.org/content/351/6280/1454.long.

42. Mitelman, F., Mertens, F., and Johansson, B. (2005). Prevalence estimates of recurrent balanced cytogenetic aberrations and gene fusions in unselected patients with neoplastic disorders. Genes Chromosom. Cancer *43*, 350–366.

43. Forbes, S.A., Beare, D., Gunasekaran, P., Leung, K., Bindal, N., Boutselakis, H., Ding, M., Bamford, S., Cole, C., Ward, S., *et al.* (2015). COSMIC: Exploring the world's knowledge of somatic mutations in human cancer. Nucleic Acids Res. *43*, D805–D811.

44. Nikiforov, Y.E. (2002). RET/PTC rearrangement in thyroid tumors. Endocr. Pathol. *13*, 3–16. Available at: https://pubmed.ncbi.nlm.nih.gov/12114746/ [Accessed February 11, 2021].

45. Sarkar, F.H., Sakr, W., Li, Y. -W, Macoska, J., Ball, D.E., and Crissman, J.D. (1992). Analysis of retinoblastoma (RB) gene deletion in human prostatic carcinomas. Prostate *21*, 145–152.

46. Marshall, A.E., Roes, M. V., Passos, D.T., DeWeerd, M.C., Chaikovsky, A.C., Sage, J., Howlett, C.J., and Dick, F.A. (2019). RB1 Deletion in Retinoblastoma Protein Pathway-Disrupted Cells Results in DNA Damage and Cancer Progression . Mol. Cell. Biol. *39*. Available at: https://pubmed.ncbi.nlm.nih.gov/31138663/ [Accessed February 11, 2021].

47. Levan, A. (1966). Non-random Representation of Chromosome Types in Human Tumor Stemlines. Hereditas *55*, 28–38. Available at: http://doi.wiley.com/10.1111/j.1601-5223.1966.tb02032.x [Accessed March 28, 2021].

48. van Steenis, H. (1966). Chromosomes and Cancer. Nature *209*, 819–821. Available at: https://www.nature.com/articles/209819a0 [Accessed March 28, 2021].

49. Latt, S.A. (1976). Optical Studies of Metaphase Chromosome Organization. Annu. Rev. Biophys. Bioeng. *5*, 1–37. Available at: http://www.annualreviews.org/doi/abs/10.1146/annurev.bb.05.060176.000245 [Accessed March 28, 2021].

50. Schreck, R.R., and Distèche, C.M. (1994). Chromosome Banding Techniques. In Current Protocols in Human Genetics (Hoboken, NJ, USA: John Wiley & Sons, Inc.), pp. 4.2.1-4.2.36. Available at: http://doi.wiley.com/10.1002/0471142905.hg0402s00 [Accessed March 28, 2021].

51. Cremer, T., Lichter, P., Borden, J., Ward, D.C., and Manuelidis, L. (1988). Detection of chromosome aberrations in metaphase and interphase tumor cells by in situ hybridization using chromosome-specific library probes. Hum. Genet. *80*, 235–246. Available at: https://pubmed.ncbi.nlm.nih.gov/3192213/ [Accessed March 28, 2021].

52. Gray, J.W., and Pinkel, D. (1992). Molecular cytogenetics in human cancer diagnosis. Cancer *69*, 1536–1542. Available at: https://pubmed.ncbi.nlm.nih.gov/1540892/ [Accessed March 28, 2021].

53. Mitelman, F. (2000). Recurrent chromosome aberrations in cancer. Mutat. Res. - Rev. Mutat. Res. *462*, 247–253.

54. Mitelman, F., Johansson, B., and Mertens, F. (2007). The impact of translocations and gene fusions on cancer causation. Nat Rev Cancer *7*, 233–245. Available at: http://www.ncbi.nlm.nih.gov/pubmed/17361217.

55.   Andersson, A., Olofsson, T., Lindgren, D., Nilsson, B., Ritz, C., Edén, P., Lassen, C., Råde, J., Fontes, M., Mörse, H., *et al.* (2005). Molecular signatures in childhood acute leukemia and their correlations to expression patterns in normal hematopoietic subpopulations. Proc. Natl. Acad. Sci. U. S. A. *102*, 19069–19074. Available at: https://pubmed.ncbi.nlm.nih.gov/16354839/ [Accessed March 30, 2021].

56.   Yeoh, E.J., Ross, M.E., Shurtleff, S.A., Williams, W.K., Patel, D., Mahfouz, R., Behm, F.G., Raimondi, S.C., Relling, M. V., Patel, A., *et al.* (2002). Classification, subtype discovery, and prediction of outcome in pediatric acute lymphoblastic leukemia by gene expression profiling. Cancer Cell *1*, 133–143. Available at: https://pubmed.ncbi.nlm.nih.gov/12086872/ [Accessed March 30, 2021].

57.   Aplan, P.D. (2006). Chromosomal translocations involving the MLL gene: Molecular mechanisms. DNA Repair (Amst). *5*, 1265–1272.

58.   Debatisse, M., Le Tallec, B., Letessier, A., Dutrillaux, B., and Brison, O. (2012). Common fragile sites: Mechanisms of instability revisited. Trends Genet. *28*, 22–32.

59.   Boteva, L., Nozawa, R.-S., Naughton, C., Samejima, K., Earnshaw, W.C., Correspondence, N.G., and Gilbert, N. (2020). Common Fragile Sites Are Characterized by Faulty Condensin Loading after Replication Stress. Available at: https://doi.org/10.1016/j.celrep.2020.108177 [Accessed June 19, 2022].

60.   Toledo, L.I., Altmeyer, M., Rask, M.-B., Lukas, C., Larsen, D.H., Povlsen, L.K., Bekker-Jensen, S., Mailand, N., Bartek, J., and Lukas, J. (2014). ATR Prohibits Replication Catastrophe by Preventing Global Exhaustion of RPA. Cell *156*, 374. Available at: https://linkinghub.elsevier.com/retrieve/pii/S0092867414000026.

61.   Roukos, V., Burman, B., and Misteli, T. (2013). The cellular etiology of chromosome translocations. Curr. Opin. Cell Biol. *25*, 357–364. Available at: http://dx.doi.org/10.1016/j.ceb.2013.02.015.

62.   Wei, P.C., Chang, A.N., Kao, J., Du, Z., Meyers, R.M., Alt, F.W., and Schwer, B. (2016). Long Neural Genes Harbor Recurrent DNA Break Clusters in Neural Stem/Progenitor Cells. Cell *164*, 644–655.

63.   Le Tallec, B., Dutrillaux, B., Lachages, A.M., Millot, G.A., Brison, O., and Debatisse, M. (2011). Molecular profiling of common fragile sites in human fibroblasts. Nat. Struct. Mol. Biol. *18*, 1421–1423. Available at: https://www.nature.com/articles/nsmb.2155 [Accessed June 19, 2022].

64.   Harrigan, J.A., Belotserkovskaya, R., Coates, J., Dimitrova, D.S., Polo, S.E., Bradshaw, C.R., Fraser, P., and Jackson, S.P. (2011). Replication stress induces 53BP1-containing OPT domains in G1 cells. J. Cell Biol. *193*, 97–108. Available at: www.jcb.org/cgi/doi/10.1083/jcb.201011083JCB97 [Accessed June 19, 2022].

65.   Lukas, C., Savic, V., Bekker-Jensen, S., Doil, C., Neumann, B., Pedersen, R.S., Grøhfte, M., Chan, K.L., Hickson, I.D., Bartek, J., *et al.* (2011). 53BP1 nuclear bodies form around DNA lesions generated by mitotic transmission of chromosomes under replication stress. Nat. Cell Biol. *13*, 243–253. Available at: https://www.nature.com/articles/ncb2201 [Accessed June 19, 2022].

66.   Chan, Y.W., Fugger, K., and West, S.C. (2018). Unresolved recombination intermediates lead to ultra-fine anaphase bridges, chromosome breaks and aberrations. Nat. Cell Biol. *20*, 92–103. Available at: https://doi.org/10.1038/s41556-017-0011-1 [Accessed June 19, 2022].

67.   Aymard, F., Aguirrebengoa, M., Guillou, E., Javierre, B.M., Bugler, B., Arnould, C., Rocher,

V., Iacovoni, J.S., Biernacka, A., Skrzypczak, M., *et al.* (2017). Genome-wide mapping of long-range contacts unveils clustering of DNA double-strand breaks at damaged active genes. Nat. Struct. Mol. Biol. *24*, 353–361.

68. Bester, A.C., Roniger, M., Oren, Y.S., Im, M.M., Sarni, D., Chaoat, M., Bensimon, A., Zamir, G., Shewach, D.S., and Kerem, B. (2011). Nucleotide deficiency promotes genomic instability in early stages of cancer development. Cell *145*, 435–446.

69. Gothe, H.J., Bouwman, B.A.M., Gusmao, E.G., Piccinno, R., Petrosino, G., Sayols, S., Drechsel, O., Minneker, V., Josipovic, N., Mizi, A., *et al.* (2019). Spatial Chromosome Folding and Active Transcription Drive DNA Fragility and Formation of Oncogenic MLL Translocations. Mol. Cell *75*, 267-283.e12.

70. Yu, X., Davenport, J.W., Urtishak, K.A., Carillo, M.L., Gosai, S.J., Kolaris, C.P., Byl, J.A.W., Rappaport, E.F., Osheroff, N., Gregory, B.D., *et al.* (2017). Genome-wide TOP2A DNA cleavage is biased toward translocated and highly transcribed loci. Genome Res. *27*, 1238–1249. Available at: http://genome.cshlp.org/lookup/doi/10.1101/gr.211615.116.

71. Canela, A., Maman, Y., Huang, S. yin N., Wutz, G., Tang, W., Zagnoli-Vieira, G., Callen, E., Wong, N., Day, A., Peters, J.M., *et al.* (2019). Topoisomerase II-Induced Chromosome Breakage and Translocation Is Determined by Chromosome Architecture and Transcriptional Activity. Mol. Cell *75*, 252-266.e8.

72. Schwer, B., Wei, P.-C., Chang, A.N., Kao, J., Du, Z., Meyers, R.M., Alt, F.W., Ferguson, D., Sleckman, B., and Yu, K. (2015). Transcription-associated processes cause DNA double-strand breaks and translocations in neural stem/progenitor cells. PNAS.

73. Burman, B., Zhang, Z.Z., Pegoraro, G., Lieb, J.D., and Misteli, T. (2015). Histone modifications predispose genome regions to breakage and translocation. Genes Dev. *29*, 1393–1402. Available at: http://www.ncbi.nlm.nih.gov/pmc/articles/PMC4511214/pdf/1393.pdf.

74. Bochman, M.L., Paeschke, K., and Zakian, V.A. (2012). DNA secondary structures: Stability and function of G-quadruplex structures. Nat. Rev. Genet. *13*, 770–780. Available at: https://www.nature.com/articles/nrg3296 [Accessed July 3, 2022].

75. Helmrich, A., Ballarino, M., Nudler, E., and Tora, L. (2013). Transcription-replication encounters, consequences and genomic instability. Nat. Struct. Mol. Biol. *20*, 412–418. Available at: https://www.nature.com/articles/nsmb.2543 [Accessed July 3, 2022].

76. Lu, S., Wang, G., Bacolla, A., Zhao, J., Spitser, S., and Vasquez, K.M. (2015). Short inverted repeats are hotspots for genetic instability: Relevance to cancer genomes. Cell Rep. *10*, 1674–1680.

77. Wang, G., Christensen, L.A., and Vasquez, K.M. (2006). Z-DNA-forming sequences generate large-scale deletions in mammalian cells. Proc. Natl. Acad. Sci. U. S. A. *103*, 2677–2682. Available at: www.pnas.orgcgidoi10.1073pnas.0511084103 [Accessed July 3, 2022].

78. Sinclair, P.B., Parker, H., An, Q., Rand, V., Ensor, H., Harrison, C.J., and Strefford, J.C. (2011). Analysis of a breakpoint cluster reveals insight into the mechanism of intrachromosomal amplification in a lymphoid malignancy. Hum. Mol. Genet. *20*, 2591–2602. Available at: https://academic.oup.com/hmg/article/20/13/2591/2527075 [Accessed July 3, 2022].

79. Zhang, Y., McCord, R.P., Ho, Y.J., Lajoie, B.R., Hildebrand, D.G., Simon, A.C., Becker, M.S., Alt, F.W., and Dekker, J. (2012). Spatial organization of the mouse genome and its role in recurrent chromosomal translocations. Cell *148*, 908–921. Available at:

http://dx.doi.org/10.1016/j.cell.2012.02.002.

80.   Roukos, V., Voss, T.C., Schmidt, C.K., Lee, S., Wangsa, D., and Misteli, T. (2013). Spatial Dynamics of Chromosome Translocations in Living Cells. Science (80-.). *341*, 660–664. Available at: https://www.sciencemag.org/lookup/doi/10.1126/science.1237150.

81.   Sunder, S., and Wilson, T.E. (2019). Frequency of DNA end joining in trans is not determined by the predamage spatial proximity of double-strand breaks in yeast. Proc. Natl. Acad. Sci. U. S. A. *116*, 9481–9490. Available at: https://www.pnas.org/content/116/19/9481 [Accessed April 11, 2021].

82.   Agmon, N., Liefshitz, B., Zimmer, C., Fabre, E., and Kupiec, M. (2013). Effect of nuclear architecture on the efficiency of double-strand break repair. Nat. Cell Biol. *15*, 694–699.

83.   Wang, G., Zhao, J., and Vasquez, K.M. (2009). Methods to determine DNA structural alterations and genetic instability. Methods *48*, 54–62.

84.   Dion, V., and Gasser, S.M. (2013). Chromatin movement in the maintenance of genome stability. Cell *152*, 1355–1364.

85.   Lisby, M., Mortensen, U.H., and Rothstein, R. (2003). Colocalization of multiple DNA double-strand breaks at a single Rad52 repair center. Nat. Cell Biol. *5*, 572–577. Available at: https://www.nature.com/articles/ncb997 [Accessed April 11, 2021].

86.   Miné-Hattab, J., and Rothstein, R. (2013). DNA in motion during double-strand break repair. Trends Cell Biol. *23*, 529–536.

87.   Seeber, A., Dion, V., and Gasser, S.M. (2013). Checkpoint kinases and the INO80 nucleosome remodeling complex enhance global chromatin mobility in response to DNA damage. Genes Dev. *27*, 1999–2008. Available at: http://www.genesdev.org/cgi/ [Accessed April 11, 2021].

88.   Gothe, H.J., Minneker, V., and Roukos, V. (2018). Dynamics of Double-Strand Breaks: Implications for the Formation of Chromosome Translocations. In, pp. 27–38. Available at: http://link.springer.com/10.1007/978-981-13-0593-1_3.

89.   McVey, M., and Lee, S.E. (2008). MMEJ repair of double-strand breaks (director's cut): deleted sequences and alternative endings. Trends Genet. *24*, 529–538.

90.   Caridi, C.P., D'agostino, C., Ryu, T., Zapotoczny, G., Delabaere, L., Li, X., Khodaverdian, V.Y., Amaral, N., Lin, E., Rau, A.R., *et al.* (2018). Nuclear F-actin and myosins drive relocalization of heterochromatic breaks. Nature *559*, 54–60. Available at: https://doi.org/10.1038/s41586-018-0242-8 [Accessed April 11, 2021].

91.   Hurst, V., Shimada, K., and Gasser, S.M. (2019). Nuclear Actin and Actin-Binding Proteins in DNA Repair. Trends Cell Biol. *29*, 462–476. Available at: https://doi.org/10.1016/j.tcb.2019.02.010 [Accessed August 21, 2022].

92.   Lamm, N., Rogers, S., and Cesare, A.J. (2021). Chromatin mobility and relocation in DNA repair. Trends Cell Biol. *31*, 843–855.

93.   Kilic, S., Lezaja, A., Gatti, M., Bianco, E., Michelena, J., Imhof, R., and Altmeyer, M. (2019). Phase separation of 53 BP 1 determines liquid-like behavior of DNA repair compartments. EMBO J. *38*. Available at: https://pubmed.ncbi.nlm.nih.gov/31267591/ [Accessed April 11, 2021].

94.   Pessina, F., Giavazzi, F., Yin, Y., Gioia, U., Vitelli, V., Galbiati, A., Barozzi, S., Garre, M., Oldani, A., Flaus, A., *et al.* (2019). Functional transcription promoters at DNA double-strand breaks mediate RNA-driven phase separation of damage-response factors. Nat. Cell Biol. *21*, 1286–1299. Available at: https://doi.org/10.1038/s41556-019-0392-4 [Accessed April

11, 2021].

95.   Costantino, L., Sotiriou, S.K., Rantala, J.K., Magin, S., Mladenov, E., Helleday, T., Haber, J.E., Iliakis, G., Kallioniemi, O.P., and Halazonetis, T.D. (2014). Break-Induced Replication Repair of Damaged Forks Induces Genomic Duplications in Human Cells. Science (80-.). *343*, 1–5.

96.   Haber, J.E. (1999). DNA recombination: The replication connection. Trends Biochem. Sci. *24*, 271–275.

97.   Novo, F.J., de Mendíbil, I.O., and Vizmanos, J.L. (2007). TICdb: a collection of gene-mapped translocation breakpoints in cancer. BMC Genomics *8*. Available at: http://www.pubmedcentral.nih.gov/articlerender.fcgi?artid=1794234&tool=pmcentrez&ren dertype=abstract%5Cnhttp://www.scopus.com/inward/record.url?eid=2-s2.0-33846910723&partnerID=tZOtx3y1.

98.   Richardson, C., Moynahan, M.E., and Jasin, M. (1998). Double-strand break repair by interchromosomal recombination : suppression of chromosomal translocations. Genes Dev. *12*, 3831–3842.

99.   Zhang, Y., and Rowley, J.D. (2006). Chromatin structural elements and chromosomal translocations in leukemia. DNA Repair (Amst). *5*, 1282–1297.

100.   Simsek, D., and Jasin, M. (2010). Alternative end-joining is suppressed by the canonical NHEJ component Xrcc4/ligase IV during chromosomal translocation formation. Nat Struct Mol Biol *17*, 410–416.

101.   Ghezraoui, H., Piganeau, M., Renouf, B., Renaud, J.-B., Sallmyr, A., Ruis, B., Oh, S., Tomkinson, A.E., Hendrickson, E.A., Giovannangeli, C., *et al.* (2014). Chromosomal Translocations in Human Cells Are Generated by Canonical Nonhomologous End-Joining. Mol. Cell *55*, 829–942. Available at: http://dx.doi.org/10.1016/j.molcel.2014.08.002.

102.   Renouf, B., Piganeau, M., Ghezraoui, H., Jasin, M., and Brunet, E. (2014). Creating Cancer Translocations in Human Cells Using cas9 DSBs and nCas9 paired nicks. Methods Enzymol. *546*, 251–271.

103.   Shibata, A., Conrad, S., Birraux, J., Geuting, V., Barton, O., Ismail, A., Kakarougkas, A., Meek, K., Taucher-Scholz, G., Löbrich, M., *et al.* (2011). Factors determining DNA double-strand break repair pathway choice in G2 phase. EMBO J. *30*, 1079–92. Available at: http://www.pubmedcentral.nih.gov/articlerender.fcgi?artid=3061033&tool=pmcentrez&ren dertype=abstract.

104.   Zeman, M.K., and Cimprich, K.A. (2013). Causes and consequences of replication stress. Nat. Cell Biol. *16*, 2–9. Available at: http://www.nature.com/doifinder/10.1038/ncb2897.

105.   Pommier, Y. (2013). Drugging topoisomerases: Lessons and Challenges. ACS Chem. Biol. *8*, 82–95. Available at: http://pubs.acs.org/doi/abs/10.1021/cb300648v.

106.   Berger, J.M. (1998). Structure of DNA topoisomerases. Biochim. Biophys. Acta *1400*, 3–18.

107.   Wu, C., Li, Y.-C., Wang, Y., Li, T., and Chan, N. (2013). On the structural basis and design guidelines for type II topoisomerase-targeting anticancer drugs. Nucleic Acids Res. *41*, 10630–40.   Available   at: http://www.pubmedcentral.nih.gov/articlerender.fcgi?artid=3905874&tool=pmcentrez&ren dertype=abstract%5Cnhttp://www.ncbi.nlm.nih.gov/pubmed/24038465.

108.   Maxwell, A., Bush, N.G., and Evans-Roberts, K. (2015). DNA Topoisomerases. EcoSal Plus *6*. Available at: http://www.ncbi.nlm.nih.gov/pubmed/26435256.

109. Lee, J.H., and Berger, J.M. (2019). Cell Cycle-Dependent Control and Roles of DNA Topoisomerase II. Genes (Basel). *10*, 859. Available at: https://www.mdpi.com/2073-4425/10/11/859 [Accessed March 30, 2021].

110. Azarova, A.M., Lyu, Y.L., Lin, C.-P., Tsai, Y., Lau, J.Y., Wang, J.C., and Liu, L.F. (2007). Roles of DNA topoisomerase II isozymes in chemotherapy and secondary malignancies. Proc. Natl. Acad. Sci. USA *104*, 11014–11019.

111. Canela, A., Maman, Y., Jung, S., Wong, N., Callen, E., Day, A., Kieffer-Kwon, K.R., Pekowska, A., Zhang, H., Rao, S.S.P., *et al.* (2017). Genome Organization Drives Chromosome Fragility. Cell *170*, 507-521.e18.

112. Pommier, Y., Huang, S. yin N., Gao, R., Das, B.B., Murai, J., and Marchand, C. (2014). Tyrosyl-DNA-phosphodiesterases (TDP1 and TDP2). DNA Repair (Amst). *19*, 114–129.

113. Gómez-Herreros, F., Zagnoli-Vieira, G., Ntai, I., Martínez-Macías, M.I., Anderson, R.M., Herrero-Ruíz, A., and Caldecott, K.W. (2017). TDP2 suppresses chromosomal translocations induced by DNA topoisomerase II during gene transcription. Nat. Commun. *8*, 233. Available at: http://dx.doi.org/10.1038/s41467-017-00307-y.

114. Riccio, A.A., Schellenberg, M.J., and Williams, R.S. (2020). Molecular mechanisms of topoisomerase 2 DNA–protein crosslink resolution. Cell. Mol. Life Sci. *77*, 81–91. Available at: https://doi.org/10.1007/s00018-019-03367-z [Accessed March 30, 2021].

115. Kim, N., and Jinks-Robertson, S. (2017). The Top1 paradox: friend and foe of the eukaryotic genome. DNA Repair (Amst). Available at: http://www.sciencedirect.com/science/article/pii/S1568786417302057 [Accessed June 20, 2017].

116. Ledesma, F.C., El Khamisy, S.F., Zuma, M.C., Osborn, K., and Caldecott, K.W. (2009). A human 5′-tyrosyl DNA phosphodiesterase that repairs topoisomerase-mediated DNA damage. Nature *461*, 674–678. Available at: https://www.nature.com/articles/nature08444 [Accessed March 31, 2021].

117. Schellenberg, M.J., Perera, L., Strom, C.N., Waters, C.A., Monian, B., Appel, C.D., Vilas, C.K., Williams, J.G., Ramsden, D.A., and Williams, R.S. (2016). Reversal of DNA damage induced Topoisomerase 2 DNA–protein crosslinks by Tdp2. Nucleic Acids Res. *44*, 3829–3844. Available at: https://academic.oup.com/nar/article/44/8/3829/2467446 [Accessed March 31, 2021].

118. Schellenberg, M.J., Schellenberg, M.J., Lieberman, J.A., Herrero-ruiz, A., Butler, L.R., Williams, J.G., Muñoz-cabello, A.M., Mueller, G.A., London, R.E., and Williams, R.S. (2017). ZATT (ZNF451)– mediated resolution of topoisomerase 2. Science (80-.). *6468*, 1–11.

119. van den Boom, J., Wolf, M., Weimann, L., Schulze, N., Li, F., Kaschani, F., Riemer, A., Zierhut, C., Kaiser, M., Iliakis, G., *et al.* (2016). VCP/p97 Extracts Sterically Trapped Ku70/80 Rings from DNA in Double-Strand Break Repair. Mol. Cell *64*, 189–198. Available at: http://dx.doi.org/10.1016/j.molcel.2016.08.037.

120. Meyer, H., Bug, M., and Bremer, S. (2012). Emerging functions of the VCP/p97 AAA-ATPase in the ubiquitin system. Nat. Cell Biol. *14*, 117–123. Available at: https://www.nature.com/articles/ncb2407 [Accessed December 28, 2021].

121. Meyer, H., and Weihl, C.C. (2014). The VCP/p97 system at a glance: Connecting cellular function to disease pathogenesis. J. Cell Sci. *127*, 3877–3883.

122. Bug, M., and Meyer, H. (2012). Expanding into new markets - VCP/p97 in endocytosis and autophagy. J. Struct. Biol. *179*, 78–82.

123. Sun, Y., Jenkins, L.M.M., Su, Y.P., Nitiss, K.C., Nitiss, J.L., and Pommier, Y. (2020). A conserved SUMO pathway repairs topoisomerase DNA-protein cross-links by engaging ubiquitin-mediated proteasomal degradation. Sci. Adv. *6*, 6290–6303. Available at: http://advances.sciencemag.org/ [Accessed April 2, 2021].

124. Azuma, Y., Arnaoutov, A., Anan, T., and Dasso, M. (2005). PIASy mediates SUMO-2 conjugation of Topoisomerase-II on mitotic chromosomes. EMBO J. *24*, 2172–2182. Available at: https://pubmed.ncbi.nlm.nih.gov/15933717/ [Accessed April 2, 2021].

125. Bandele, O.J., and Osheroff, N. (2008). The efficacy of topoisomerase II-targeted anticancer agents reflects the persistence of drug-induced cleavage complexes in cells. Biochemistry *47*, 11900–11908.

126. Montecucco, A., and Biamonti, G. (2007). Cellular response to etoposide treatment. Cancer Lett. *252*, 9–18.

127. Xie, B.S., Zhao, H.C., Yao, S.K., Zhuo, D.X., Jin, B., Lv, D.C., Wu, C.L., Ma, D.L., Gao, C., Shu, X.M., *et al.* (2011). Autophagy inhibition enhances etoposide-induced cell death in human hepatoma G2 cells. Int. J. Mol. Med. *27*, 599–606. Available at: http://www.spandidos-publications.com/10.3892/ijmm.2011.607/abstract [Accessed April 5, 2021].

128. Blasiak, J., Pawlowska, E., Szczepanska, J., and Kaarniranta, K. (2019). Interplay between Autophagy and the Ubiquitin-Proteasome System and Its Role in the Pathogenesis of Age-Related Macular Degeneration. Int. J. Mol. Sci. *20*, 210. Available at: https://www.mdpi.com/1422-0067/20/1/210 [Accessed April 5, 2021].

129. Allan, J.M., and Travis, L.B. (2005). Mechanisms of Therapy-Related Carcinogenesis. Nat. Rev. Cancer *5*, 943–955. Available at: http://www.nature.com/doifinder/10.1038/nrc1749.

130. Travis, W.D., Brambilla, E., and Riely, G.J. (2013). New pathologic classification of lung cancer: Relevance for clinical practice and clinical trials. J. Clin. Oncol. *31*, 992–1001. Available at: http://ascopubs.org/doi/10.1200/JCO.2012.46.9270 [Accessed April 10, 2021].

131. Lo-Coco, F., and Hasan, S.K. (2014). Understanding the molecular pathogenesis of acute promyelocytic leukemia. Best Pract. Res. Clin. Haematol. *27*, 3–9. Available at: http://linkinghub.elsevier.com/retrieve/pii/S1521692614000243.

132. Cowell, I.G., and Austin, C.A. (2012). Mechanism of generation of therapy related leukemia in response to anti-topoisomerase II agents. Int. J. Environ. Res. Public Health *9*, 2075–2091.

133. Libura, J., Slater, D.J., Felix, C.A., and Richardson, C. (2005). Therapy-related acute myeloid leukemia–like MLL rearrangements are induced by etoposide in primary human CD34+ cells and remain stable after clonal expansion. Blood *105*, 2124–2131. Available at: https://pubmed.ncbi.nlm.nih.gov/15528316/ [Accessed April 5, 2021].

134. Meyer, C., Hofmann, J., Burmeister, T., Gröger, D., Park, T.S., Emerenciano, M., Pombo de Oliveira, M., Renneville, A., Villarese, P., Macintyre, E., *et al.* (2013). The MLL recombinome of acute leukemias in 2013. Leukemia *27*, 2165–2176. Available at: http://www.nature.com/doifinder/10.1038/leu.2013.135.

135. Wang, J., Iwasaki, H., Krivtsov, A., Febbo, P.G., Thorner, A.R., Ernst, P., Anastasiadou, E., Kutok, J.L., Kogan, S.C., Zinkel, S.S., *et al.* (2005). Conditional MLL-CBP targets GMP and models therapy-related myeloproliferative disease. EMBO J. *24*, 368–381. Available at: http://emboj.embopress.org/cgi/doi/10.1038/sj.emboj.7600521 [Accessed April 5, 2021].

136. Wright, R.L., and Vaughan, A.T.M. (2014). A systematic description of MLL fusion gene

formation. Crit. Rev. Oncol. Hematol. *91*, 283–291.

137. Sirulnik, A., Melnick, A., and Zelent, A. (2003). Molecular pathogenesis of acute promyelocytic leukaemia and APL variants. Best Pract. Res. Clin. Haematol. *16*, 387–408.

138. Pendleton, M., Lindsey, R.H., Felix, C.A., Grimwade, D., and Osheroff, N. (2014). Topoisomerase II and leukemia. Ann. N. Y. Acad. Sci. *1310*, 98–110.

139. Kakizuka, A., Miller, W.H., Umesono, K., Warrell, R.P., Frankel, S.R., Murty, V.V.V.S., Dmitrovsky, E., and Evans, R.M. (1991). Chromosomal translocation t(15;17) in human acute promyelocytic leukemia fuses RARα with a novel putative transcription factor, PML. Cell *66*, 663–674.

140. Noguera, N.I., Catalano, G., Banella, C., Divona, M., Faraoni, I., Ottone, T., Arcese, W., and Voso, M.T. (2019). Acute promyelocytic Leukemia: Update on the mechanisms of leukemogenesis, resistance and on innovative treatment strategies. Cancers (Basel). *11*. Available at: https://pubmed.ncbi.nlm.nih.gov/31635329/ [Accessed April 11, 2021].

141. Laurenzana, A., Pettersson, F., and Miller, W.H. (2006). Role of PML/RARα in the pathogenesis of APL. Drug Discov. Today Dis. Mech. *3*, 499–505.

142. Briggs, F.B.S., Goldstein, B.A., McCauley, J.L., Zuvich, R.L., De Jager, P.L., Rioux, J.D., Ivinson, A.J., Compston, A., Hafler, D.A., Hauser, S.L., *et al.* (2010). Variation within DNA repair pathway genes and risk of multiple sclerosis. Am. J. Epidemiol. *172*, 217–24. Available at: http://www.pubmedcentral.nih.gov/articlerender.fcgi?artid=3658128&tool=pmcentrez&rendertype=abstract.

143. Hasan, S.K., Buttari, F., Ottone, T., Voso, M.T., Hohaus, S., Marasco, E., Mantovani, V., Garagnani, P., Sanz, M.A., Cicconi, L., *et al.* (2011). Risk of acute promyelocytic leukemia in multiple sclerosis Coding variants of DNA repair genes. Neurology *76*, 1–7.

144. Hasan, S.K., Ottone, T., Schlenk, R.F., Xiao, Y., Wiemels, J.L., Mitra, M.E., Bernasconi, P., Di Raimondo, F., Stanghellini, M.T.L., Marco, P., *et al.* (2010). Analysis of t(15;17) chromosomal breakpoint sequences in therapy-related versus de novo acute promyelocytic leukemia: Association of DNA breaks with specific DNA motifs at PML and RARA loci. Genes, Chromosom. Cancer *49*, 726–732. Available at: http://doi.wiley.com/10.1002/gcc.20783.

145. Hasan, S.K., Mays, A.N., Ottone, T., Ledda, A., Nasa, G. La, Cattaneo, C., Borlenghi, E., Melillo, L., Montefusco, E., Stephen, C., *et al.* (2008). Molecular analysis of t (15;17) genomic breakpoints in secondary acute promyelocytic leukemia arising after treatment of multiple sclerosis. Blood *112*, 3383–3390.

146. Mistry, A.R., Felix, C.A., Whitmarsh, R.J., Mason, A., Reiter, A., Cassinat, B., Parry, A., Walz, C., Wiemels, J.L., Segal, M.R., *et al.* (2005). DNA Topoisomerase II in Therapy-Related Acute Promyelocytic Leukemia. N Engl J Med *352*, 1529–1538.

147. Brunet, E., Simsek, D., Tomishima, M., DeKelver, R., Choi, V.M., Gregory, P., Urnov, F., Weinstock, D.M., and Jasin, M. (2009). Chromosomal translocations induced at specified loci in human stem cells. Proc. Natl. Acad. Sci. U. S. A. *106*, 10620–10625. Available at: https://www.pnas.org/content/106/26/10620 [Accessed April 10, 2021].

148. Piganeau, M., Ghezraoui, H., De Cian, A., Guittat, L., Tomishima, M., Perrouault, L., René, O., Katibah, G.E., Zhang, L., Holmes, M.C., *et al.* (2013). Cancer translocations in human cells induced by zinc finger and TALE nucleases. Genome Res. *23*, 1182–1193. Available at: http://www.genome.org/cgi/doi/10.1101/gr.147314.112. [Accessed April 10, 2021].

149. Zhang, H., and Cohen, S.N. (2004). Smurf2 up-regulation activates telomere-dependent

senescence. Genes Dev. *18*, 3028–3040. Available at: http://www.genesdev.org/cgi/doi/10.1101/gad.1253004.

150. Lund, H.L., Hughesman, C.B., Fakhfakh, K., McNeil, K., Clemens, S., Hocken, K., Pettersson, R., Karsan, A., Foster, L.J., and Haynes, C. (2016). Initial Diagnosis of ALK-Positive Non-Small-Cell Lung Cancer Based on Analysis of ALK Status Utilizing Droplet Digital PCR. Anal. Chem. *88*, 4879–4885. Available at: https://pubs.acs.org/sharingguidelines [Accessed April 10, 2021].

151. Mertens, F., Johansson, B., Fioretos, T., and Mitelman, F. (2015). The emerging complexity of gene fusions in cancer. Nat. Rev. Cancer *15*, 371–381. Available at: www.nature.com/reviews/cancer [Accessed April 10, 2021].

152. Hu, J., Meyers, R.M., Dong, J., Panchakshari, R.A., Alt, F.W., and Frock, R.L. (2016). Detecting DNA double-stranded breaks in mammalian genomes by linear amplification mediated high-throughput genome-wide translocation sequencing. Nat. Protoc. *11*, 853–871.

153. Burman, B., Misteli, T., and Pegoraro, G. (2015). Quantitative detection of rare interphase chromosome breaks and translocations by high-throughput imaging. Genome Biol. *16*, 146. Available at: https://genomebiology.biomedcentral.com/articles/10.1186/s13059-015-0718-x [Accessed April 19, 2021].

154. Difilippantonio, M.J., Zhu, J., Chen, H.T., Meffre, E., Nussenzweig, M.C., Max, E.E., Ried, T., and Nussenzweig, A. (2000). DNA repair protein Ku80 suppresses chromosomal aberrations and malignant transformation. Nature *404*, 510–4. Available at: http://www.pubmedcentral.nih.gov/articlerender.fcgi?artid=4721590&tool=pmcentrez&rendertype=abstract.

155. Weinstock, D.M., Richardson, C.A., Elliott, B., and Jasin, M. (2006). Modeling oncogenic translocations: Distinct roles for double-strand break repair pathways in translocation formation in mammalian cells. DNA Repair (Amst). *5*, 1065–1074.

156. Iliakis, G., Murmann, T., and Soni, A. (2015). Alternative end-joining repair pathways are the ultimate backup for abrogated classical non-homologous end-joining and homologous recombination repair: Implications for the formation of chromosome translocations. Mutat. Res. - Genet. Toxicol. Environ. Mutagen. *793*, 166–175. Available at: http://dx.doi.org/10.1016/j.mrgentox.2015.07.001.

157. Stingele, J., Bellelli, R., and Boulton, S.J. (2017). Mechanisms of DNA–protein crosslink repair. Nat. Rev. Mol. Cell Biol. *18*, 563–573. Available at: http://dx.doi.org/10.1038/nrm.2017.56.

158. Thattikota, Y., Tollis, S., Palou, R., Vinet, J., Tyers, M., and D'Amours, D. (2018). Cdc48/VCP Promotes Chromosome Morphogenesis by Releasing Condensin from Self-Entrapment in Chromatin. Mol. Cell *69*, 664-676.e5. Available at: https://www.sciencedirect.com/science/article/abs/pii/S1097276518300595?via%3Dihub [Accessed November 15, 2018].

159. Aymard, F., Bugler, B., Schmidt, C.K., Guillou, E., Caron, P., Briois, S., Iacovoni, J.S., Daburon, V., Miller, K.M., Jackson, S.P., *et al.* (2014). Transcriptionally active chromatin recruits homologous recombination at DNA double-strand breaks. Nat. Struct. &Amp; Mol. Biol. *21*, 366. Available at: https://doi.org/10.1038/nsmb.2796.

160. Sternberg, S.H., Redding, S., Jinek, M., Greene, E.C., and Doudna, J.A. (2014). DNA interrogation by the CRISPR RNA-guided endonuclease Cas9. Nature *507*, 62–67. Available at: http://www.nature.com/articles/nature13011 [Accessed November 25, 2019].

161. Wiedenheft, B., Sternberg, S.H., and Doudna, J.A. (2012). RNA-guided genetic silencing systems in bacteria and archaea. Nature *482*, 331–338. Available at: https://www.nature.com/articles/nature10886 [Accessed April 25, 2021].

162. Ferreira, C.B., Sumner, R.P., Rodriguez-Plata, M.T., Rasaiyaah, J., Milne, R.S., Thrasher, A.J., Qasim, W., and Towers, G.J. (2020). Lentiviral Vector Production Titer Is Not Limited in HEK293T by Induced Intracellular Innate Immunity. Mol. Ther. - Methods Clin. Dev. *17*, 209–219. Available at: https://doi.org/10.1016/j.omtm.2019.11.021. [Accessed April 25, 2021].

163. Sentmanat, M.F., Peters, S.T., Florian, C.P., Connelly, J.P., and Pruett-Miller, S.M. (2018). A Survey of Validation Strategies for CRISPR-Cas9 Editing. Sci. Rep. *8*, 888. Available at: www.nature.com/scientificreports/ [Accessed April 25, 2021].

164. Oh, S., Harvey, A., Zimbric, J., Wang, Y., Nguyen, T., Jackson, P.J., and Hendrickson, E.A. (2014). DNA ligase III and DNA ligase IV carry out genetically distinct forms of end joining in human somatic cells. DNA Repair (Amst). *21*, 97–110. Available at: http://dx.doi.org/10.1016/j.dnarep.2014.04.015.

165. Dörsam, B., Seiwert, N., Foersch, S., Stroh, S., Nagel, G., Begaliew, D., Diehl, E., Kraus, A., McKeague, M., Minneker, V., *et al.* (2018). PARP-1 protects against colorectal tumor induction, but promotes inflammation-driven colorectal tumor progression. Proc. Natl. Acad. Sci. U. S. A. *115*, E4061–E4070. Available at: https://pubmed.ncbi.nlm.nih.gov/29632181/ [Accessed April 25, 2021].

166. Smart, D.J., Halicka, H.D., Schmuck, G., Traganos, F., Darzynkiewicz, Z., and Williams, G.M. (2008). Assessment of DNA double-strand breaks and γH2AX induced by the topoisomerase II poisons etoposide and mitoxantrone. Mutat. Res. - Fundam. Mol. Mech. Mutagen. *641*, 43–47.

167. Sørensen, C.S., Syljuåsen, R.G., Falck, J., Schroeder, T., Rönnstrand, L., Khanna, K.K., Zhou, B.B., Bartek, J., and Lukas, J. (2003). Chk1 regulates the S phase checkpoint by coupling the physiological turnover and ionizing radiation-induced accelerated proteolysis of Cdc25A. Cancer Cell *3*, 247–258.

168. Bartek, J., and Lukas, J. (2003). Chk1 and Chk2 kinases in checkpoint control and cancer. Cancer Cell *3*, 421–429.

169. Zhou, Y., Caron, P., Legube, G., and Paull, T.T. (2014). Quantitation of DNA double-strand break resection intermediates in human cells. Nucleic Acids Res. *42*, 1–11.

170. Caron, P., Choudjaye, J., Clouaire, T., Bugler, B., Daburon, V., Aguirrebengoa, M., Mangeat, T., Iacovoni, J.S., Álvarez-Quilón, A., Cortés-Ledesma, F., *et al.* (2015). Non-redundant Functions of ATM and DNA-PKcs in Response to DNA Double-Strand Breaks. Cell Rep. *13*, 1598–1609.

171. Raftopoulou, C., Roumelioti, F.M., Dragona, E., Gimelli, S., Sloan-Béna, F., Gorgoulis, V., Antonarakis, S.E., and Gagos, S. (2020). Karyotypic flexibility of the complex cancer genome and the role of polyploidization in maintenance of structural integrity of cancer chromosomes. Cancers (Basel). *12*. Available at: https://pubmed.ncbi.nlm.nih.gov/32150835/ [Accessed February 27, 2022].

172. Srivastava, M., Nambiar, M., Sharma, S., Karki, S.S., Goldsmith, G., Hegde, M., Kumar, S., Pandey, M., Singh, R.K., Ray, P., *et al.* (2012). An inhibitor of nonhomologous end-joining abrogates double-strand break repair and impedes cancer progression. Cell *151*, 1474–1487.

173. Carpenter, A.J., and Porter, A.C.G. (2004). Construction, Characterization, and

Complementation of a Conditional-Lethal DNA Topoisomerase II Mutant Human Cell Line. Mol. Biol. Cell *15*, 5700–5711. Available at: http://www.molbiolcell.org/cgi/doi/10.1091/mbc.E04-08-0732.

174. Roukos, V., Pegoraro, G., Voss, T.C., and Misteli, T. (2015). Cell cycle staging of individual cells by fluorescence microscopy. Nat. Protoc. *10*, 334–348. Available at: https://www.nature.com/articles/nprot.2015.016 [Accessed March 20, 2022].

175. Reiter, A., Saußele, S., Grimwade, D., Wiemels, J.L., Segal, M.R., Lafage-Pochitaloff, M., Walz, C., Weisser, A., Hochhaus, A., Willer, A., *et al.* (2003). Genomic anatomy of the specific reciprocal translocation t(15;17) in acute promyelocytic leukemia. Genes Chromosom. Cancer *36*, 175–188.

176. Huberman, J.A. (1981). New views of the biochemistry of eucaryotic DNA replication revealed by aphidicolin, an unusual inhibitor of DNA polymerase α. Cell *23*, 647–648.

177. Chodosh, L.A., Fire, A., Samuels, M., and Sharp, P.A. (1989). 5,6-Dichloro-1-β-D-ribofuranosylbenzimidazole inhibits transcription elongation by RNA polymerase II in vitro. J. Biol. Chem. *264*, 2250–2257. Available at: http://www.jbc.org/article/S0021925818941694/fulltext [Accessed January 16, 2022].

178. Stingele, J., Schwarz, M.S., Bloemeke, N., Wolf, P.G., and Jentsch, S. (2014). A DNA-dependent protease involved in DNA-protein crosslink repair. Cell *158*, 327–338. Available at: http://dx.doi.org/10.1016/j.cell.2014.04.053 [Accessed December 28, 2021].

179. Heidelberger, J.B., Voigt, A., Borisova, M.E., Petrosino, G., Ruf, S., Wagner, S.A., and Beli, P. (2018). Proteomic profiling of VCP substrates links VCP to K6-linked ubiquitylation and c-Myc function. EMBO Rep., e44754. Available at: http://embor.embopress.org/lookup/doi/10.15252/embr.201744754.

180. Acs, K., Luijsterburg, M.S., Ackermann, L., Salomons, F.A., Hoppe, T., and Dantuma, N.P. (2011). The AAA-ATPase VCP/p97 promotes 53BP1 recruitment by removing L3MBTL1 from DNA double-strand breaks. Nat. Struct. Mol. Biol. *18*, 1345–1350.

181. Ramadan, K., Halder, S., Wiseman, K., and Vaz, B. (2017). Strategic role of the ubiquitin-dependent segregase p97 (VCP or Cdc48) in DNA replication. Chromosoma *126*, 17–32. Available at: https://link.springer.com/article/10.1007/s00412-016-0587-4 [Accessed December 28, 2021].

182. Anderson, D.J., Le Moigne, R., Djakovic, S., Kumar, B., Rice, J., Wong, S., Wang, J., Yao, B., Valle, E., Kiss von Soly, S., *et al.* (2015). Targeting the AAA ATPase p97 as an Approach to Treat Cancer through Disruption of Protein Homeostasis. Cancer Cell *28*, 653–665.

183. Zhou, H.J., Wang, J., Yao, B., Wong, S., Djakovic, S., Kumar, B., Rice, J., Valle, E., Soriano, F., Menon, M.K., *et al.* (2015). Discovery of a First-in-Class, Potent, Selective, and Orally Bioavailable Inhibitor of the p97 AAA ATPase (CB-5083). J. Med. Chem. *58*, 9480–9497. Available at: https://pubs.acs.org/sharingguidelines [Accessed December 28, 2021].

184. Gothe, H.J. (2020). Dissertation von Henrike Johanna Gothe.

185. Sciascia, N., Wu, W., Zong, D., Sun, Y., Wong, N., John, S., Wangsa, D., Ried, T., Bunting, S.F., Pommier, Y., *et al.* (2020). Suppressing proteasome mediated processing of topoisomerase II DNA-protein complexes preserves genome integrity. Elife *9*.

186. Jasin, M., and Haber, J.E. (2016). The democratization of gene editing: Insights from site-specific cleavage and double-strand break repair. DNA Repair (Amst). Available at: http://dx.doi.org/10.1016/j.dnarep.2016.05.001.

187. Bindra, R.S., Goglia, A.G., Jasin, M., and Powell, S.N. (2013). Development of an assay to

measure mutagenic non-homologous end-joining repair activity in mammalian cells. Nucleic Acids Res. *41*.

188. Gelot, C., Guirouilh-Barbat, J., Le Guen, T., Dardillac, E., Chailleux, C., Canitrot, Y., and Lopez, B.S. (2016). The Cohesin Complex Prevents the End Joining of Distant DNA Double-Strand Ends. Mol. Cell *61*, 15–26.

189. Mani, R.S., Tomlins, S.A., Callahan, K., Ghosh, A., Nyati, M.K., Varambally, S., Palanisamy, N., and Chinnalyan, A.M. (2009). Induced chromosomal proximity and gene fusions in prostate cancer. Science (80-.). *326*, 1230.

190. Mladenov, E., Magin, S., Soni, A., and Iliakis, G. (2016). DNA double-strand-break repair in higher eukaryotes and its role in genomic instability and cancer: Cell cycle and proliferation-dependent regulation. Semin. Cancer Biol. *37–38*, 51–64.

191. Jasin, M., and Zhang, Y. (2011). An essential role for CtIP in chromosomal translocation formation through an alternative end-joining pathway. Nat Struct Mol Biol *18*, 80–84.

192. Mateos-Gomez, P.A., Gong, F., Nair, N., Miller, K.M., Lazzerini-Denchi, E., and Sfeir, A. (2015). Mammalian polymerase θ promotes alternative NHEJ and suppresses recombination. Nature *518*, 254–7. Available at: http://www.pubmedcentral.nih.gov/articlerender.fcgi?artid=4718306&tool=pmcentrez&rendertype=abstract.

193. Joannides, M., Mays, A.N., Mistry, A.R., Hasan, S.K., Reiter, A., Wiemels, J.L., Felix, C.A., Lo Coco, F., Osheroff, N., Solomon, E., *et al.* (2011). Molecular pathogenesis of secondary acute promyelocytic leukemia. Mediterr. J. Hematol. Infect. Dis. *3*.

194. Panousis, C., and Phillips, D.R. (1994). DNA sequence specificity of mitoxantrone. Nucleic Acids Res. *22*, 1342–1345.

195. Hoa, N.N., Shimizu, T., Zhou, Z.W., Wang, Z.Q., Deshpande, R.A., Paull, T.T., Akter, S., Tsuda, M., Furuta, R., Tsusui, K., *et al.* (2016). Mre11 Is Essential for the Removal of Lethal Topoisomerase 2 Covalent Cleavage Complexes. Mol. Cell *64*, 580–592.

8 Tables of Figures

8.1 Introduction

8.2   Results

8.3 Discussion

9   List of abbreviations

Abbreviation	Meaning
DRB	5,6-dichloro-1-β-D-ribofuranosylbenzimidazole
DSB	(DNA) double strand break
DSE	double strand end
VCP	Valosin containing protein (p97)
AML	acute myeloid leukaemia
APL	acute promyelocytic leukaemia
ORI	origin of replication initiation
SUMO	small Ubiquitin-like modifier
SIM	sumo interacting motif
CFS	common fragile site
ERFS	early replicating fragile site
FBS	Fetal bovine serum
DPC	DNA-protein crosslink
FISH	fluorescent *in situ* hybridization
MS	multiple sclerosis
MIDAS	mitotic DNA synthesis
DDR	DNA damage response
HR	homologous recombination
SSA	single strand annealing
ER	endoplasmic reticulum
ERAD	ER-associated degradation
HTGTS	high-throughput genome-wide translocation sequencing
LAM-HTGTS	Linear-amplification mediated high-throughput genome-wide sequencing
ATRA	all-trans retinoic acid
MMEJ	microhomology-mediated end joining
dsDNA	double stranded DNA
ssDNA	single stranded DNA
EJ	end joining
NHEJ	non-homologous end joining
cNHEJ	canonical/classical non-homologous end joining
aEJ	alternative end joining

Acknowledgments

Getting a PhD and writing a thesis ain't easy. Therefore…

… I would like to thank the following people who have helped me undertake this research and/or supported me along the way:

My supervisor Vassilis Roukos, for his support, understanding and patience – even in difficult times;

The former and current members of the Roukos lab for their moral support – could not have done this without you.

Everyone at the Institute of Molecular Biology gGmbH and within the International PhD Programme for scientific input or support from behind the scenes.

My friends and family for their support and patience during this journey, I cannot believe you are all still sticking around.

Most importantly my partner Jonas – I simply could not have done this without you and your support, especially in the last couple of months!

Vera Minneker

Virchowstr. 17,
50935 Köln, Germany
Tel: +49-177-1738472
DOB: 25/06/1989

Email: v.minneker@web.de
Nationality: German

Education

2016 - present	**Johannes-Gutenberg University Mainz**	
	PhD student in the International PhD program (IPP)	
2013 - 2015	**University Duisburg-Essen**	
	M.Sc. Medical Biology. Final Grade 1.6	
2010 - 2013	**Westfälische Hochschule (WHS) University of Applied Sciences**	
	B.Sc. molecular Biology. Final Grade 1.8	

Laboratory Experience

April 2016 – March 2021
Institute for Molecular Biology gGmbH in Mainz, Roukos Lab
Doctoral researcher
Study of the dynamics of chromosome translocation formation

April – October 2015
MPI for Molecular Physiology in Dortmund, Vader Lab
Master thesis: *Characterization of the meiotic roles of Cdc48 and its cofactor Wss1 in budding yeast*

January – February 2015
MPI for Molecular Biomedicine in Münster, Vaquerizas Lab
6 week internship: *Study of chromatin organization in D. melanogaster*

November – December 2014
MPI for Molecular Physiology in Dortmund, Vader Lab
6 week internship: *Study of the relationship between Pch2, Hop1 and Orc1 during meiosis in S. cerevisiae*

October 2014
Westfälische Hochschule (WHS) University of Applied Sciences
Part time job: Supervision of first semester students' lab projects

September – October 2014
Westfälische Hochschule (WHS) University of Applied Sciences
6 week internship: *Recombinant expression and purification of human BMP2 in B. subtilis*

November 2013 – March 2015
Biophysics department at Ruhr University Bochum
Part time job: Data mining on data from MALDI imaging and FTIR imaging. Part of the PURE project

July – August 2013
Biophysics department at Ruhr University Bochum
Bachelor thesis: *FTIR data mining on data from colon cancer tissue slices using discrete wavelet transform in MATLAB and LASAGNE software*

April – June 2013
Biophysics department at Ruhr University Bochum, Germany and CAS-MPG-PICB Shanghai, China
13 week internship of which 6 weeks were done at the PICB in Shanghai

Publications

Lucic B, Chen H-C, Kuzman M, Zorita E, Wegner J, Minneker V, Roukos V, Benkirane M, Weng W, Schmidt M, Fronza R, Stadhouders R, Vlahovicek K, Filion GJ, Lusic M (2019) **Spatially clustered loci with multiple enhancers are frequent targets of HIV-1** *NatCom*

Piccinno R, Minneker V, Roukos V (2019) **53BP1-DNA repair enters a new liquid phase** *EMBO J.*

Gothe HJ, Bouwman BAM, Gusmao EG, Piccinno R, Petrosino G, Sayols S, Drechsel O, Minneker V, Josipovic N, Mizi A, Nielsen CF, Wagner EM, Takeda S, Sasanuma H, Hudson DF, Kindler T, Baranello L, Papantonis A, Crosetto N, Roukos V. (2019) **Spatial Chromosome Folding and Active Transcription Drive DNA Fragility and Formation of Oncogenic MLL Translocations.** *Mol Cell.*

Gothe HJ, Minneker V, Roukos V. (2018) **Dynamics of Double-Strand Breaks: Implications for the Formation of Chromosome Translocations**. *Adv Exp Med Biol*

Dörsam B, Seiwert N, Foersch S, Stroh S, Nagel G, Begaliew D, Diehl E, Kraus A, McKeague M, Minneker V, Roukos V, Reißig S, Waisman A, Moehler M, Stier A, Mangerich A, Dantzer F, Kaina B, Fahrer J. (2018) **PARP-1 protects against colorectal tumor induction, but promotes inflammation-driven colorectal tumor progression.** *Proc Natl Acad Sci U S A.*

Conference participation

November 2019	**IMB Conference: "Chromosome Territories & Nuclear Architecture"** Poster presentation "C-Fusion 3D: a novel tool to probe spatial gene positioning and rare chromosome rearrangements in single cells"
October 2019	**EMBO Workshop: DNA damage response** Poster presentation "C-Fusion 3D: a novel tool to probe spatial gene positioning and rare chromosome rearrangements in single cells"
May 2019	**EMBO Workshop: The genome in 3 dimensions** Poster presentation "C-Fusion 3D: a novel tool to probe spatial gene positioning and rare chromosome rearrangements in single cells"

Further work experience

Since June 2021	**Referentin im Vorstandsbüro, Forschungszentrum Jülich GmbH**
August 2020 – August 2021	**Coordinator of the International PhD Programme (IPP) in Mainz** (varying weekly working hours)
May 2020	**Co-organized the first "Pint of Science" event in Mainz** (postponed due to COVID-19)
May 2020	**Co-organized the IPP retreat** to Tübingen (60 participants, postponed due to COVID-19)
January 2020	**Founded the IMB sustainability group "IMB Green"**
November 2019	**Co-organizer of the "2019 N² Joint Event: From Research to Application"** (350 participants)
June 2019 – August 2020	**SFB1361 IRTG student representative**
May 2019 – August 2020	**Board Member of the N² network of networks**
May 2019 – August 2020	**IPP representative**
March 2019	**Co-organized the "Girls Day" at IMB** (14 participants)
September 2017	**Co-organized a joint lab retreat with the Beli lab** to Porto (15 participants)
April 2017	**Co-organized the IPP retreat** to Cologne (90 participants)